

DOE/BC/14942-4
(DE98000463)

Advanced Reservoir Characterization And Evaluation Of CO2
Gravity Drainage In The Naturally Fractured Spraberry Trend
Area

Annual Report
September 1, 1995 - August 31, 1996

By
David S. Schechter

December 1997

Performed Under Contract No. DE-FC22-95BC14942

New Mexico Petroleum Recovery Research Center
New Mexico Institute of Mining and Technology
Socorro, New Mexico



National Petroleum Technology Office
U. S. DEPARTMENT OF ENERGY
Tulsa, Oklahoma

DISCLAIMER

This report was prepared as an account of work sponsored by an agency of the United States Government. Neither the United States Government nor any agency thereof, nor any of their employees, makes any warranty, expressed or implied, or assumes any legal liability or responsibility for the accuracy, completeness, or usefulness of any information, apparatus, product, or process disclosed, or represents that its use would not infringe privately owned rights. Reference herein to any specific commercial product, process, or service by trade name, trademark, manufacturer, or otherwise does not necessarily constitute or imply its endorsement, recommendation, or favoring by the United States Government or any agency thereof. The views and opinions of authors expressed herein do not necessarily state or reflect those of the United States Government.

This report has been reproduced directly from the best available copy.

Available to DOE and DOE contractors from the Office of Scientific and Technical Information, P.O. Box 62, Oak Ridge, TN 37831; prices available from (615) 576-8401.

Available to the public from the National Technical Information Service, U.S. Department of Commerce, 5285 Port Royal Rd., Springfield VA 22161

DOE/BC/14942-4
Distribution Category UC-122

Advanced Reservoir Characterization And Evaluation of CO₂ Gravity Drainage In The
Naturally Fractured Spraberry Trend Area

Annual Report
September 1, 1995 to August 31, 1996

By
David S. Schechter

December 1997

Work Performed Under Contract No. DE-FC22-95BC14942

Prepared for
U.S. Department of Energy
Assistant Secretary for Fossil Energy

Jerry F. Casteel, Project Manager
National Petroleum Technology Office
P.O. Box 3628
Tulsa, OK 74101

Prepared by:
New Mexico Petroleum Recovery Research Center
New Mexico Institute of Mining and Technology
Socorro, NM

TABLE OF CONTENTS

TABLE OF CONTENTS	iii
LIST OF TABLES	iv
LIST OF FIGURES	v
ABSTRACT	vii
EXECUTIVE SUMMARY	viii
ACKNOWLEDGEMENTS	xi
I. INTRODUCTION	1
II. TECHNICAL PROGRESS	2
1. RESERVOIR CHARACTERIZATION	2
1.1 Geological Characterization of the Spraberry Formation	2
1.2 Core-Log Integration for Characterization of the Spraberry Trend Shaly Sands	14
2. INVESTIGATION OF CRUDE OIL/BRINE/ROCK INTERACTION	32
2.1 Determination of Initial Water Saturation	32
2.2 Rock Wettability as Determined by Imbibition Experiments	32
2.3 Water-Oil Interfacial Tension Measurements	35
2.4 Water-Oil Capillary Pressure Determination	35
3. RESERVOIR PERFORMANCE ANALYSES	46
3.1 Scaling Analysis of Water Imbibition Results	46
3.2 Analysis of Inflow Performance of Spraberry Trend Wells	50
3.3 Simulation of a Spraberry Waterflood Pilot	81
4. INVESTIGATION OF CO ₂ /CRUDE OIL PHASE BEHAVIOR AND RECOVERY MECHANISM BY CO ₂ INJECTION IN FRACTURED SYSTEMS	103
4.1 Minimum Miscibility Pressure (MMP)	103
4.2 Interfacial Tension Measurements	103
4.3 Vaporization of Oil Fractions into CO ₂	104
4.4 Investigation of CO ₂ Gravity Drainage	104
4.5 Mathematical Modeling of CO ₂ Gravity Drainage	106
5. CORING CENTRAL PRODUCTION WELL IN THE CO ₂ PILOT AREA ..	126
III. CONCLUSIONS	133

LIST OF TABLES

Table 1.1 - XRD analysis, parts in 10	8
Table 1.2 - Log-based rock model	24
Table 2.1 - Estimated macroscopic displacement efficiency (E_{dm}) in cores from Spraberry Trend Area reservoirs	37
Table 2.2 - Properties of rock and fluids used in 8 completed tests	37
Table 2.3 - Rock properties and results of water imbibition experiments	38
Table 3.1 - Well productivity before and after hydraulic fracture treatment	64
Table 3.2 - Data used for matching productivity decline of X.B. Cox A-4 shut-in well test	64
Table 3.3 - Productivity of depleted wells in Driver Unit before and after large scale hydraulic treatments	65
Table 3.4 - Reservoir properties for the Humble pilot flood	91
Table 3.5 - Reservoir fluid properties	91
Table 3.6 - Matched parameters for rock matrix	92
Table 3.7 - Matched parameters for fractures	92
Table 4.1 - Composition of separator oil and produced oils	117

LIST OF FIGURES

Figure 1.1 - Gamma-ray log, porosity and permeability.	9
Figure 1.2 - Gamma-ray response, porosity and clay content.	10
Figure 1.3 - Gamma-ray response, porosity and percentage of carbonate.	11
Figure 1.4 - Porosity and clays plus carbonate percentage	12
Figure 1.5 - Relative contributions of percent clay and carbonate.	13
Figure 1.6 - Log-derived water saturation	25
Figure 1.7 - Open-hole log for the DOE pilot well E.T.O'Daniel #37	26
Figure 1.8 - Open-hole logs from the E.T.O'Daniel #26.	27
Figure 1.9 - Open-hole logs from the E.T. O'Daniel # 28	28
Figure 1.10 - Cased-hole logs from the E.T. O'Daniel "G" #1.	29
Figure 1.11 - Effective porosity vs. volume of shale	30
Figure 1.12 - Fractured zone identification from logs for E.T. O'Daniel #37.	31
Figure 2.1 - Initial water saturation in Spraberry sandstone	39
Figure 2.2 - Oil recovery from untreated cores during water imbibition.	39
Figure 2.3 - Oil recovery from cleaned cores during water imbibition.	40
Figure 2.4 - Effect of permeability on final oil recovery.	40
Figure 2.5 - Brine recovery from a cleaned core during oil imbibition.	41
Figure 2.6 - Final recovery versus corresponding aging time in oil	41
Figure 2.7 - Effect of aging of core in oil on wettability to water.	42
Figure 2.8 - Diagram of experimental setup for IFT measurements.	42
Figure 2.9 - J-function from mercury injection capillary pressure, cores from Shackelford #1-38A.	43
Figure 2.10 - J-function from mercury injection capillary pressure, cores from Judkins A#5.	43
Figure 2.11 - Average J-function developed from mercury injection capillary pressure curves, cores from Shackelford #138A and Judkins A#5.	44
Figure 2.12 - Estimated water-oil capillary pressure in Spraberry sand.	44
Figure 2.13 - Drainage water-oil capillary pressure in Spraberry sand.	45
Figure 3.1 - Imbibition oil recovery from cleaned Spraberry cores	66
Figure 3.2 - Dimensionless imbibition oil recovery curves.	66
Figure 3.3 - Calculated imbibition oil recovery for Spraberry reservoirs.	67
Figure 3.4 - Calculated imbibition oil recovery for 5U Unit, Upper Spraberry.	67
Figure 3.5 - Oil-water relative permeability curves for Spraberry sands.	68
Figure 3.6 - Calculated imbibition oil recovery for 5U Unit, Upper Spraberry.	68
Figure 3.7 - Matching between calculated and actual productivity for Cox A-4.	69
Figure 3.8 - Calculated and actual productivity for Davenport B-5.	69
Figure 3.9 - Calculated and actual productivity for Davenport B-7	70
Figure 3.10 - Calculated and actual productivity for Davenport C-6	70
Figure 3.11 - Calculated and actual productivity for Davenport C-8	71
Figure 3.12 - Calculated and actual productivity for Bryans A-2.	71
Figure 3.13 - Calculated and actual production rates for 6 wells.	72
Figure 3.14 - Calculated and actual productivity indices for 6 wells	72
Figure 3.15 - Calculated pressure distribution along a stress-insensitive fracture.	73

Figure 3.16 - Calculated pressure distribution along a stress-sensitive fracture.	73
Figure 3.17 - A model to interpret cyclic waterflooding performance.	74
Figure 3.18 - Geometry of a reservoir drained by a wing of a fracture.	74
Figure 3.19 - The Spraberry Trend Area, showing location of Humble pilot.	93
Figure 3.20 - Humble pilot test showing dramatic increase in production of central well ..	94
Figure 3.21 - High water injection rates were used to reopen the fractures.	95
Figure 3.22 - Three years performance of the Humble pilot waterflood.	96
Figure 3.23 - Sheet model for naturally fractured reservoirs	97
Figure 3.24 - Grid model after orientation to the major fracture trend.	97
Figure 3.25 - Matrix and fracture relative permeabilities.	98
Figure 3.26 - Plot of generated imbibition capillary pressures.	98
Figure 3.27 - The flood fronts as of Feb. 1, 1958	99
Figure 3.28 - Water production after water flooding from the middle producer.	100
Figure 3.29 - History match of data for cumulative water injection.	100
Figure 3.30 - History match of data for oil production rate in central production well ...	100
Figure 3.31 - History match of data for cumulative oil production.	100
Figure 3.32 - History match of observed and simulated data for gas production rate.	101
Figure 3.33 - History match of observed and simulated data for gas-oil ratio.	101
Figure 3.34 - History match of observed and simulated data for water production rate. ...	101
Figure 3.35 - History match of data for cumulative water production.	101
Figure 3.36 - History match of observed and simulated data for water-oil ratio	102
Figure 3.37 - History match of observed and simulated data for water cut.	102
Figure 3.38 - History match of observed and simulated data for bottom hole pressure. ...	102
Figure 4.1 - Estimated minimum miscibility pressure for Spraberry reservoir oil	118
Figure 4.2 - Measured densities of CO ₂ /oil systems at reservoir temperature of 138°F. ...	118
Figure 4.3 - Effect of pressure on IFT of two CO ₂ /oil systems at 138°F.	119
Figure 4.4 - Relationship between density difference and IFT for two CO ₂ /oil systems at 138°F.	119
Figure 4.5 - Oil recovery during CO ₂ gravity drainage from a 500 md Berea.	120
Figure 4.6 - Oil recovery during CO ₂ gravity drainage from a 50 md Berea.	120
Figure 4.7 - Pressure history of the 0.01 md Spraberry core experiment.	121
Figure 4.8 - Oil recovery during CO ₂ gravity drainage from a 0.01 md Spraberry core, oil collected at reservoir temperature	121
Figure 4.9 - Corrected oil recovery during CO ₂ gravity drainage from a 0.01md Spraberry core	122
Figure 4.10 - Solution to demarcator and recovery for Fs = 1.	122
Figure 4.16 - Comparison of calculated recovery with experimental data, CO ₂ /oil gravity drainage in a 0.01 md Spraberry core	125
Figure 5.1 - Pilot pattern configuration in E.T. O'Daniel Unit.	129
Figure 5.2 - Whole core observation of fractures compared with FMI log for the 5U pay zone.	130
Figure 5.3 - Injection profile performed by Humble Oil Co. in 1968.	131
Figure 5.4 - Orientation of fractures in the Spraberry Trend Area.	132

ABSTRACT

The overall goal of this project is to assess the economic feasibility of CO₂ flooding the naturally fractured Spraberry Trend Area in West Texas. This objective is being accomplished by conducting research in four areas: 1) extensive characterization of the reservoirs, 2) experimental studies of crude oil/brine/rock (COBR) interaction in the reservoirs, 3) analytical and numerical simulation of Spraberry reservoirs, and, 4) experimental investigations on CO₂ gravity drainage in Spraberry whole cores. This report provides results of the first year of the five-year project for each of the four areas.

In the first area, reservoir characterization has been established based on petrophysical and geological analysis combined with core-log integration. A shaly sand rock model for describing the Spraberry Trend Area Reservoir has been established, and as a result, a better log interpretation algorithm for identifying Spraberry pay zones has been developed.

In the second area, COBR interaction in the Spraberry matrix has been analyzed based on results of laboratory experiments. Initial water saturation and historical water saturation in the Spraberry sands has been determined to be between 0.20 and 0.40 depending on permeability of the sand. Macroscopic displacement efficiency during water imbibition has been estimated to be about 50%. Wettability of the Spraberry sands has been determined. The Amott wettability index to water was estimated to be about 0.55 indicating that the Spraberry sands are weakly water wet. Water-oil capillary pressure has been established. The experimental capillary pressure curve confirms the rock wettability determined based imbibition test. Interfacial tension (IFT) between Spraberry oil and brine has been measured to be 32 mN/m. Experimental results have been used in analytical and numerical reservoir simulations.

In the third area, performance of the Spraberry reservoirs has been explored based on reservoir characterization and laboratory investigations. Scaling of imbibition oil recovery results to reservoir geometry indicates that higher oil recovery should have been achieved during water flooding, although the Spraberry sands are weakly water wet. Reasons for the poor performance of water flood were analyzed. Inflow performance of Spraberry Trend wells has been analyzed using a new mathematical model developed for wells intersecting long fractures. Computer simulation of a Spraberry waterflood pilot has been conducted using laboratory measured parameters to understand Spraberry waterflood performance.

In the fourth area, efficiency of CO₂ gravity drainage has been investigated based on laboratory experiments. Minimum Miscibility Pressure (MMP) was measured to be 1,550 psig. IFT of the CO₂/Spraberry oil under reservoir conditions was determined. The IFT at the MMP is about 1.5 mN/m. Investigation of vaporization of oil fractions into CO₂ was initiated. Preliminary result shows insignificance of the mechanism. CO₂ gravity drainage experiments were carried out using Spraberry oil and whole cores. 51% of original oil in place was recovered from a 0.01 md Spraberry whole core within 200 days during CO₂ gravity drainage. Experimental data were matched by a mathematical model.

EXECUTIVE SUMMARY

The goal of this project is to test the economic feasibility of CO₂ injection in the naturally fractured Spraberry Trend Area in the Permian Basin. CO₂ injection in naturally fractured reservoirs does not meet classic screening criteria due to the expectation of excessive channeling of low viscosity CO₂ through the natural fractures. However, the number of naturally fractured reservoirs and the low recovery usually attendant with these reservoirs combined with abundance of natural CO₂ sources strongly suggests the necessity of exploring counter-intuitive process options. The success of a CO₂ pilot in the naturally fractured Midale reservoir fortified by laboratory experiments performed under the Department of Energy's Extraction Technology Program were the driving force behind the undertaking of such a risky venture. Both lab and field results indicated that injection of IFT-lowering gas could result in gravity drainage of oil in the matrix blocks if the fractures had sufficient vertical relief and significant density.

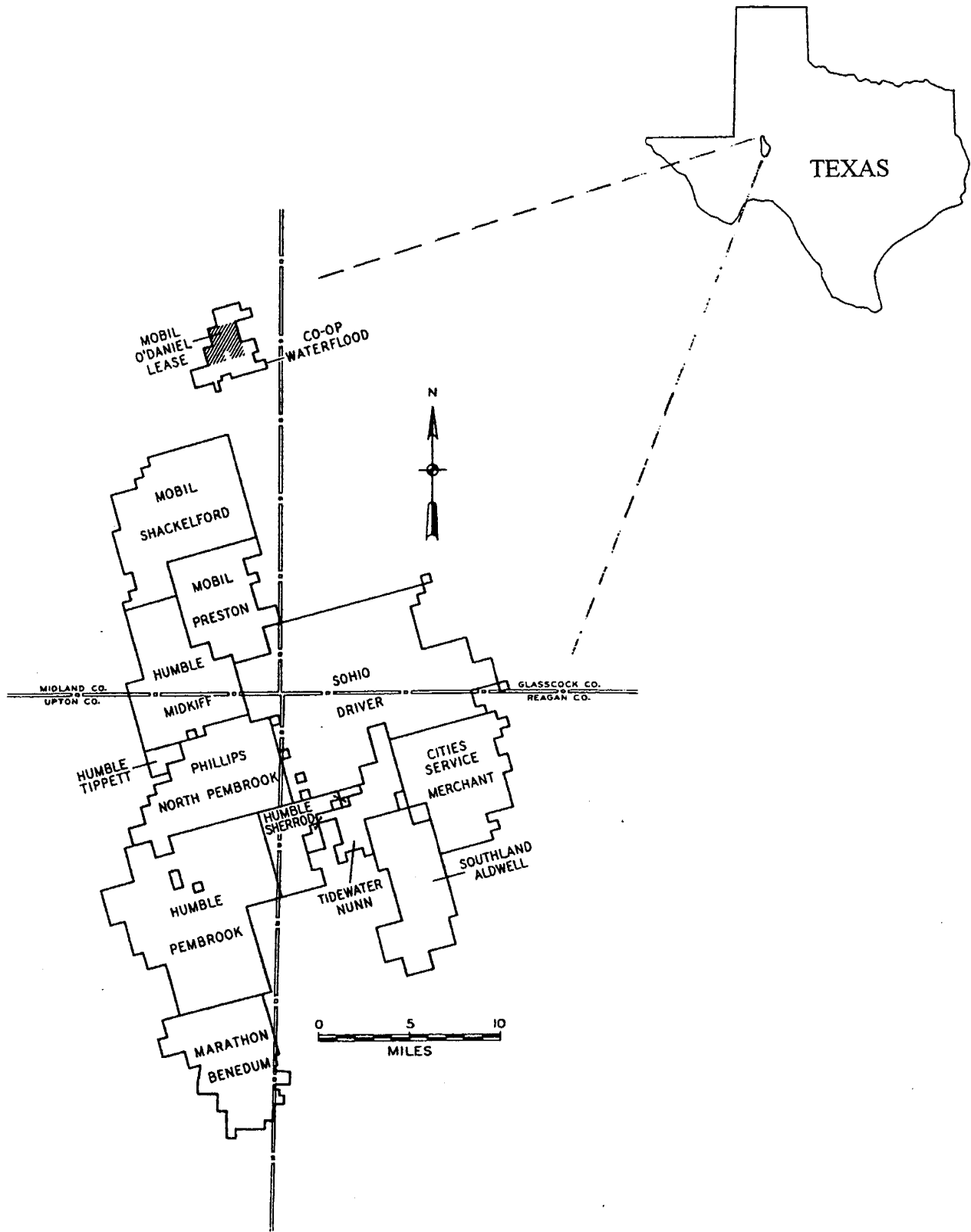
Several other factors are prominent in the decision to attempt a pilot CO₂ project in the Spraberry Trend Area. The magnitude of the target is a serious consideration. Spraberry reservoirs contained some 10 Bbbl OOIP of which less than 10% has been recovered over the course of 45 years of production. Secondly, whereas major oil companies once dominated Spraberry production, now independent operators own a majority of oil production. These companies are just as reliant, yet less accessible to technology than major oil companies. In addition, major oil companies had little incentive to attempt risky projects in this notoriously unyielding reservoir. However Spraberry production is far more important to the independent operators that currently produce many of the 7,000+ active wells, many of which are reaching their economic limit. CO₂ supply, a crucial question in any reservoir considered as a potential candidate, is abundant and in close proximity to Spraberry Trend Area fields. All of these factors combined with the favorable performance of the Midale pilot and concurrent DOE extraction research work led to the inexorable conclusion that a pilot CO₂ injection in the Spraberry was a prime candidate for the DOE Class III Field Demonstration Program. Furthermore, teaming of an independent oil company and a university research laboratory encompasses the spirit of technology transfer embodied in the DOE Program. So far, the teamwork between New Mexico Tech's Petroleum Recovery Research Center and Parker and Parsley Petroleum Co. has been beneficial for both organizations and exemplary of the purpose of the Department of Energy's Class Program.

Significant progress is reported on the characterization and fluid flow aspects of the project, both from an experimental and analytical viewpoint. At the time of the writing of this summary, the first horizontal core ever retrieved from the Spraberry Trend Area has been recovered and is currently being analyzed. We expect to address more of the field activities in the upcoming year as we reach the point of obtaining sufficient reservoir characterization to continue into the pilot phase of the project. The field activity in the first year was restricted to coring the central production well in the pilot area. The results of the coring operation are presented in Section V of this report. A shaly sand algorithm was developed which provides improved methodology of identifying the pay zones that strongly fluoresce. This core-based model is corroborated by petrophysical and geological

information provided in Section I. The model has been developed using QLA2 (Geographix Inc.) and we are currently working on developing a more accurate cased-hole analogy for extrapolation to other fields and areas in the vast Spraberry Trend Area. We now have dozens of Spraberry core plugs from Upper Spraberry pay zones and are currently pursuing a detailed study of imbibition, capillary pressure and wettability. Such information is crucial in understanding waterflood performance in tight, naturally fractured reservoirs. We provide a simulation of a forty year old waterflood pilot in Section IV which utilizes the most current data available. This pilot is unique in that detailed well by well information is available, a rarity in Spraberry. We have performed slim tube tests to determine MMP and measured Spraberry crude oil/CO₂ IFT at reservoir conditions with a pendant drop apparatus. We also report on CO₂ gravity drainage experiments with Spraberry and Berea whole core performed at reservoir conditions. The results indicate that given sufficient fracture density and containment of CO₂ in the pilot area, the pilot CO₂ injection will mobilize incremental reserves.

In effect, this document and the planned work in the upcoming Field Demonstration will eventually provide a “how to” manual outlining the essential ingredients to plan, study, design and implement water and gas injection strategies in naturally fractured reservoirs.

David S. Schechter
December 1996



Location of the Spraberry Trend Area Field, West Texas

ACKNOWLEDGMENTS

This work was financially supported by the United States Department of Energy and the following consortium of companies; Marathon Oil Co., Mobil Research and Development Corp., Mobil E&P USA, Parker and Parsley Petroleum Co., Petroglyph Operating Co., Texaco E&P Technology Dept. and The Wiser Oil Co. This support is gratefully acknowledged. In addition, we would like to recognize Exxon Co. USA for providing data from the Pembroke Unit and Geographix Inc. for donation of software used in reservoir characterization. I greatly appreciate diligent efforts from the following individuals who contributed to this project. Dr. Boyun Guo played a key role in development of the material reported in Section 2, parts of Section 3 and Section 4. Ashish Banik interpreted open-hole logs and developed the shaly-sand rock-log model reported in Section 1. Claudio Saleta and Martha Cather performed the geological and petrophysical work described in Section 1. Eli Kindem and Erwin Putra conducted the Humble waterflood pilot simulation. Hujun Li measured both imbibition curves and IFT reported in Section 4. Dr. John Lorenz from Sandia National Laboratory performed the fracture analysis reported in Section 5. Other acknowledgments go to Richard Baker of Epic Consulting Ltd., Steve Melzer and Loren Stiles of UTPB-CEED, Randy Miller of Reservoirs Inc. and Lincoln Elkins. Finally, I would like to personally recognize Paul McDonald, project manager from Parker and Parsley, for his steadfast guidance and attention to detail and Tom Sheffield of Parker and Parsley Petroleum Co. for providing New Mexico Tech's Petroleum Recovery Research Center a wealth of data from the Spraberry Trend Area.

I. INTRODUCTION

The objective of the Spraberry CO₂ pilot project is to determine the technical and economic feasibility of continuous CO₂ injection in the naturally fractured reservoirs of the Spraberry Trend. In order to describe, understand, and model CO₂ flooding in the naturally fractured Spraberry reservoirs, characterization of the fracture system is a *must*. The reservoir characterization was based on core and log data analyses in the first year of the project. A rock model for describing the Spraberry Trend Shaly Sands has been identified and established. A better method for identifying Spraberry pay zones has been developed.

Characterization of the crude oil/brine/rock interaction in the Spraberry matrix has been carried out based on results of laboratory experiments. Initial water saturation and historical water saturation in the Spraberry sands was determined to be between 0.2 and 0.4 depending upon rock permeability. Macroscopic displacement efficiency during water imbibition has been estimated to be about 50%. Wettability of the Spraberry sands has been determined to be weakly water wet. Water-oil capillary pressure has been established. The experimental capillary pressure curve confirms the rock wettability determined based on imbibition test. Interfacial tension (IFT) between Spraberry oil and brine has been measured to be 36 mN/m. Experimental results have been used in analytical and numerical reservoir simulations. In order to fully understand the behavior of the naturally fractured Spraberry reservoirs, the results of the characterization of matrix, fracture, and fluids have been employed in reservoir performance analyses. Scaling of imbibition oil recovery results to reservoir geometry indicates that higher oil recovery should have been achieved during water flooding, although the Spraberry sands are weakly water wet. Inflow performance of Spraberry Trend wells has been analyzed using a new mathematical model developed for wells intersecting long fractures. Computer simulation of a Spraberry Trend reservoir has been conducted. The overall goal of this project is to enhance the prospects for miscible CO₂ flooding the naturally fractured Spraberry oil reservoirs. The efficiency of CO₂ gravity drainage was investigated based on laboratory experiments. Minimum Miscibility Pressure (MMP) was measured to be 1,550 psig. IFT of the CO₂/Spraberry oil under reservoir conditions was determined. The IFT at the MMP is about 1.5 mN/m. CO₂ gravity drainage experiments were carried out using Spraberry oil and whole cores. Experimental data were matched by a newly developed mathematical model.

In summary, we have gained significant understanding of the naturally fractured Spraberry Trend reservoirs through this study. The weakly-wet Spraberry sands should be partially responsible for the low performance of water flooding in the Spraberry Trend reservoirs. Result of oil recovery from a low permeability Spraberry core during CO₂ gravity drainage experiment is promising. This result indicates a good potential of CO₂ flooding in the Spraberry Trend reservoirs.

II. TECHNICAL PROGRESS

1. RESERVOIR CHARACTERIZATION

1.1 Geological Characterization of the Spraberry Formation

Introduction

Spraberry reservoirs are typically low porosity, low permeability fine sandstones and siltstones that are interbedded with shaly non-reservoir rocks. Large scale geological characterization of Spraberry reservoirs has in general been limited to definition of reservoir targets based primarily on the shape and strength of the gamma ray response (GR).¹ Some information has been published on lithology and reservoir heterogeneity,² but there has been very limited work performed concerning detailed description and understanding of individual reservoirs and units within the Spraberry. Basing reservoir models primarily on gamma response has several drawbacks: different amounts and types of clays emit different levels of radioactivity, distortion in GR response can be caused by the presence of potassium feldspar, micas, and accessory minerals like rutile and zircon, and, GR curves provide little information on the presence of porosity-occluding authigenic minerals like calcite and quartz. Therefore, one can either erroneously assume that all high gamma response units are poor quality reservoirs, or that all low gamma responses correspond to clean sandstone, when neither may be true. To accurately define relationships between lithology, reservoir quality, and log response, various techniques were used to examine the Spraberry Trend Area reservoir and non-reservoir rocks.

During the first year, most work has been directed at understanding the vertical heterogeneity of lithofacies. Cores from three Upper Spraberry wells were evaluated by various techniques including X-ray diffraction (XRD) analysis, Scanning Electron Microscopy (SEM), petrographic analysis, detailed minipermeameter analysis, and log evaluation. The three main wells that have been used as a sources of information for geological characterization are the Arthur Judkins A#5, the Shackelford 1-38A, and the E.T. O'Daniel #37.

Core Analysis

Detailed lithologic studies of cores were performed using a variety of techniques. Petrographic thin sections were cut from cores from three wells. An attempt was made to obtain representative material from all the various lithologies, however most of the thin sections were made from the reservoir portions of the Spraberry 1U unit. Point counts were made from most thin sections to assess framework and cement mineralogy. Diagenetic features were described. Additional detailed analysis of certain portions of the core were made by XRD and SEM analysis. XRD was done to determine clay mineralogy and the relative proportions of clay minerals within the various rock types, also to identify

fracture-filling minerals. Scanning electron microscopy was used to examine pore structure and also to perform qualitative identification of various mineral phases. Minipermeameter measurements were performed using a close spacing of half to one inch separation between measurements. This close spacing of measurements allowed for observation of permeability variability at small scales, as well as creating relatively long sequences of measurements in a log profile type showing larger scale behavior that is easily correlated with wireline logs. An analysis of the relationship between log behavior and reservoir quality is presented, using supporting evidence from the core analysis.

Results

Figures 1.1 through 1.5 present a series of log profiles for the petrographic data, minipermeameter measurements, and gamma ray logs from the Shackelford 1-38A core that cover the 1U unit (7083-7093 ft) of the Upper Spraberry. Also included are cross-plots for some petrographic data showing the principal quality controls on porosity. Figure 1.1 shows log tracks of permeability, porosity, and the gamma ray log. It can be seen that there is a reasonably close relationship between the porosity and the gamma ray curve, however not everywhere does the high gamma ray (usually corresponding to high clay content) correspond to a low porosity. The same can be seen from a permeability/gamma ray plot. The two arrows in the porosity plot point to depths that, by gamma ray curve interpretation alone, would be probably considered to be an oil saturated sand unit. A look at porosity logs shows that these zones are also low porosity and should not be included in net pay calculations.

By examination of log profiles of various components, it is possible to determine lithologic variations that correlate to the gamma ray response. Figure 1.2 shows a log of porosity, gamma ray response, and percent clay (determined by point count). High gamma ray values, in general, correspond to high percentages of clay. Especially in tracking the sandy ten feet of the 1U unit (7083-7093 ft) along each log, it is noticeable that the sections with lowest amounts of clay have the highest overall porosities of the 1U. The two sand peaks and the high GR of the shale layer in between are easily correlated to the clay content derived from petrographic data and the minipermeameter measurements. However, at 7076 feet, there is a GR low that corresponds to a region of lower porosity. In Figure 1.3, it can be seen that a high percentage of carbonate cement is completely occluding the porosity of this layer. Figure 1.4 combines both the carbonate and clay matrix. As can be seen, the log track of the combined totals of percent clay and carbonate very closely parallel the track of porosity with depth.

Figure 1.5 shows a comparison of the relative contributions of percent clay matrix and percent carbonate cement to the overall reservoir porosity degradation. It can be seen that there is a reasonably well defined trend of increasing clay and decreasing porosity. The contribution of carbonate cement is less obvious, but it is clear that rocks with a high proportion of carbonate cement usually have low porosities and indeed there are a few layers within the 1U that are almost entirely carbonate. Gamma logs alone will not provide enough

information to define these zones, and additional logs are necessary in order to delineate the best reservoir rocks within the Spraberry. Data from core analysis agree well with the log analysis presented in the following section. If effective porosity is plotted against shale volume, it is found that there are three basic groups of rock in the Upper Spraberry: one with porosity <7% and shale volume >15% (mostly mudstones and siltstones), one with porosity <7% and shale volume <15% (dolostones and dolomitic siltstones), and the reservoir pay zones that have shale volume of <15% and porosity >7%. Additionally, log and core analysis demonstrates that the best pay zone targets are most probably those that show considerable thickness, good porosities and a low GR response. Thin layers showing very low GR values are very common within the stratigraphic column but these are not considered to be significant contributors to overall reservoir quality because of their relatively insignificant volume and the fact that many of the low gamma ray zones are also low porosity carbonate-rich layers.

Diagenesis

Detailed petrographic analysis of diagenetic events has not yet been completed. Preliminary results showing results of XRD investigations on clay mineralogy are presented here.

Clay Diagenesis

Hoffman and Hower³ proposed a time-temperature model for illitization of smectite with increase of depth. Such models have been found applicable to other geologic and petroleum studies of sedimentary rocks and basins of Miocene age or older,^{4,5} thus should apply to the Permian-aged Spraberry. In a previous study of the Spraberry Formation, Houde⁶ mentioned that XRD analysis of rocks contained primarily illite and kaolinite. Part of Houde's investigation is a very complete study on source bed geochemistry of the shales in the Spraberry Formation. In this work, Houde calculated temperatures from the present geothermal gradient of the area, which indicate that the minimum temperature at which the Spraberry was exposed is at least 63°C and could be as much as approximately 77°C near the base of the core studied. His kerogen coloration data agrees well with the previous geothermal gradient calculated temperatures, which showed that the Spraberry was exposed to temperature ranges at which initial generation of oil should begin. The temperature information suggests that the potassic clays in the Spraberry Formation should have compositions smectite to randomly-ordered mixed illite/smectite (R=0 (I/S)) region, assuming that clay behavior is similar to Gulf Coast models of smectite diagenesis.⁷

In the present study, however, clay assemblages (Table 1.1) show very small amounts of smectite and illite/smectite mixed layer (typical of the ordering range mentioned above) clays. Instead illite and chlorite are more abundant. These results are supported by additional XRD data from Reservoirs Inc. for the E.T. O'Daniel # 37 and Shackelford # 1-38A wells, and suggest that perhaps Spraberry clays may have been exposed to higher burial temperatures than previously believed. There are several alternate explanations. Smectite

may have been relatively insignificant in abundance in the original detrital sediments. Additionally, brine chemistry and pressure are also important controls on clay diagenesis and can accelerate or slow various reactions. Without a more complete study of polytypes assemblages and clay mineralogy data from younger and older rocks within the stratigraphic sequence as well as age equivalent rocks of different burial depths, it is difficult to interpret properly clay mineralogy data.

Some lines of evidence do relate the clay mineralogy of this formation to diagenetic alteration of smectitic detrital clays with increase with burial depth and temperature. First, the geological setting of a basin fill rich in argillaceous material and organic matter is a common setting for highly smectitic clays.⁸ Second, there is a significant amount of partially dissolved or altered K-feldspar to provide a source of potassium necessary to drive the reaction of smectite to illite. This reaction in turn liberates a number of cations such as Si, Mg, Ca, and Fe. The assemblage of diagenetic minerals within the Spraberry rocks examined (to be discussed in more detail in future reports) includes quartz, dolomite, and ferroan dolomite. These cements could easily be byproducts of the smectite/illite conversion. Also, organic matter present might be associated with the production of acidic fluids and CO₂ that in turn are responsible for widespread dissolution of grains and cements (secondary porosity enhancement). Although the temperatures found⁹ are considered good enough for a first stage of ordering polytypes (smectite-to-R=0 I/S) (based on Hoffman and Hower model³), the assemblages of clays found in our study with dominant amounts of illite and chlorites and absence of good amounts of expandable layers, resembles better the higher temperature polytypes. This ambiguity could be solved by pursuing XRD analysis of unoriented samples, and sample examination of younger and older strata.

Fracture Diagenesis

Study of the diagenesis of natural fractures can provide useful information about the timing of natural fractures, as well as something of the nature of the fluids and relationships to cements in the matrix rock. Fractures within the Spraberry Formation are both mineralized and unmineralized; to date, two samples of mineralized fractures have been examined petrographically, as well as two unmineralized fractures.

Paragenesis of a large (>1 mm wide) mineralized fracture, recovered from a depth of 7088 feet in Shackelford # 1-38A consists of the following sequence:

After fracturing, a thin layer of minerals was precipitated on fracture walls. This layer consisted of quartz and dolomite in subequal proportions, with dolomite being more abundant. The minerals were precipitated into void space, as evidenced by the presence of many euhedral crystal faces and terminations, only possible where minerals are growing into unoccupied (or fluid-filled) space. This early generation of mineralization utilized the grains of the matrix as nucleation sites, quartz growing on detrital quartz grains and dolomite growing on detrital and authigenic dolomite within the matrix. When examined by UV

fluorescent light microscopy, it is clear that there are at least two generations of dolomite cement within the sample aside from the original detrital carbonate grains; one generation (the first) has a brownish fluorescence while the second generation does not fluoresce. It is nonfluorescing dolomite that forms one of the early fracture cements, whereas fluorescing dolomite comprises a significant proportion of the dolomite in some thin sections. The early fracture mineralization only comprises a layer about one crystal thick within this fracture.

The bulk of the mineralized fracture is comprised of the mineral barite ($\text{Ba}(\text{SO})_4$), a common fracture-filling mineral. The barite may possibly have replaced precursor quartz and dolomite, there are inclusions of both minerals within the fracture. As well as inclusions of these minerals, the barite contains numerous 2-phase fluid inclusions (liquid and vapor phase). In one area of the thin section, a fourth mineral phase is present as a surface lining on the barite crystals. This is a very fine-grained, highly birefringent material. It may be very finely crystalline dolomite, anhydrite, clay (unlikely), or possibly even some kind of drilling mud; it is too fine-grained to be identified with certainty through standard petrographic microscopy. The smooth, draping quality of this coating indicates possible deposition from a liquid (as opposed to growth as a crystal), and it could possibly be some component of the drilling mud.

A second thin section from Sun Oil Co. Hutchinson #7 contained several hairline fractures that were both mineralized and unmineralized. The mineralization in the fractures appears to be exclusively nonfluorescing carbonate, possibly dolomite, and no barite was seen. This thin section contained numerous fossil echinoderm fragments which may have been a source of Ca for fracture mineralization. The unmineralized fracture terminated against the mineralized one, suggesting formation at a later period. More fractures will need to be examined before any significant conclusions can be drawn concerning fracture timing, sources of cementation, and relationships between mineralized and unmineralized fractures and lithology.

Fracture Model

Reasons for fracturing may be varied, but one possible model is that fracturing was caused by overpressuring. The gradual increase in burial depth produced an increase in compaction, pressure, and temperature. The Spraberry Formation is dominantly fine clay material with minor amounts of fine sands and siltstones, a typical lithologic environment for production of significant overpressuring. Clay sediments mixed with organic matter are characterized by having the highest initial porosity. Burial compaction and diagenesis of this material usually results in almost total destruction of porosity within the clay sediments accompanied by a tremendous loss of fluids. At the same time the principal vertical stresses are being increased by burial, the pore pressure mainly within the sandy, less porous and more competent layers of the formation are increasing because of migration of a large volume fluid derived from shale dewatering and possible diagenesis. These conditions probably caused the necessary reduction of principal effective stresses to a level where enough unconfinement⁷ is created to

give way to fracturing. Pressure solution features, typical of overpressured sands, have been found during petrographic analysis. Also, matrix free sandy siltstones and very fine sandstones show the effect of compaction and grains show both flat and concave-convex contacts.

References

1. Tyler, N., and Gholston, J.C.: "Heterogeneous Deep-Sea Fan Reservoir, Shackelford and Preston Waterflood Units, Spraberry Trend, West Texas," Report of Investigation No. 171, Bureau of Economic Geology, The University of Texas, Austin, 1988.
2. Guevara, E.H.: "Geological Characterization of Permian Submarine Fan Reservoirs of the Driver Waterflood Unit, Spraberry Trend, West Texas," Report of Investigation No. 172, Bureau of Economic Geology, The University of Texas, Austin, 1988.
3. Hoffman, J. and Hower, J., 1979. Clay mineral assemblages as low grade metamorphic geothermometers: application to the thrust faulted disturbed belt of Montana, U.S.A., in: Scholle, P. A. and Schluger, P.R. (eds.) Aspects of Diagenesis. SEPM Special Publication No. 26, p. 55-79.
4. Pollastro, R. M., 1989, Clay Minerals as Geothermometers and Indicators of Thermal Maturity--Application to Basin History and Hydrocarbon Generation, AAPG Bull., v. 73, No. 9, p. 1171.
5. Lanson, B., Champion, D, 1997, The I/S-To-Illite Reaction in the Late Stage Diagenesis, Am. J. Sci., Vol 291, p. 473-506.
6. Houde, R.F., 1979: Sedimentology, diagenesis, and source bed geochemistry of the Spraberry sandstone, subsurface Midland basin, west Texas. Unpub. MS thesis, U. Texas Dallas.
7. Boles, J., and Franks, S., 1979: Clay diagenesis in Wilcox sandstones of southwest Texas: implications of smectite diagenesis on sandstone cementation: J. Sed. Petrol. v. 49, p. 55-70.
8. Eslinger, E. and Pevear, D., 1988: Clay Minerals: SEPM Short Course Notes No. 22., SEPM, Tulsa OK.
9. Lorenz, J.C., Teufel, L. W. and Warpinski, N.R., 1991: Regional fractures 1: A mechanism for the formation of regional fractures at depth in flat-lying reservoirs. AAPG Bull, V. 75, no. 11, p. 1714-1737.

Table 1.1. XRD Analysis, Parts in 10

Depth (ft)	illite	chlorite	kaolinite
7069.4	4	1	1
7081.6	2	1	1
7082.6	2	1	1
7083.5	3	2	1
7085.7	2	1	---
7087.4	4	1	1
7090.6	3	1	---
7092.1	3	1	---

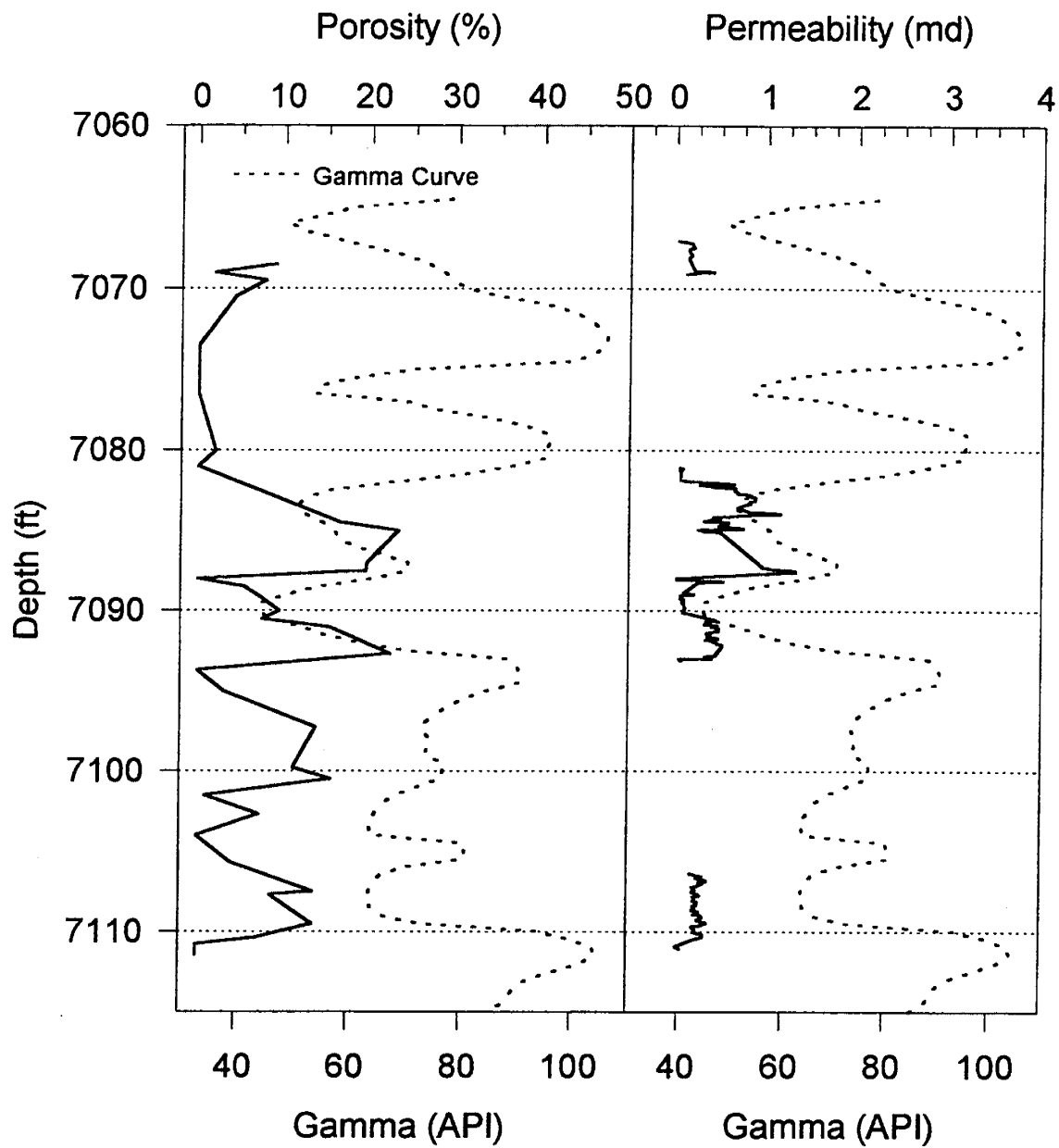


Fig. 1.1. Log tracks of permeability, porosity, and the gamma ray. 1U pay sand occurs from 7082-7092 ft.

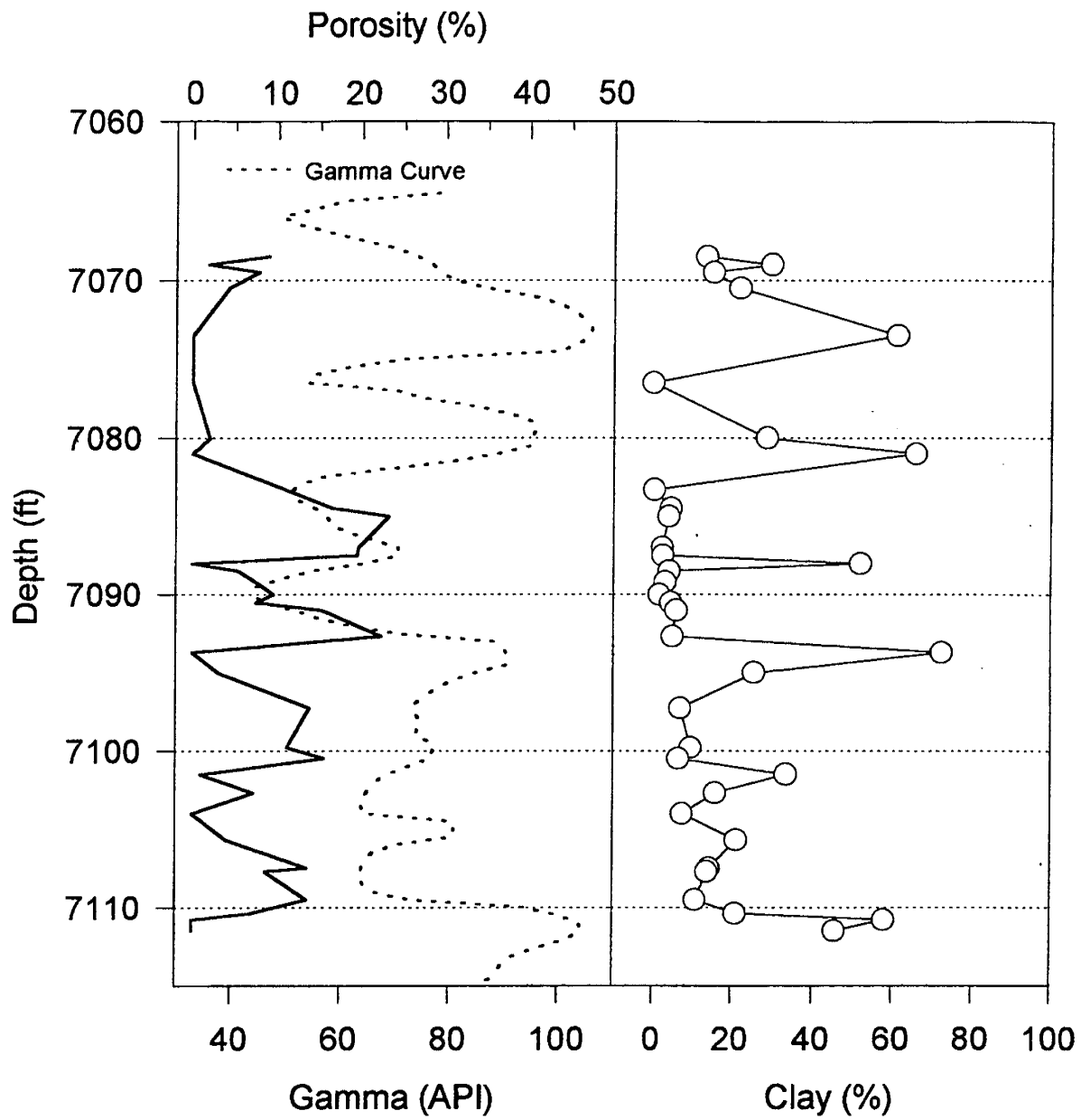


Fig. 1.2. Logs of porosity, gamma ray response, and percent clay (determined by point count)

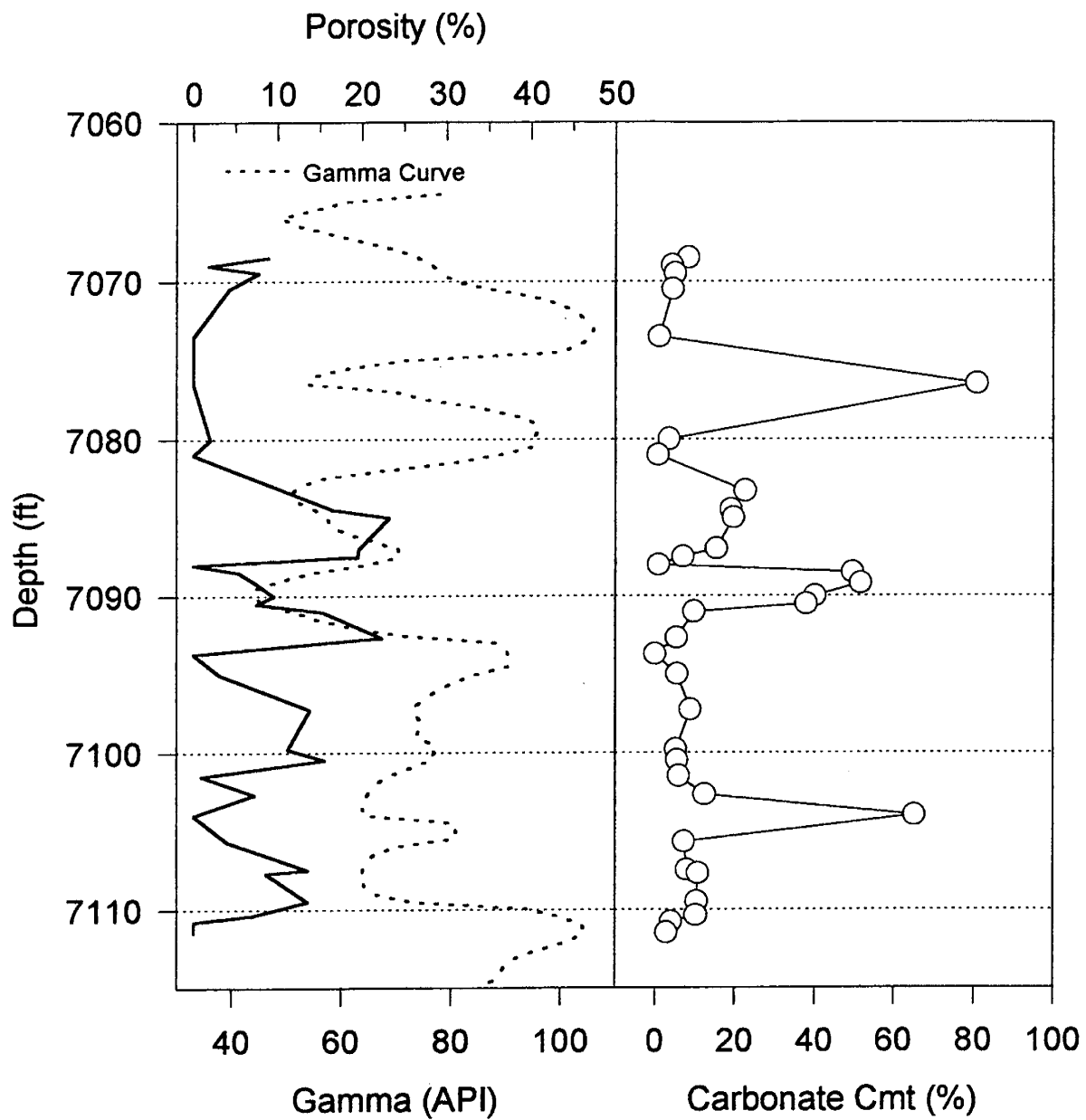


Fig. 1.3. A high percentage of carbonate cement is completely occluding the porosity at a depth of 7076 ft even though gamma-ray response indicates sandstone pay.

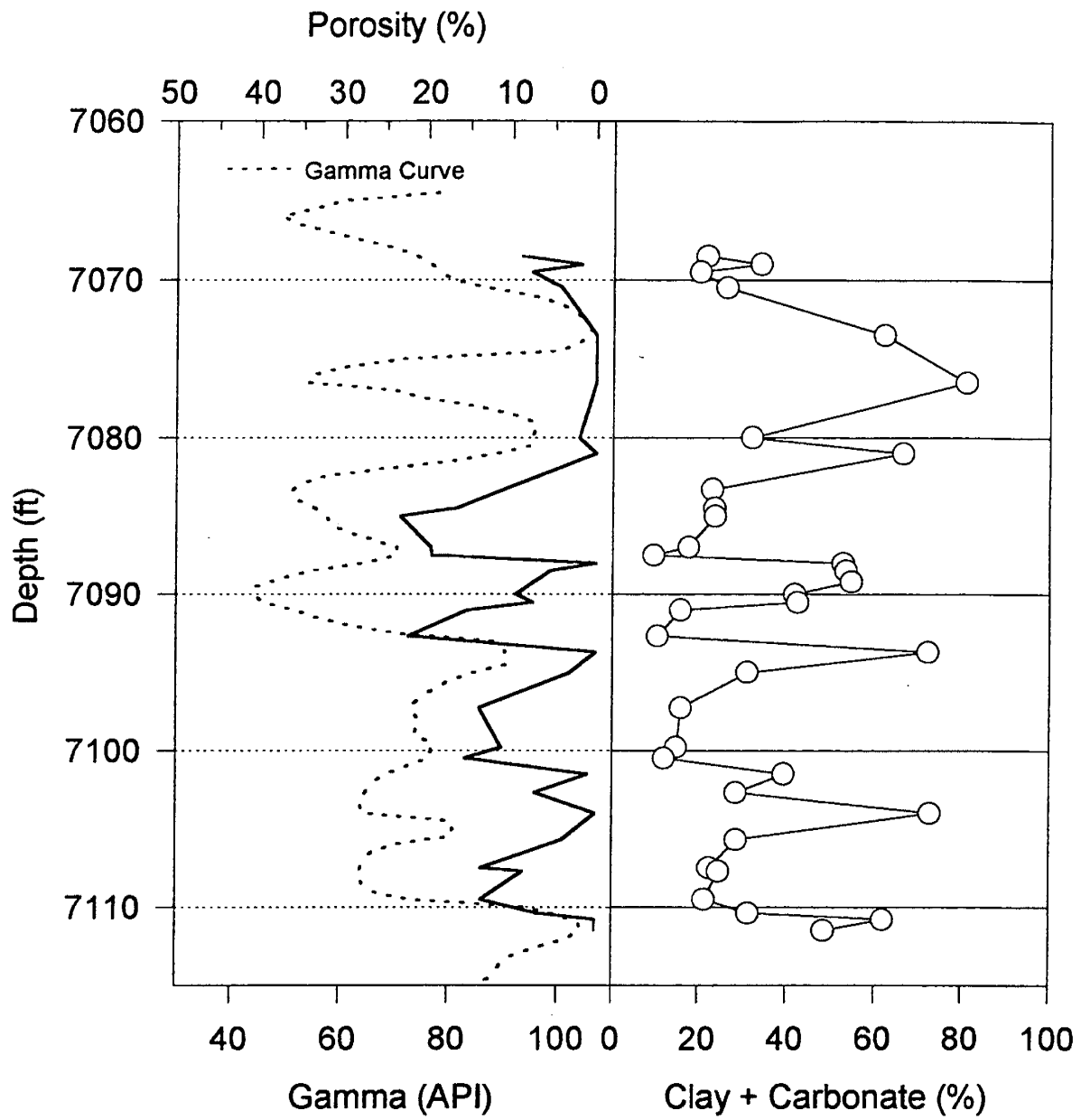


Fig. 1.4. Combination of the carbonate and clay matrix

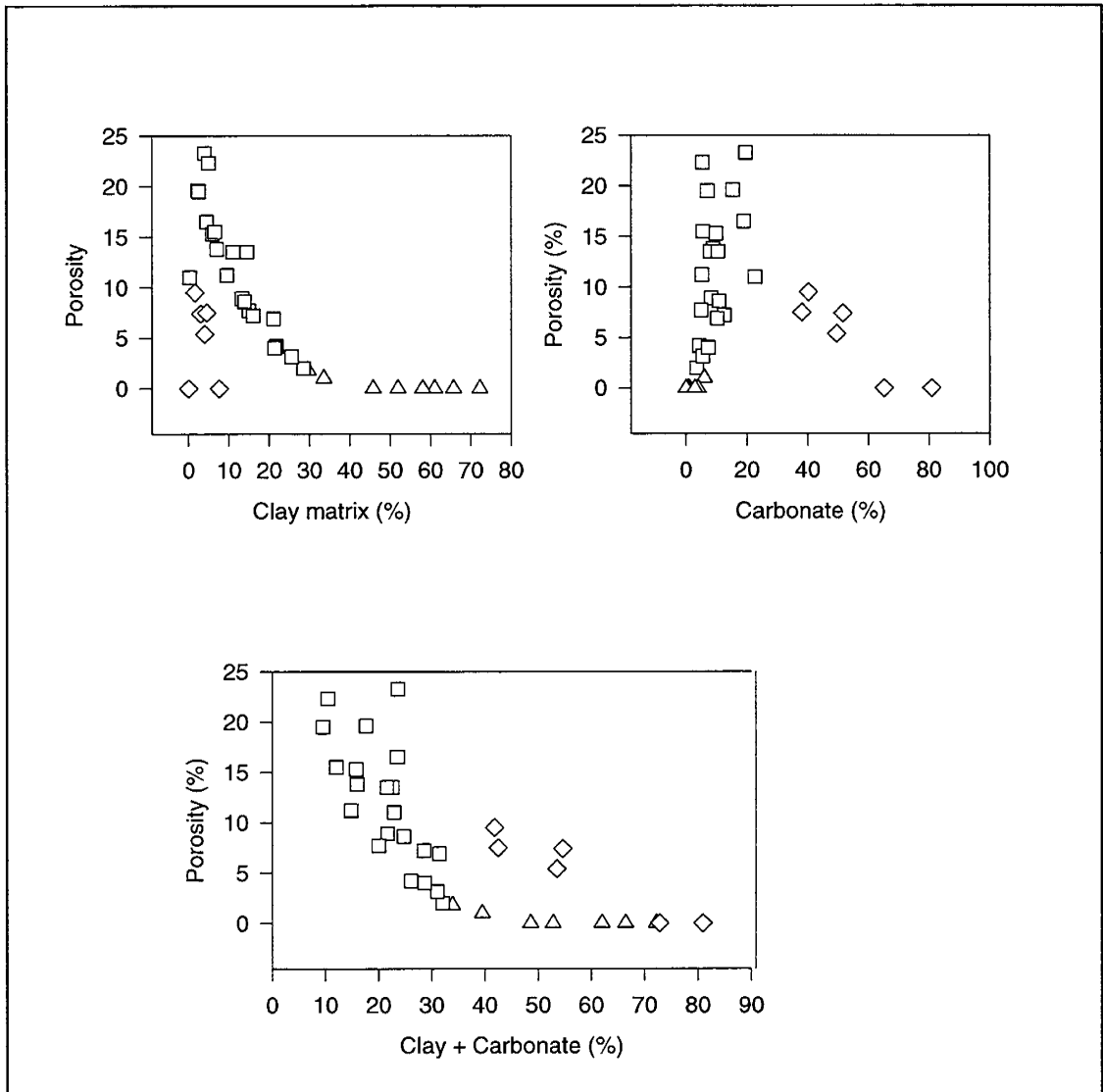


Fig. 1.5. A comparison of the relative contributions of percent clay matrix and percent carbonate cement to the overall reservoir porosity degradation.

1.2 Core-Log Integration for Characterization of the Spraberry Trend Shaly Sands

Abstract

In this section, Spraberry Trend Area reservoirs have been characterized with emphasis on identification of oil-bearing sands based on core-log correlation. Integration of extensive geological and petrophysical data presented in the previous section into a modern shaly-sand log interpretation model has been performed to characterize the Spraberry Trend. Quantitative cut-off criteria based on core-log integration was developed which allows log based identification of thin, oil-bearing intervals suitable for hydraulic fracture treatment. The Archie parameters (a , m , and n) have been derived from core data to improve log-derived water saturation. Core-derived porosity and water saturation have been compared with log-derived values for the purpose of identification of oil-bearing intervals. We present a log based rock model which distinguishes pay and non-pay zones. This allows definition of true net pay throughout the Trend regardless of depositional environment. The results from this investigation provide recommendations for logging suites that will allow a better description of thin pay sands which characterize the Spraberry Trend throughout the Midland Basin. The methodology developed may be used primarily to understand the areal extent and pinch-off of productive intervals and the water saturation within the pay intervals.

Introduction

The tremendous areal coverage and large amount of remaining oil warrant further investigation to expend all possible process options before large numbers of Spraberry wellbores need to be plugged and abandoned (Schechter *et al*^{1,2}). Identification and mapping of the thin pay zones that comprise Spraberry Trend pay is an important first step when considering any IOR process in the future.

Mardock & Myers¹⁴ and Lytle & Ricke¹⁵ first published techniques for evaluating the Spraberry Trend using radioactive and induction logs. These efforts provided reasonable results for distinguishing lithologies. However, quantitative analysis was not possible at that time. Since then, many interpretative techniques have been developed. Fairly recent studies of the Spraberry Trend were carried out by Tyler & Gholston¹⁸ and Guevara¹⁹. These studies attempted to ascertain the distribution of the sedimentologic attributes of Spraberry Trend by analysis of the shape and magnitude of the gamma ray log. Quantitative shaly-sand log interpretation and core-log integration was not presented. Several authors^{7, 20} provide a qualitative geological characterization of the Spraberry Trend depositional sequences, however no quantitative log analysis is available to map these sequences, especially the thin, oil-bearing pay zones.

On a lease basis, the pay sands are relatively easy to recognize yet correlation of pay sands throughout the Trend has not been attempted. Thousands of wells have been completed in the Spraberry Trend Area in the last 45 years. The logs run in many of these wells are old, cased-hole gamma-ray, sometimes with a porosity log and in many cases, a porosity log may not be available. We therefore need to develop methodology whereby pay zones can be distinguished in areas where 1) no core is available, 2) a porosity log may or may not be available and 3) perhaps the only log available might be vintage, cased-hole gamma-ray.

In this investigation, we demonstrate the applicability of modern shaly-sand log analysis in determining net pay as observed in three recent core wells discussed in Section 1.1. We recommend a logging suite which provides the most reliable technique for net pay determination. This investigation will clearly show that true reservoir rock (primarily massive/clean siltstone) in the Spraberry Trend Area cannot be identified by gamma-ray response alone. We also provide the methodology to convert old cased-hole gamma-ray logs into porosity logs. Good agreement is demonstrated between generated porosity logs and actual porosity logs. Finally a rock-model is presented which identifies essentially three rock types:

- Rock Type A - massive, clean siltstone, low clay and dolomite content and strongly fluorescent, low water saturation
- Rock Type B - low clay, high dolomitic content with weak or no fluorescence and high water saturation, and
- Rock Type C - muddy clay rich zones that do not fluoresce.

The methodology presented provides the basis for mapping the extent, thinning and pinch-off of Rock Type A pay intervals throughout the Midland Basin for Upper Spraberry, Lower Spraberry (Jo-Mill) or Dean reservoirs. The methodology used in this investigation integrates the following data: ultraviolet photographs of whole core, thin-section analysis, minipermeameter measurements, whole core analysis, open and cased-hole logs.

Archie Parameter a , m , and n

Log interpretation models are sensitive to the uncertainty in both m and n . m and n are usually derived from core data. It was reported that the Archie parameter a is a weak-fitting parameter with no physical significance and can generally be set to unity (Maute *et al*²²). According to Aguilera²⁸, m should be relatively small (ranging from about 1.1 to 1.3) for naturally fractured systems. m and n values were derived from Spraberry core data. Based on our analysis (Banik & Schechter^{5,6}), we found that the value of m is 1.35 for the upper pay zone, 2.49 for the upper non-pay zones, 1.10 for the lower pay zones, 2.22 for the lower non-pay zones and 2.41 for the Dean zones. Similarly, the value of n is 1.74 for the lower pay zones, and 1.15 for the lower non-pay zones. Therefore overall m and n values for the Spraberry Trend Area are 1.66 and 1.46.

Core Analysis

Upper Spraberry core from the Shackelford 1-38A, Judkins "A" No. 5 and the first DOE pilot well the E.T.O'Daniel # 37 were available for this investigation. The cores were examined to determine gross lithologic properties and to correlate core properties with the wireline response in addition to development of a rock model. Thin-sections were made to determine the distribution of microscopically visible porosity and for investigation of diagenesis, cementation etc., as reported in Section 1.1. Porosity, water saturation and permeability were obtained from whole core analysis⁸. Permeability distribution in the main pay was measured by minipermeametry and found to correlate well with whole core analysis. Minipermeameter measurement of the entire pay zone indicated that the matrix by itself is relatively homogeneous, usually in the range of 0.1 to 1.0 md. The two main pay zones 1U & 5U (each is approximately 8-15 ft in thickness separated by 150 ft. of non-pay) were clearly identified by oil fluorescence and are indicated in the log shown in Fig. 1.7.

Core-Log Integration

Effective water saturation and effective porosity were calculated from shaly-sand log interpretation using both conventional m & n ($m=2$ & $n=2$) and core derived m & n ($m=1.66$ & $n=1.46$). It has been observed that conventional m & n values overestimate the water saturation, whereas water saturation calculated using core derived m & n values shows good agreement with core measured water saturation (Fig. 1.6). It has also been observed that for the Spraberry Trend, the Automatic Compensation Method (ACM)⁹ and the Fertl²⁹ method of shaly-sand interpretation performs better than the Dual water method³⁰. Effective water saturation calculated from the Dual Water method is much higher than the effective water saturation calculated from the ACM and the Fertl method.

Shaly-Sand Log Interpretation

Volume of shale was calculated from gamma-ray logs using the Larionov non-linear relationship⁹. The result was compared with ultraviolet observation of fluorescing intervals. The fluorescent intervals show a clear distinction between oil bearing sand and muddy zones containing no oil due to sharp contrast seen at the interface between these lithologies. Effective porosity was calculated from log data, and was cross-plotted along with volume of shale on a modified shaly-sand producibility chart to determine if the volume of shale is high enough to drastically reduce producibility. Based on fluorescing intervals observed in the core along with the modified shaly-sand producibility chart, we contend that shale volume less than 15% and effective porosity greater than 7% provide accurate cut-off criteria for identification of fluorescing intervals in Spraberry Trend Area reservoirs. Thin-section analysis confirms the cut-off criteria by observation of visible porosity in oil bearing intervals whereas no visible porosity is observed in the non-pay muddy zones.

Identification of the Pay Zones

We previously demonstrated^{5,6} that classic shaly-sand analysis could accurately quantify thin fractured pay zones which characterize the Spraberry Trend. The acquisition of core data reaffirmed our analysis that Upper Spraberry net pay consists of two primary, thin (8-15 ft) pay zones, the 1U and 5U. We mentioned previously that sharp contrast is observed by fluorescence between shales containing no oil and the 1U and 5U pay zones. The 1U and 5U pay zones are easily identified by integrating whole core analysis and open-hole logs into a calibrated shaly-sand model. However, there is inconsistency with the 2U, 3U and 4U zones shown in Fig. 1.7 through Fig. 1.10. Gamma-ray cut-off criteria indicate these zones are pay, yet core data demonstrates these zones are not pay. To resolve this dilemma, volume of shale was correlated with neutron-density, sonic and bulk-density porosity logs. It has been observed that the porosity of the 2U, 3U and 4U zones which have low gamma-ray response, is less than 7%. Thin-section point counts presented in Section 1.1 indicates a large concentration of dolomite in these zones. Thin section analysis also reveals that the porosity of the 2U, 3U and 4U zones is drastically reduced due to dolomitic cement, thus effectively rendering these zones as non-pay. A closer look at porosity logs is necessary to distinguish low gamma-ray zones which are oil saturated and those zones which contain no oil.

Effective Porosity from Different Log Suites

Thin section results indicated the necessity of refining porosity cut-off. Different porosity logs (both open-hole and cased-hole) have been investigated to confirm the above mentioned cut-off criteria for identification of the pay zones. Sonic, bulk-density and neutron-density cross-plot porosity along with gamma ray log were utilized in this study to isolate and differentiate pay and non-pay zones that demonstrate similar gamma ray response.

Open-Hole Logs

The E.T. O'Daniel lease consists of 2,100 acres in the middle of the Spraberry Trend Area. This relatively small lease is the site for the pilot CO₂ project. Fig. 1.7 is an example of open-hole log from the E.T. O'Daniel #37 (Upper Spraberry). Fig. 1.7 shows shale volume derived from gamma ray response using the non-linear Larionov relationship (Asquith⁹). Fig. 1.7 also shows neutron, density and bulk-density porosity logs along with the neutron-density cross-plot porosity. The effective porosity derived from the neutron-density cross-plot clearly identified 1U and 5U pay zones having porosity >7%, whereas the 2U, 3U, 4U zones which have low amounts of clay and porosity less than 7% due to dolomitic cement. This result correlates well with point count data presented in Fig. 1.3.

Fig. 1.8 is an example of an open-hole log from the E.T. O'Daniel # 26 (Upper Spraberry). Fig. 1.8 shows the gamma-ray and volume of shale as was seen in Fig. 1.7. A bulk-density log was run in this well. Bulk-density clearly indicates much greater density in the 2U, 3U and 4U zones than in the 1U and 5U zones. Matrix density for sandstones and quartzites is

2.65, for limey-sands or sandy-limes is 2.68, for limestone 2.71 and for dolomites 2.87 (Dewan¹⁰). Higher bulk-density indicates lower porosity. Effective porosity, calculated from bulk-density accurately distinguishes between the 1U and 5U pay zones with porosity >7% and the 2U, 3U and 4U zones with porosity <7%. Fig. 1.8 also shows reduction of caliper log in the 1U and 5U pay zones whereas there are no changes are evident in the caliper log for the 2U, 3U and 4U non-pay zones. This indicates borehole diameter is reduced due to mudcake buildup. The presence of mudcake itself is proof of the presence of permeability in the 1U and 5U pay-zones. Mud losses are generally observed in the 1U and 5U pay zones. This observation correlates with the observation that natural fractures tend to occur in the pay zones and terminate at gradual or sharp non-pay contacts. This suggests that natural fractures tend to be concentrated in the pay zones. Mudcake is likely to accumulate within the fractures. Fracture indications may be obtained from the density correction curve¹¹. Since the density correction curve corrects the density log for effects of rough borehole and mud cake, the density correction curve may be affected by mud in the fractures and indicate a correction in the 1U and 5U pay-zones, which tends to confirm the presence of open fractures in the 1U and 5U pay zones (Fig. 1.8).

Fig. 1.9 is an example of an open-hole log from the E.T. O'Daniel # 28 (Upper Spraberry). This log suite consists of gamma ray and sonic transit time. Volume of shale was derived from gamma ray log as before and porosity was derived from sonic transit time. Sonic transit time in the 2U, 3U and 4U is lower than in the 1U and 5U pay zones. Lower transit time indicates lower porosity. Sonic transit time is 1) 54 $\mu\text{sec}/\text{ft}$ for sandstone, 2) 49 $\mu\text{sec}/\text{ft}$ for limestone and 3) 44 $\mu\text{sec}/\text{ft}$ for dolomite (Dewan¹⁰). Effective porosity calculated from sonic transit time also indicates high porosity (>7%) in the 1U and 5U pay zones and low porosity (<7%) in the 2U, 3U and 4U non-pay zones. Thus effective porosity cut-off of 7% accurately differentiate 1U and 5U pay zones from 2U, 3U and 4U non-pay zones.

Porosity Generation from Gamma Ray Log

We have shown that sandstone zones with low gamma-ray response and high percentage of carbonate cement can be distinguished from pay by effective porosity derived from 1) neutron-density cross-plots, 2) bulk-density log, and 3) sonic transit time log. However, it is possible that only old cased-hole gamma ray logs might be available. But for accurate log-based identification of pay zones, the minimum requirement is a gamma ray log and any porosity log. So we made an attempt to generate porosity logs from gamma ray logs using established cut-off criteria as presented in previous sections. Fig. 1.9 shows sonic transit time generated from the gamma ray log and is compared with the original sonic transit time log. Good agreement is observed between original sonic transit time log and the generated sonic transit time log from the gamma ray log.

Cased-Hole Log

Fig. 1.10 is an example of a cased-hole log from the O'Daniel "G" # 1. This log consists of gamma ray log and old neutron log (API). Fig. 1.10 shows that the neutron log accurately distinguishes the 1U and 5U pay zones from the 2U, 3U, and 4U non-pay zones. The neutron log shows high CPS (count per second) in the 2U, 3U and 4U non-pay zones. High neutron counts indicates low porosity.

Log Based Rock Model

A rock-log model⁴ has been developed to identify the highest quality pay intervals using available open-hole well log data. Volume of shale was cross-plotted against effective porosity in Fig. 1.11. Three general rock types have been identified, of which only one can be classified as pay. Rock Type A has volume of shale <15%, and porosity >7% with little dolomitic cement and strongly fluoresces. Rock Type B has volume of shale <15%, yet the porosity <7% and primarily occluded by dolomitic cement and may be weakly fluorescent. Rock Type C has volume of shale >15% and does not fluoresce. Rock Type A is the primary reservoir rock (1U and 5U) in the Upper Spraberry. This rock type consist of mainly massive/clean siltstone. This rock type fluoresces strongly under ultraviolet light, has high oil saturations and visible porosity is observed as seen in thin section photographs. Rock Type B has low volume of shale and low porosity occluded by dolomitic cement as shown in Fig. 1.11., and is considered non-pay (2U, 3U and 4U zones). This rock type mainly consist of siltstone and dolomite and fluoresces weakly relative to the 1U and 5U. Rock Type C is non-pay mudstones with high shale volume. Rock Type C does not fluoresce under ultraviolet light. The schematic representation of the log based rock model is given in the Table 1.2.

Potential for Fractured Zone Identification

Fig. 1.12 shows the effective porosity derived from neutron-density cross-plot and compared with core derived porosity for the DOE pilot well E.T.O'Daniel # 37 (Upper Spraberry). Comparison of core measured porosity with log derived porosity may be helpful in determining the zones that may be fractured in the reservoir. In this method, it is assumed that the core represents porosity in the matrix. The neutron-density cross-plot is assumed to read total porosity (both matrix and fracture). Consequently, the difference between the two porosity curves is interpreted as near wellbore fracture porosity. From Fig. 1.12, it is observed that, in the intervals 7230-7240, there are indications of fractures due to the separation of the core-measured and log-derived porosity curves. It is also observed from Fig.1.12 that for the interval 7230-7240, log derived water saturation (total water saturation) is higher than core-measured water saturation (matrix water saturation), which may indicate the presence of water-filled fractures. These intervals were confirmed to be fractured by analysis of the whole cores and a FMI log. However, this analysis does not distinguish

between drilling induced and natural fractures. Both coring induced and natural fractures were observed in the pay interval.

Conclusions

The success of shaly-sand analysis now provides quantitative methodology to map the thin pay sands that comprise the Spraberry Trend Area. This technique can be applied to the entire Trend to understand pinch-off and thinning of the sands near the fringe of the basin or channel sand development or disappearance. The following conclusions were reached based on a detailed investigation for identification of pay zones using core-log integration:

1. Volume of shale <15% and effective porosity >7% provides adequate cut-off criteria to identify and differentiate pay zones from non-pay zones.
2. Volume of shale is derived from gamma ray using the non-linear Larionov relationship and effective porosity can be derived from 1) neutron-density cross-plots, 2) bulk-density logs and, 3) sonic transit time, etc.
3. Porosity logs can be generated from cased hole gamma-ray logs where no porosity logs may be available.
4. In the E.T. O'Daniel area, the 1U and 5U are the pay zones in the Upper Spraberry.
5. The 2U, 3U and 4U, even though the gamma ray appears favorable, is composed of siltstone with dolomitic cement occluding the porosity thereby rendering these zones as non-pay.
6. Utilization of new values of m & n integrated with shaly-sand interpretation has proven effective for identification of thin fluorescing intervals and the water saturation within these intervals. The interpretation was confirmed by whole core analysis.
7. The Automatic Compensation Method and the Fertl method of shaly-sand analysis performs better than the Dual water method in the Spraberry Trend Area.
8. Porosity exponent m, separation between log-derived porosity and core-measured porosity, and separation between log-derived water saturation and core-measured water saturation may be a good fracture indicator for the Spraberry Trend.
9. The pay-zones are relatively homogeneous and composed predominantly of quartz and feldspar with some dolomite. Clay minerals are mostly illite.
10. The methodology presented allows basin-wide mapping of the thin, fractured siltstone intervals which are oil saturated.

Nomenclature

GR	= gamma ray log, API.
VSHL	= volume of shale.
CALI	= borehole caliper log, in.
RHOB, RHOZ	= bulk-density log, gm/cc.
DPHI, DPHZ	= density porosity log, pu.
INTT	= sonic transit time log, $\mu\text{sec}/\text{ft}$.
INTT (GR)	= sonic transit time log derived from the GR, $\mu\text{sec}/\text{ft}$.
NPHI	= neutron porosity log, pu.
PHIE	= effective porosity corrected for shale.
PHIEX	= effective porosity derived from the neutron-density cross-plots porosity.
BDPE	= effective porosity derived from the bulk-density logs.
NEUT	= old neutron logs, API.
<i>m</i>	= porosity exponent.
<i>n</i>	= saturation exponent.
<i>a</i>	= cementation factor.

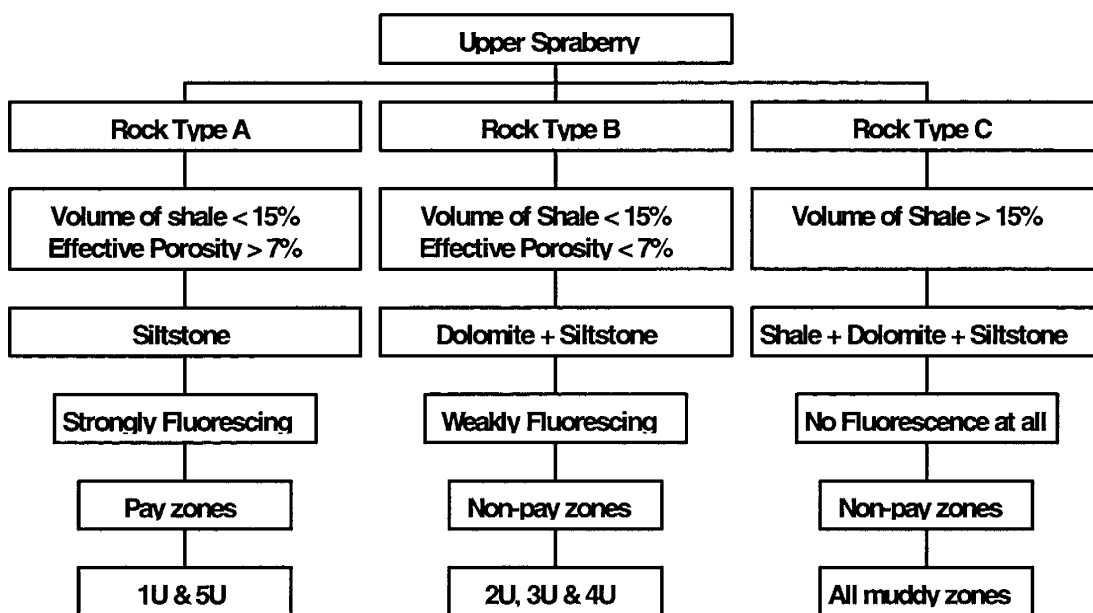
References

1. Schechter, D.S., McDonald, P., Sheffield, T., and Baker, R.: "Integration of Laboratory and Field Data for Development of a CO₂ Pilot in the Naturally Fractured Spraberry Reservoir," SPE 36657 presented at poster session of the 1996 SPE Annual Technical Conference and Exhibition, Denver, Colorado, 6-9 October 1996.
2. Schechter, D.S., McDonald, P., Sheffield, T., and Baker, R.: "Reservoir Characterization and CO₂ Pilot Design in the Naturally Fractured Spraberry Trend Area," paper SPE 35469 presented at the SPE Permian Basin Oil & Gas Recovery Conference, Midland, Texas, 27-29 March 1996.
3. Sheffield, T.D., McDonald, P., Schechter, D.S., Baker, R., and Teufel, L.: "CO₂ Pilot Design in the Naturally Fractured Spraberry Trend: Project Update and Spraberry Rock Model," paper presented at the Annual Convention of the American Association of Petroleum Geologists, May 19-22, 1996.
4. Schechter, D.S., and Banik, A.K.: "What is Spraberry Pay?," report of investigation, PRRC Report # 96-28, New Mexico Petroleum Recovery Research Center, Socorro, NM, 1996.
5. Banik, A.K., and Schechter, D.S.: "Core-Log Integration for the Naturally Fractured Spraberry Trend Area," paper presented at the Naturally Fractured Reservoir Forum (Characterization & Fluid Flow), Socorro, New Mexico, April 19, 1996.
6. Banik, A.K., and Schechter, D.S.: "Characterization of the Naturally Fractured Spraberry Trend Shaly Sands Based on Core and Log Data," paper SPE 35224 presented at the SPE Permian Basin Oil & Gas Recovery Conference, Midland, Texas, 27-29 March 1996.

7. Saleta, C.J., Banik, A.K., Cather, M.E., and Schechter, D.S.: "Application of Analytical Techniques to Evaluate the Heterogeneities of the Upper Spraberry Formation (Permian) and its Influence on the Quality of the Midland Basin Reservoirs in West Texas," SPE 35225 presented at a poster session at the SPE Permian Basin Oil & Gas Recovery Conference, Midland, Texas, 27-29 March 1996.
8. "Geological and Petrophysical Analysis of the Upper Spraberry Formation in Midland County, Texas," report prepared by Reservoirs Inc. for Parker & Parsley Development Company, 1996.
9. Asquith, G.B.: *Log Evaluation of Shaly Sandstone Reservoirs: A Practical Guide*, AAPG, Tulsa, Oklahoma, 1982.
10. Dewan, J.T.: *Essentials of Modern Open-Hole Log Interpretation*, PennWell Book, Tulsa, Oklahoma, 1983.
11. Beck, J., Schultz, A., and Fitzgerald, D.: "Reservoir Evaluation of Fractured Cretaceous Carbonates in South Texas," paper presented at the SPWLA Eighteenth Annual Logging Symposium, June 5-8, 1977.
12. Elkins, L.F.: "Reservoir Performance and Well Spacing, Spraberry Trend Area Field of West Texas," Petroleum Transaction, AIME (1953) 198, 177-196.
13. Elkins, L.F., and Skov, A.M.: "Cyclic Water Flooding the Spraberry Utilizes End Effects to Increase Oil Production Rates," JPT (August 1963A) 877-884.
14. Mardock, E.S., and Myers, J.P.: "Radioactivity Logs Define Lithology in the Spraberry Formation," Oil & Gas Journal (November 29, 1951), 90.
15. Lyttle, W.J., and Ricke, R.R.: "Well Logging in Spraberry," Oil & Gas Journal (December 13, 1951), 92.
16. Archie, G.E.: "Electrical Resistivity Log as an Aid in Determining Some Reservoir Characteristics," Trans., AIME (1942) 146, 54-62.
17. Stalheim, S.O., and Eidesmo, T.: "Is The Saturation Exponent n A Constant?," SPWLA 36th Annual Logging Symposium, June 26-29, 1995.
18. Tyler, N., and Gholston, J.C.: "Heterogeneous Deep-Sea Fan Reservoir, Shackelford and Preston Waterflood Units, Spraberry Trend, West Texas," Report of Investigation No. 171, Bureau of Economic Geology, The University of Texas, Austin, 1988.
19. Guevara, E.H.: "Geological Characterization of Permian Submarine Fan Reservoirs of the Driver Waterflood Unit, Spraberry Trend, West Texas," Report of Investigation No. 172, Bureau of Economic Geology, The University of Texas, Austin, 1988.
20. Handford, C.R.: "Sedimentology and Genetic Stratigraphy of Dean and Spraberry Formations (Permian), Midland Basin, Texas," AAPG (1981), v. 65, No. 9, 1602-1616.
21. Worthington, P.F., and Pallatt, N.: "Effective of Variable Saturation Exponent Upon the Evaluation of Hydrocarbon Saturation," paper SPE 20538 presented at the 1990 SPE Annual Technical Conference and Exhibition, New Orleans, Sept. 23-26.
22. Maute, R.E., Lyle, W.D., and Sprunt, Eve S.: "Improve Data-Analysis Method Determines Archie Parameters From Core Data," JPT (January 1992) 103-107.
23. *QLA2-A Log Interpretation System*, GeoGraphix, Inc. 1994.
24. *Log Interpretation Principles/Applications*, Schlumberger Educational Services, Houston (1989).

25. Log Interpretation Charts, Western Atlas Logging Services, Houston (1985).
26. Doublet, L.E., Pande, P.K., Clark, M.B., Nevans, J.W., and Blasingame, T.A.: "An Integrated Geological and Engineering Reservoir Characterization of the North Robertson (Clearfork) Unit: A case Study, Part 1," paper SPE 29594, presented at the 1995 Joint Rocky Mountain Regional Meeting and Low-Permeability Reservoirs Symposium, Denver, Colorado, USA, 20-22 March 1995.
27. Davies, D.K., and Vessell, R.K.: "Flow Unit Characterization of a Shallow Shelf Carbonate Reservoir: North Robertson Unit, West Texas," paper SPE/DOE 35433, presented at the 1996 SPE/DOE Tenth Symposium on Improved Oil Recovery, Tulsa, OK, 21-24 April 1996.
28. Aguilera, R.: "Analysis of Naturally Fractured Reservoirs From Sonic and Resistivity Logs," JPT (November 1974).
29. Fertl, W.H.: "Shaly Sand Analysis in Development Wells," SPWLA 16th Annual Logging Symposium Trans., paper A, 1975.
30. Clavier, C., Coates, G., and Dumanoir, J.: "The Theoretical and Experimental Basis for the 'Dual Water' Model for Interpretation of Shaly Sands," JPT (April 1984).
31. Gomez-Rivero, O.: "A Practical Method for Determining Cementation Exponents and Some Other Parameters As An Aid in Well Log Analysis," The Log Analyst (September-October 1976), 8-24.

Table 1.2. Log Based Rock Model



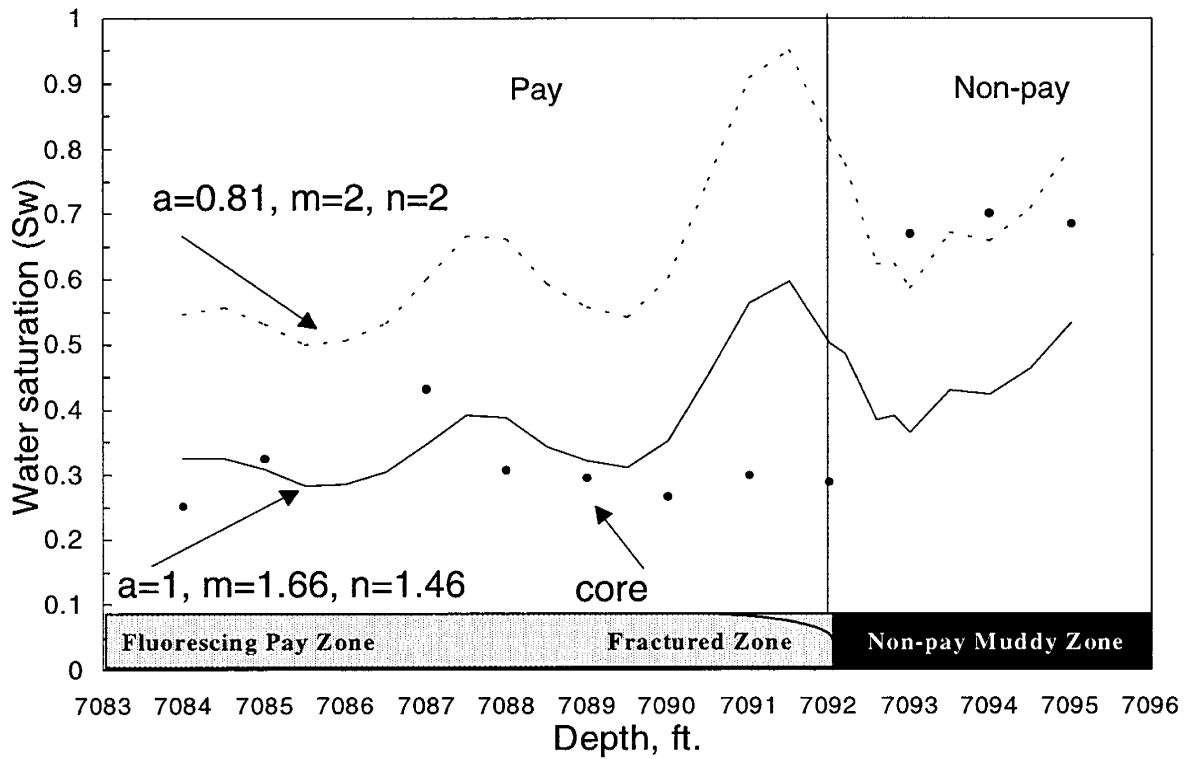


Fig. 1.6. Log-derived water saturation calculated using conventional and derived m and n values and compared with core-measured water saturation (Upper Spraberry, Shackelford 1-38 A). Sharp contrast between pay and non-pay is observed by fluorescence at a depth of 7092 ft. Geological characterization of this interval is found in Figs. 1.1 through 1.5.

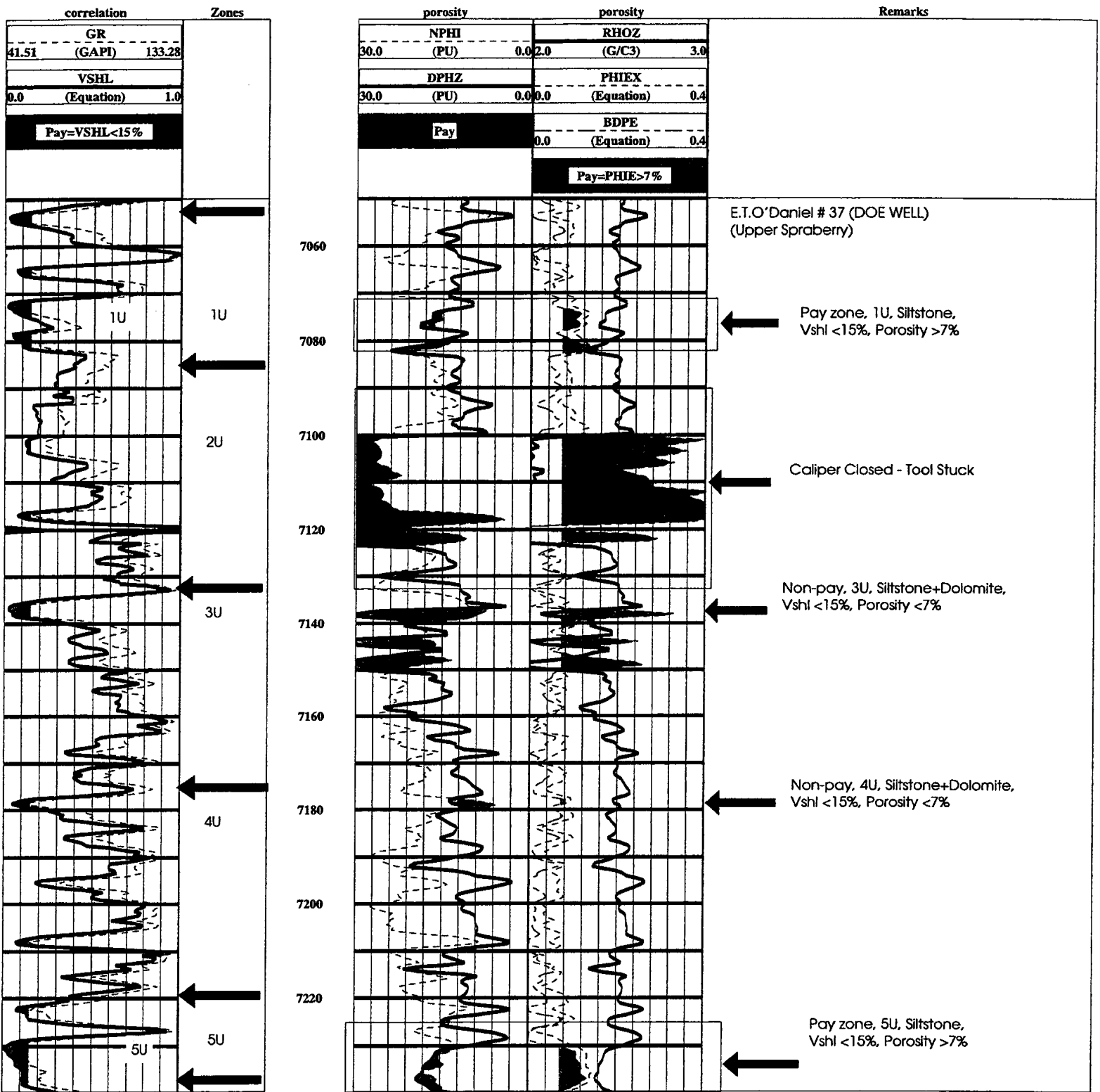


Fig. 1.7. Open-hole log for the DOE pilot well E.T.O'Daniel # 37 (Upper Spraberry).

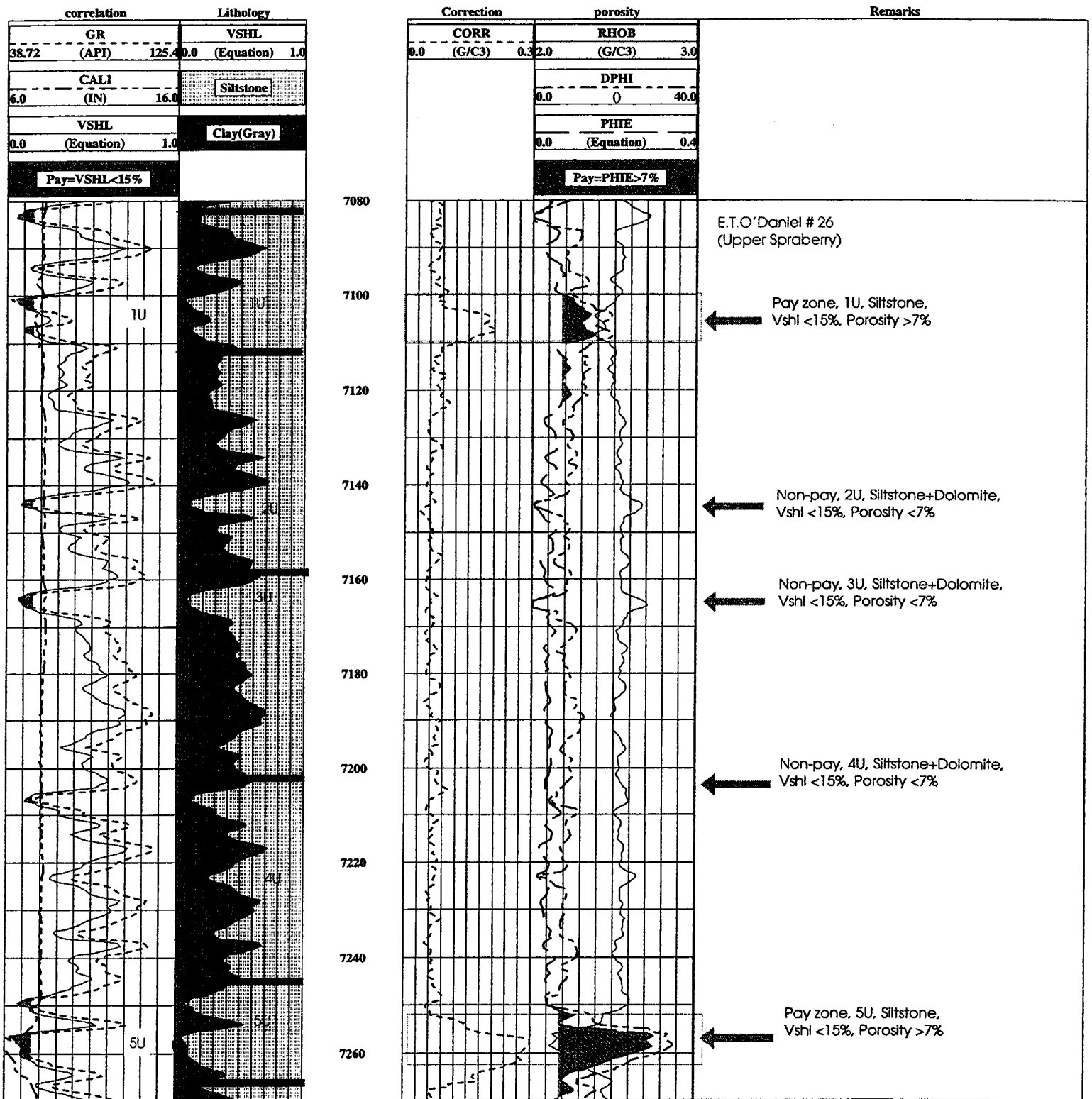


Fig. 1.8. Open-hole logs from the E.T.O'Daniel # 26 (Upper Spraberry).

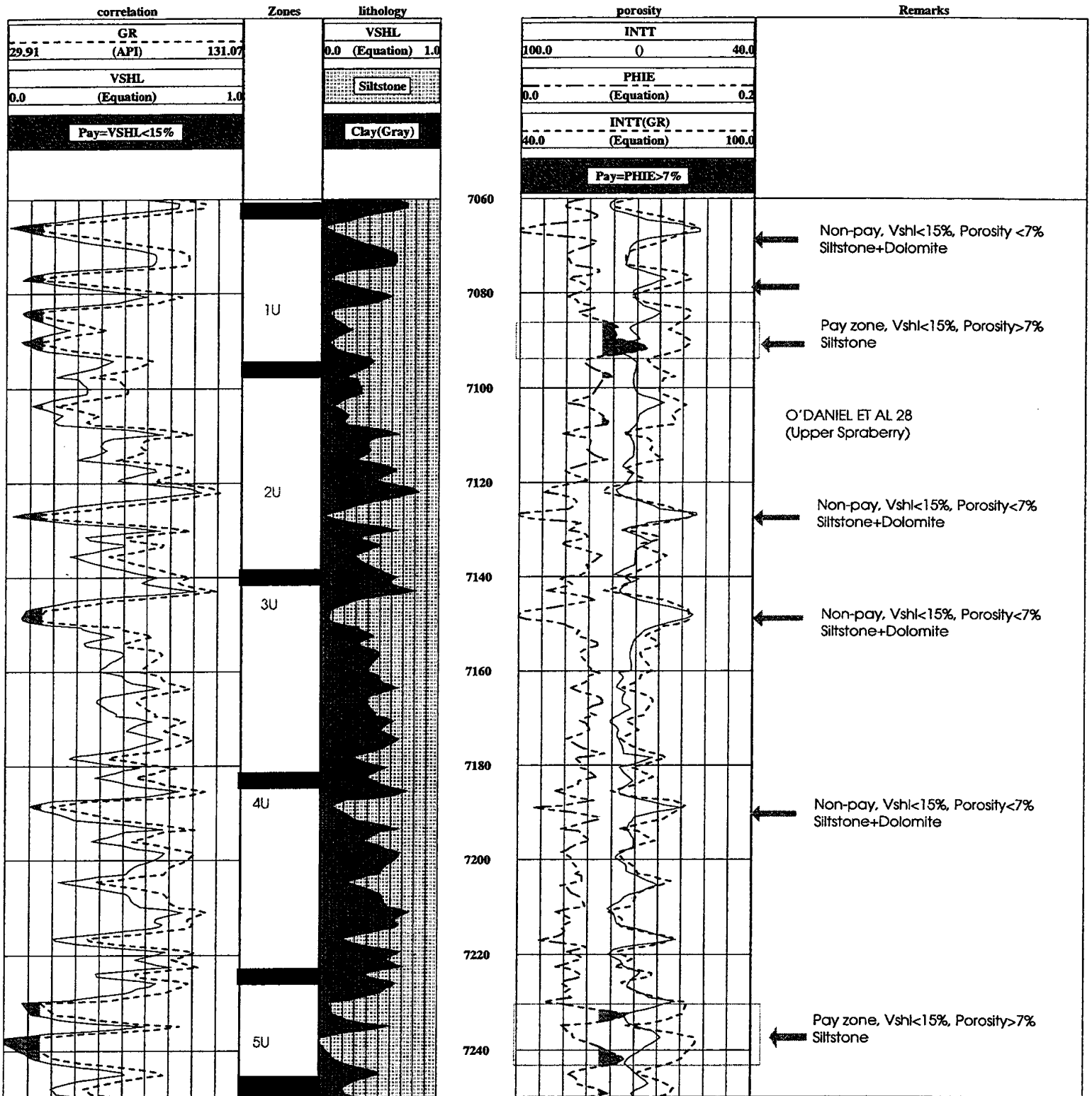


Fig. 1.9. Open-hole logs from the E.T. O'Daniel #28 (Upper Spraberry). INTT is original sonic log and INTT(GR) is sonic log generated from gamma-ray log.

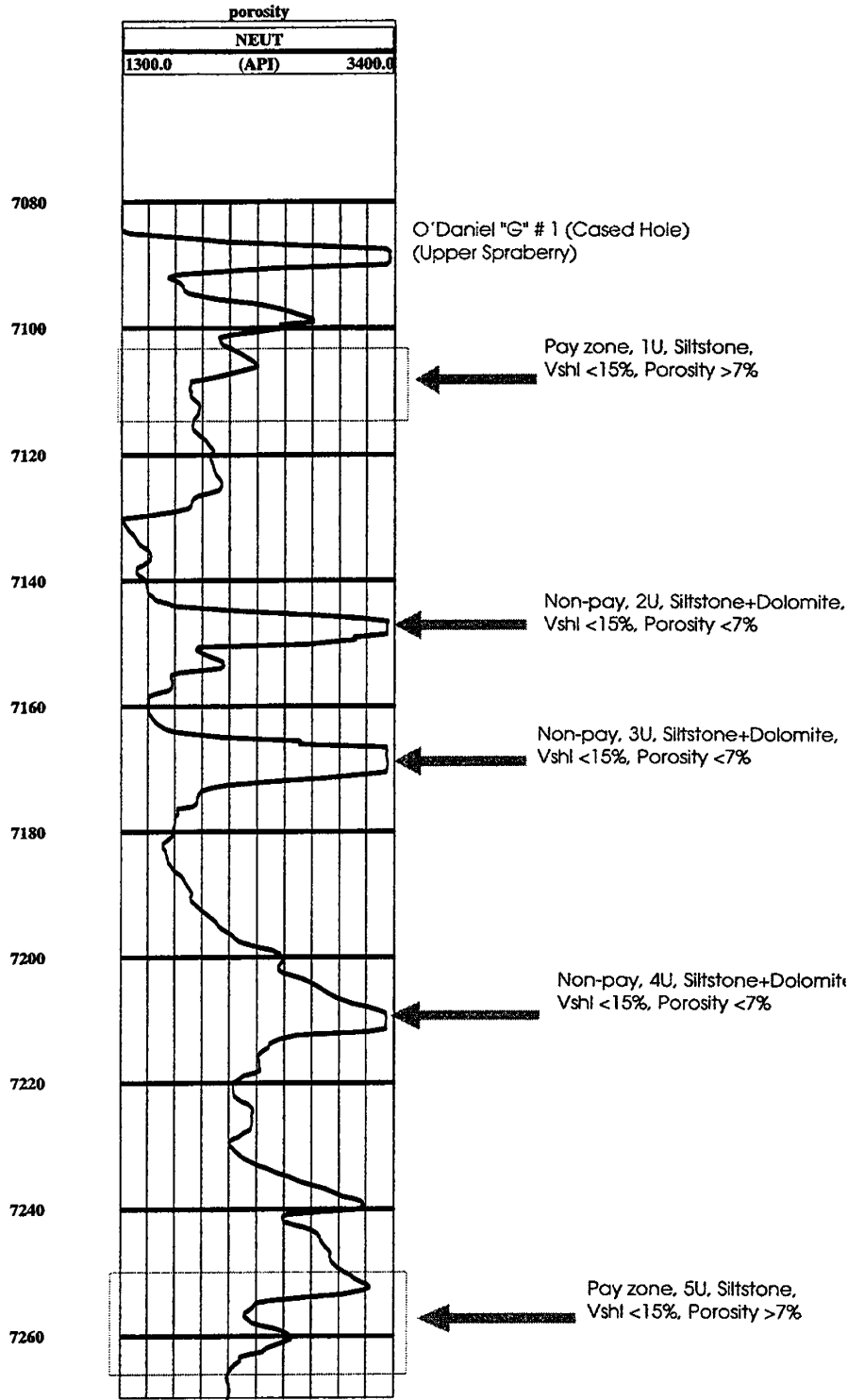
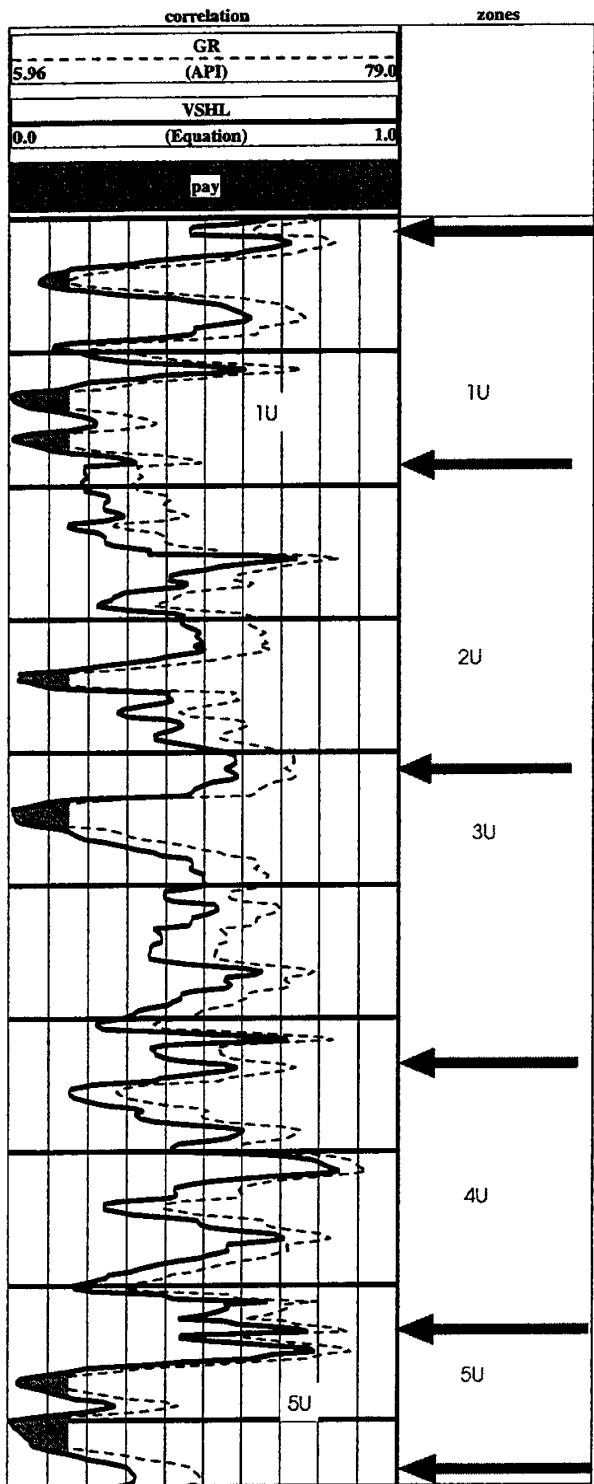


Fig. 1.10. Cased-hole logs from the E.T. O'Daniel "G" #1 (Upper Spraberry).

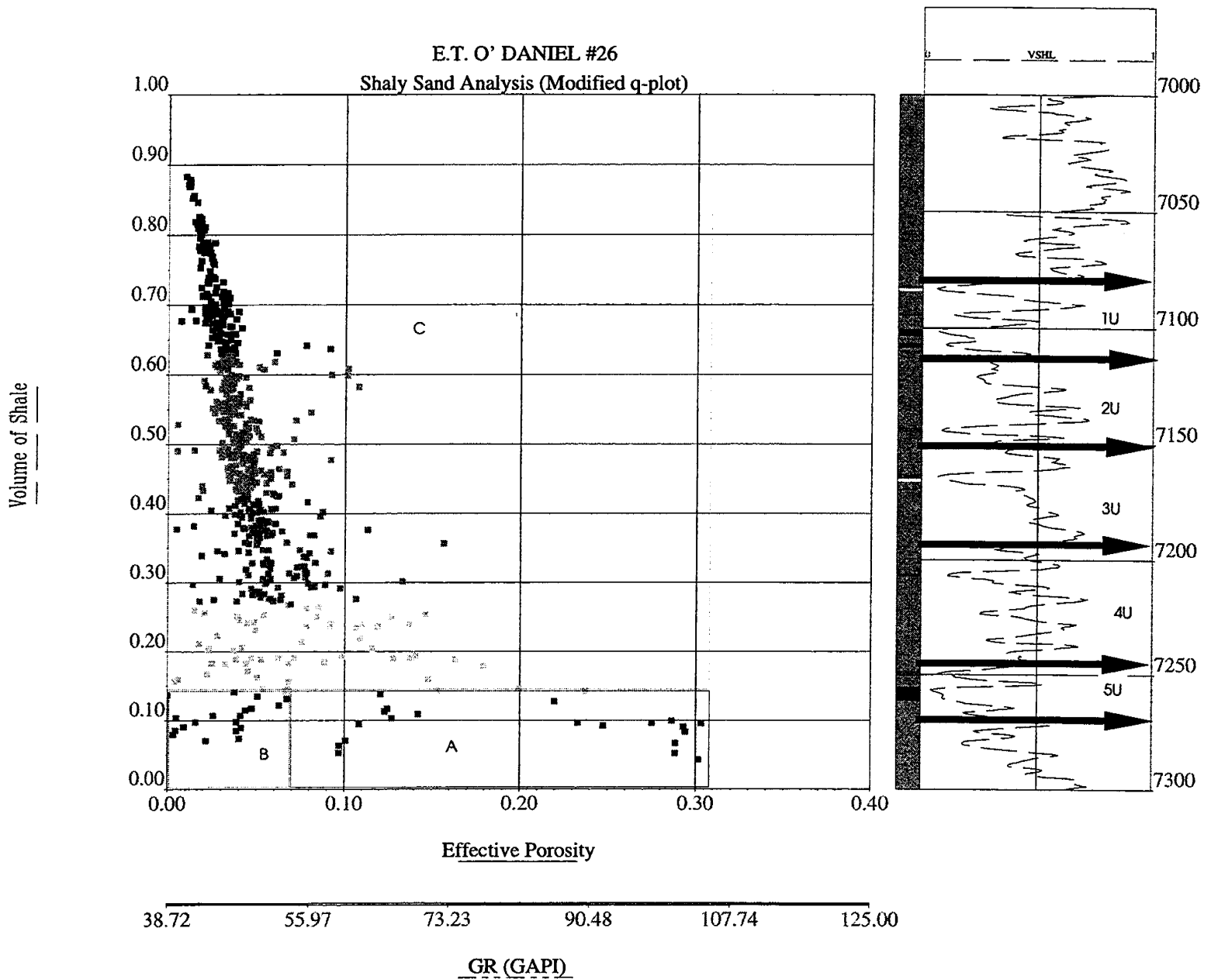


Fig. 1.11. Effective porosity vs. volume of shale for identification of rock type. Log based rock model for the Spraberry Trend Area. Data points in box A are from the 1U and 5U pay zones (rock type A, VSHL <15%, effective porosity >7%). Data points in the box B are from the 2U, 3U, and 4U non-pay zones (rock type B, VSHL <15%, effective porosity <7%). Data points in the box C are from the muddy non-pay zones (rock type C, VSHL >15%).

2. INVESTIGATION OF CRUDE OIL/BRINE/ROCK INTERACTION

2.1 Determination of Initial Water Saturation

The initial water saturation in the Spraberry Trend Area reservoirs has been carefully evaluated based on cores from 46 wells drilled before 1954. Fig. 2.1 shows a plot of the initial water saturation against air permeability of the cores. It is seen from the plot that the initial water saturation is above 0.20 pore volume (PV) for nearly all the cores. The saturation data is more scattered in the low permeability region as opposed to high permeability regions. The average water saturation can approximately be represented by the following correlation:

$$S_{wi} = 0.20 + 0.12 e^{-0.6(k-0.1)} \quad (1)$$

where S_{wi} is the initial water saturation and k is air permeability of the core in millidarcies.

Using this correlation for the initial water saturation and laboratory determined water saturation of cores, macroscopic displacement efficiencies (E_{dm}) of waterflooding in the Spraberry cores at various times have been evaluated and summarized in Table 2.1. It is seen that the macroscopic displacement efficiencies (E_{dm}) of waterflooding in these cores are much higher than field observed water flooding oil recovery which is between 5 % and 9 % in the Upper Spraberry sand. This indicates that the volumetric sweep efficiency in Spraberry Trend Area reservoirs is low.

2.2 Rock Wettability as Determined by Imbibition Experiments

Introduction

In order to understand the interaction between rock, crude oil and brine in Spraberry Trend Area reservoirs, we have performed water and oil imbibition experiments using Spraberry oil, synthetic Spraberry reservoir brine, and Spraberry reservoir rock. Macroscopic displacement efficiency of water to oil in core samples due to capillary forces has been determined by spontaneous imbibition tests. Effect of core cleaning and aging on the displacement efficiency and wettability has been investigated. Wettability of Spraberry cores taken from the Spraberry Shackelford 1-38A has been estimated based on spontaneous water and oil imbibition tests. It is concluded that the cores are weakly water-wet with mixed wetting behavior. The Amott wettability index to water (I_w) of the cores has been determined to be between 0.5 and 0.7. The macroscopic displacement efficiency during spontaneous water imbibition varies from 40% to 70% depending upon core permeability.

Experimental Procedure for Imbibition Tests

The whole cores we received are 4-inch-diameter cores taken from the Spraberry Shackelford 1-38A. We cut core plugs from whole cores to fit our core holders. The core plugs are 1.5 inch in diameter and about 2 inches long. Core plugs were dried in an oven before initiation of imbibition experiments. The experimental procedure is as follows:

1. Measure core dimensions, weigh core in air, and measure permeability to air (k_a).
2. Vacuum core for 72 hours, then saturate core in vacuum with synthetic reservoir brine, let the core age in brine and measure core weight until the weight stabilizes. Estimate core porosity (ϕ).
3. Inject brine into the core under 200 psig of injection pressure and 500 psig of overburden pressure for 2 pore volumes. Estimate core permeability to brine (k_w).
4. Inject oil into the core under 200 psig of pressure. Measure brine and oil flow rate until initial brine saturation (S_{wi}) is established in the core. Estimate permeability to oil at initial brine saturation (k_o).
5. Age the fluid-saturated core in oil and weigh core until core weight stabilizes. The aging time should be at least 2 weeks before going to the next step.
6. Place core into a beaker filled with brine at ambient conditions. Weigh core in brine after removing produced oil from the core surface. Calculate oil recovery based on change in weight of the core as a function of imbibition time. Terminate imbibition experiment when recovery stabilizes.
7. Displace the residual oil in the core by waterflooding at 200 psig injection pressure. Calculate Amott wettability index to water (I_w).

In order to assure that reservoir conditions were established in the core prior to water imbibition, we cleaned some core plugs by injecting chloroform into them. To investigate the effect of cleaning on rock properties, chloroform was injected into the core after step 3 and followed by another water injection before proceeding to step 4.

Results and Discussion

Untreated Cores. Assuming that the whole cores we received were clean, the first 10 core plugs were not treated with chloroform. Oil recovery curves obtained from some of the uncleaned core plugs are presented in Fig. 2.2. It is seen from Fig. 2.2 that brine imbibition rate varies from core to core. Final oil recovery due to imbibition varies from 10% to 40%.

Properties of the cores and fluids, final recoveries, and wettability indices to water are summarized in Table 2.2.

Cleaned Cores. In order to establish a wetting condition similar to that in the reservoir, some cores were cleaned with chloroform before imbibition tests. Oil recovery curves obtained from some of the core plugs are presented in Fig. 2.3. This figure also indicates that brine imbibition rate varies from core to core. Final oil recovery due to imbibition varies from 15% to 70%. Comparison between Fig. 2.2 and Fig. 2.3 reveals that the rate of water imbibition was significantly improved after cleaning the cores with chloroform. Final oil recovery by spontaneous imbibition was also improved. Rock properties before and after chloroform cleaning are shown in Table 2.3 indicating that both porosity and permeability increased. Comparison of the residual water saturation data in Table 2.2 and Table 2.3 indicates that the initial water saturation after oil injection under 200 psig increased from 18.6% to 42.2% due to chloroform cleaning. This result suggests that the cores became more water wet after the cleaning procedure. This was confirmed by the improved Amott wettability index to water (I_w) calculated after waterflooding the core. The average I_w was increased from 0.5 to 0.6.

Several factors may affect the final oil recovery during brine imbibition. These factors should include core permeability, initial water saturation, and core wettability. The final oil recovery is plotted in Fig. 2.4 against core permeability to brine. This figure indicates that the final oil recovery increases with core permeability. Scatter of data is probably due to variations in initial water saturation and wettability of the cores.

We have also investigated brine recovery during spontaneous imbibition of oil into a Spraberry core (core No. SP-10 in Table 2.2) fully saturated with brine. Fig. 2.5 shows the resultant recovery curve. This curve indicates that a small portion of the rock is oil wet since the core imbibes oil.

In order to exclude the effect of aging time in oil on the result, the final oil recoveries from completed tests with cleaned cores are plotted against aging time in Fig. 2.6. This figure indicates if the data beyond three weeks aging time is considered equilibrated, then the final oil recovery due to spontaneous water imbibition should be about 50% of original oil in place (OOIP). The Amott wettability indices to water for various cores are plotted versus the aging time in Fig. 2.7. This plot indicates that if the data below three weeks aging time are disregarded, the I_w of Spraberry reservoir rock should be about 0.55, which implies a weakly water wet system.

2.3 Water-Oil Interfacial Tension Measurements

Experimental Apparatus

Shown in Fig. 2.8 is a sketch of our experimental setup for IFT determination by pendant drop measurements. Up to 18 needles can be installed in a high pressure cell for forming pendant and sessile drops of different sizes. Fluids are circulated by a pump through the measuring cell, where pendant drops are formed, and then into a density meter to measure densities of the two phases. A circulating water bath is used to control the temperature of the measuring cell and the density meter. Pressure and temperature in the cell are measured by a pressure transducer and a thermometer. The temperature is regulated at measuring conditions. Pendant/sessile drops are imaged by a CCD video camera. Drop images are sent to the VCR, monitor and computer for data processing. IFT is calculated from the image profile by the computer. The density meter is a PAAR mPDS 2000. The video camera is a SANYO VCB-3524 with a 1.5X tele-conversion lens, C-Mount Lens Adapter, and a video monitor. The image processing software is EPIX SVIP version 7.0 for Windows. The circulating pump is a high speed LDC analytical mini-pump. Needle sizes range from 0.23 mm to 0.90 mm outer diameter. For calibration uses, accurately cut metal collars are attached around the needles.

Results

The IFT of synthetic Spraberry brine/Spraberry separator oil system has been measured under ambient conditions. The result is 32 mN/m. IFT measurement for this system under elevated pressures and temperatures is ongoing. The IFT of synthetic Spraberry brine/Spraberry reservoir oil system will be carried out in the near future.

2.4 Water-Oil Capillary Pressure Determination

The water-oil capillary pressure in the Upper Spraberry 1U and 5U sands has been estimated by utilizing the Leverett J-function on previously measured mercury injection capillary pressure data. Plotted in Fig. 2.9 are mercury injection capillary pressure curves converted to Leverett J-function for 9 cores taken from the Shackelford # 138A. As can be seen from Fig. 2.9, the capillary pressure measurements for 6 low permeability (<0.1 md) cores were not complete in the low saturation region indicating these samples were from non-pay zones. Therefore, those curves for low permeability cores are disregarded in this analysis. Fig. 2.10 shows mercury injection capillary pressure curves converted to Leverett J-function for 5 cores taken from the Judkins A#5. The curve for core #5 was not complete in the low saturation region because of its low permeability, and therefore is disregarded. The seven completed curves presented in Figs. 2.9 and 2.10 appear to be identical. The average J-function of the seven cores is plotted in Fig. 2.11, which can be further used for estimation of water-oil capillary pressure. Assuming that water-oil interfacial tension is 42 mN/m and contact angle

is 45 degrees, water-oil capillary pressures for a 0.5 md Spraberry core have been estimated as shown in Fig. 2.12. The imbibition capillary pressure curve was estimated by subtracting a pressure of 15 psia from the estimated drainage capillary pressure so that the curve intersects the S_w axis at a point corresponding to the Amott wettability index to water (I_w) of 0.55 as determined by imbibition tests. The water-oil capillary pressure of Spraberry core is currently being measured in the New Mexico Petroleum Recovery Research Center using Spraberry oil and synthetic Spraberry brine. Some of the experimental results are presented in Fig. 2.13 and compared with the above estimated capillary pressure from mercury injection tests.

Table 2.1 - Estimated Macroscopic Displacement Efficiency (E_{dm}) in Cores from Spraberry Trend Area Reservoirs

Year	Core Permeability (md)	Water Saturation (%PV)	E_d (%OOIP)	Well Cored
1963	0.4 - 1.3	32 - 40	10 - 16	Tippett #5
1974	0.3 - 0.5	35 - 45	20	Parish #7
1987	0.3 - 1.0	35 - 55	17 - 21	Judkins A#5
1990	0.6 - 1.2	31 - 52	15 - 26	Pembrook #9407
1995	0.2 - 1.6	20 - 50	12 - 28	E.T.O'Daniel #37

Table 2.2 - Properties of Rock and Fluids Used in 8 Completed Tests

Test No.	ϕ (%)	k_a (md)	k_w (md)	k_o (md)	S_{wi} (%)	ρ_w (g/cc)	ρ_o (g/cc)	μ_w (cp)	μ_o (cp)	R_{im} (%)	R_{wf} (%)	I_w
SP-1	10.0	0.43	0.28	0.09	13.9	1.09	0.86	1.16	16.4	38	41	0.45
SP-2	10.0	0.45	0.22	0.10	18.4	1.09	0.87	1.18	22.4	38	38	0.50
SP-3	9.8	0.44	0.23	0.14	21.3	1.08	0.87	1.17	21.8	41	22	0.64
SP-4	10.0	0.46	0.14	0.06	14.3	1.08	0.87	1.17	19.5	40	27	0.59
SP-5	10.7	0.49	0.27	0.09	15.3	1.08	0.87	1.18	19.5	35	40	0.47
SP-6	9.8	0.43	0.22	0.06	17.2	1.08	0.87	1.18	19.5	>11	25	0.31
SP-7	10.4	0.34	0.20	0.08	22.0	1.08	0.75*	1.18	1.72*	>10		
SP-8	5.9	0.06	0.03		18.8	1.08	0.87	1.18	19.8			
SP-9	6.5	0.06	0.03		18.4	1.08	0.87	1.18	19.8			
SP-10	12.8	0.36	0.15	0.05	26.5	1.08	0.87	1.18	19.5	21	24	0.46
Average	10.4	0.43	0.21	0.08	18.6	1.08	0.87	1.18	19.8	32	31	0.50

* Soltrol 220

Table 2.3 - Rock Properties and Results of Water Imbibition Experiments

Test No.	Before Cleaning			After Cleaning			t _{oil} (Day)	R _{im} (OOIP)	I _w
	φ (%)	k _w (md)	S _{wi} (%)	φ (%)	k _w (md)	S _{wi} (%)			
SP-8a	5.9	0.03		9.9	0.12	52	14	>0.36	
SP-9a	6.5	0.03		9.0	0.18	47	21	>0.16	
SP-10	12.8	0.15		14.3	0.45	32		0.09*	
SP-11	10.0	0.11		13.2	0.31	38	6	0.71	0.76
SP-15	3.1	0.02		6.9	0.06	55	16	0.70	
SP-16	2.1	0.01		9.2	0.07	53	25	>0.14	
SP-17	3.1	0.02		7.7	0.08	54	7	0.40**	
SP-19	5.0	0.03		12.3	0.32	36			
SP-21	10.8	0.10		14.4	0.35	36	15	0.45	0.64
SP-22	5.0	0.03		10.1	0.25	42	49	0.42	0.49
SP-24	4.1	0.03		11.6	0.36	38	1	0.79	0.75
SP-25	4.0	0.02		10.4	0.27	40	20	0.72	
SP-27	6.8	0.04		10.6	0.29	39	30	0.57	0.66
SP-28	2.9	0.02		7.8	0.09	53	90	0.29	0.35
SP-30	7.0	0.04		9.7	0.26	41	41	0.48	0.52
SP-33	11.8	0.21		13.9	0.41	35	60	0.47	0.55
SP-34	11.1	0.17		13.2	0.34	40	28		
SP-1	10.0	0.28	13.9	12.0	0.34	37	21	0.50	0.55
SP-3	9.8	0.23	21.3	11.2	0.34	33	21	> 0.15**	
Average						42.2			

* Brine recovery during oil imbibition

** Imbibition performed at 138 F and 1250 psig

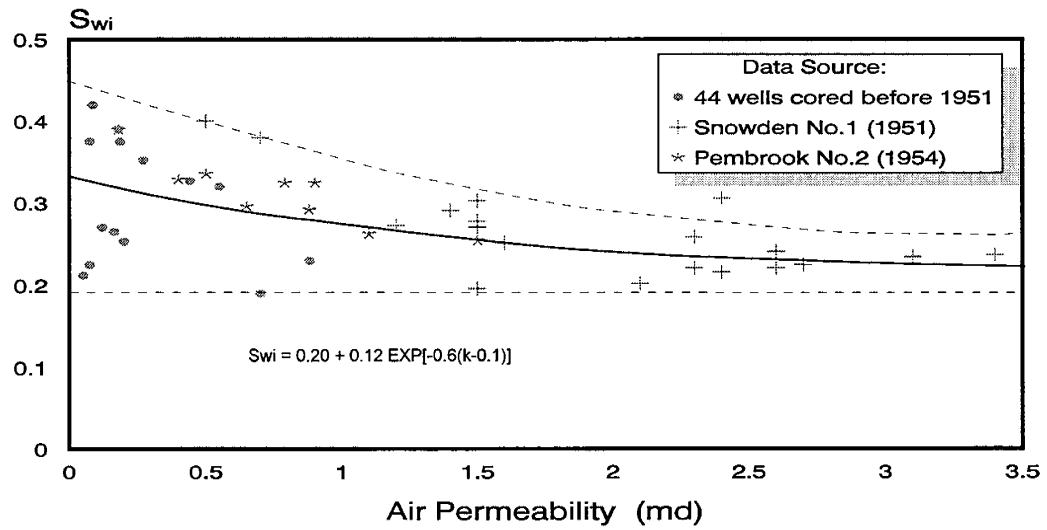


Fig. 2.1 - Initial water saturation in Spraberry sandstone

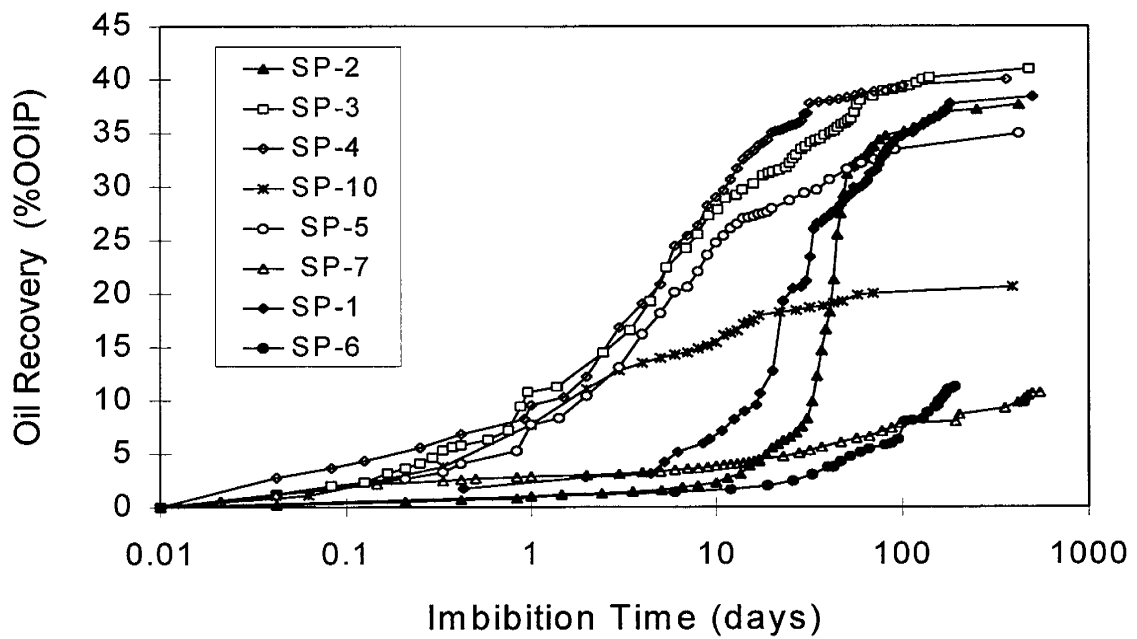


Fig. 2.2 - Oil recovery from untreated Spraberry cores during brine imbibition

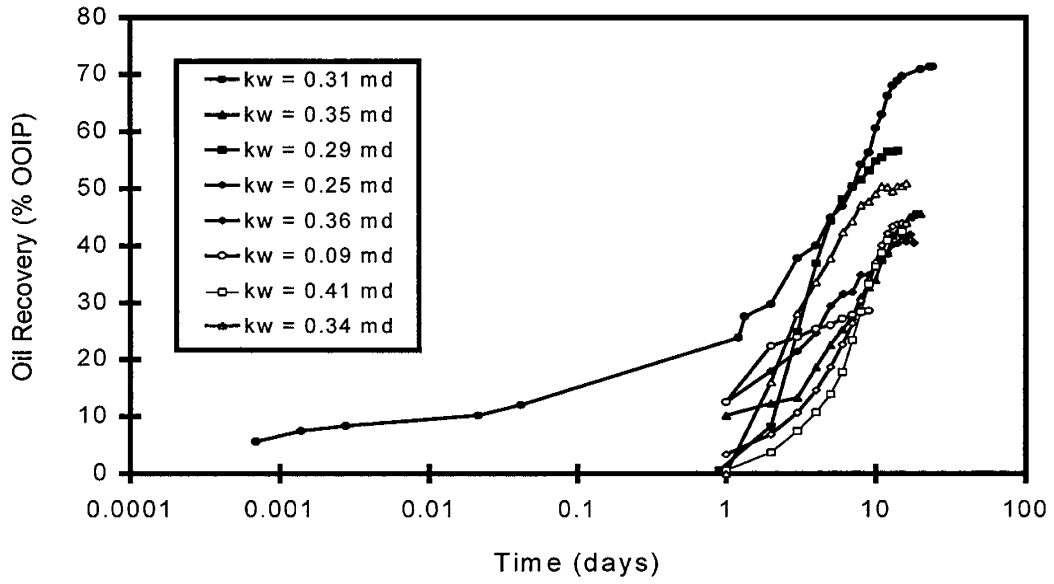


Fig. 2.3 - Oil recovery from cleaned Spraberry cores during water imbibition

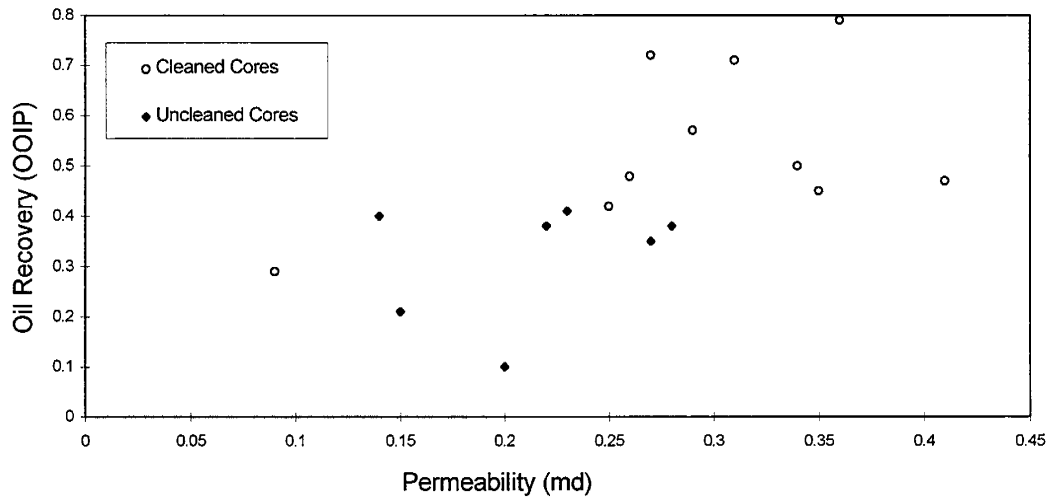


Fig. 2.4 - Effect of permeability on final oil recovery

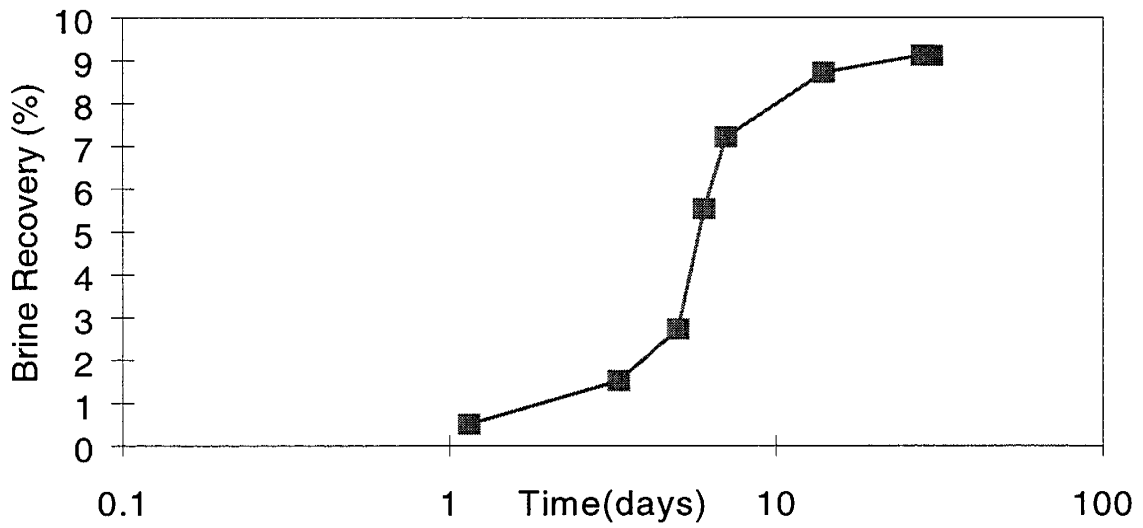


Fig. 2.5 - Brine recovery from a cleaned core during oil imbibition. Spontaneous oil imbibition indicates mixed wettability

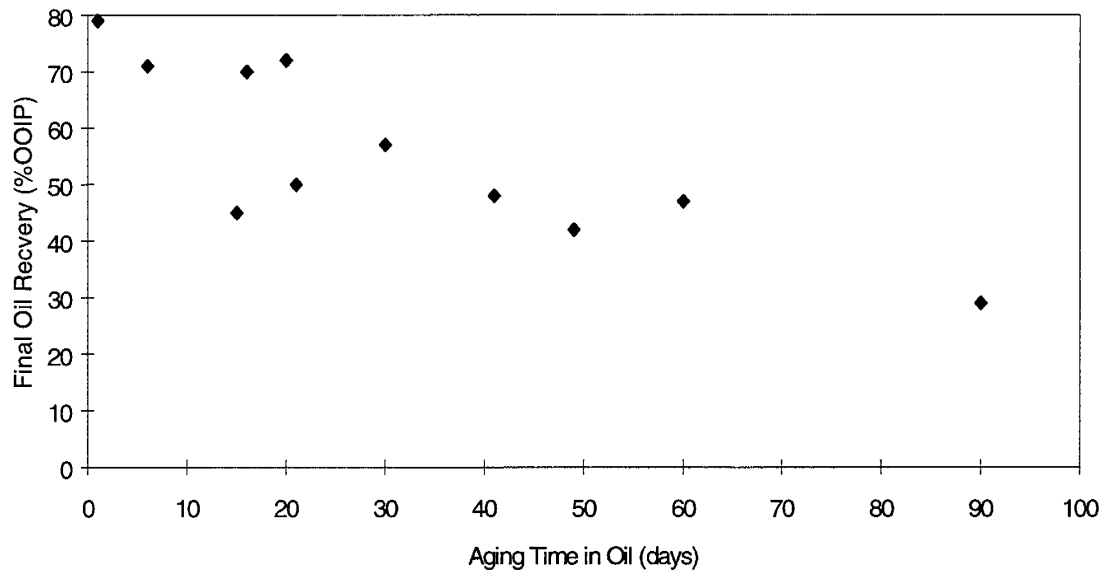


Fig. 2.6 - Final recovery versus corresponding aging time in oil.

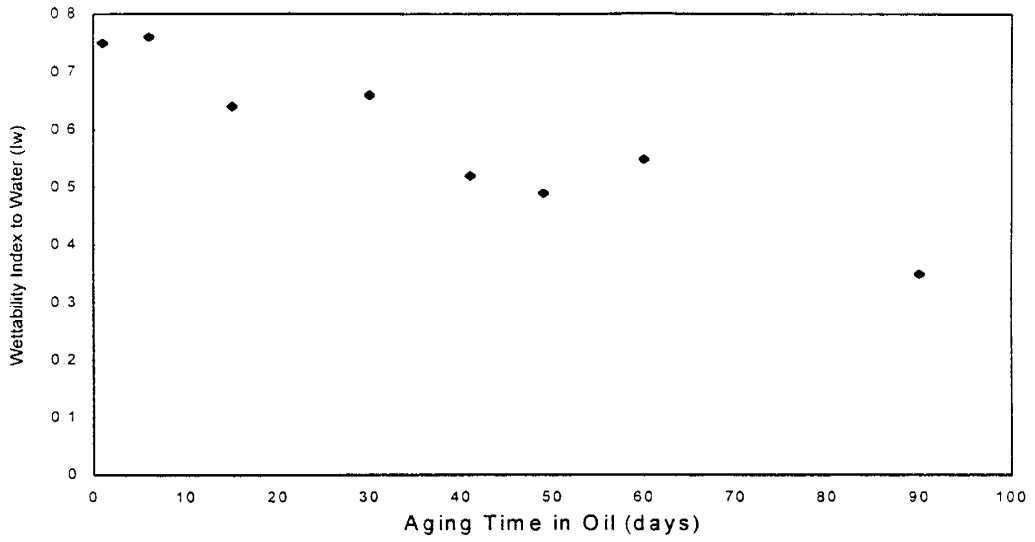


Fig. 2.7 - Effect of aging of core in oil on wettability to water

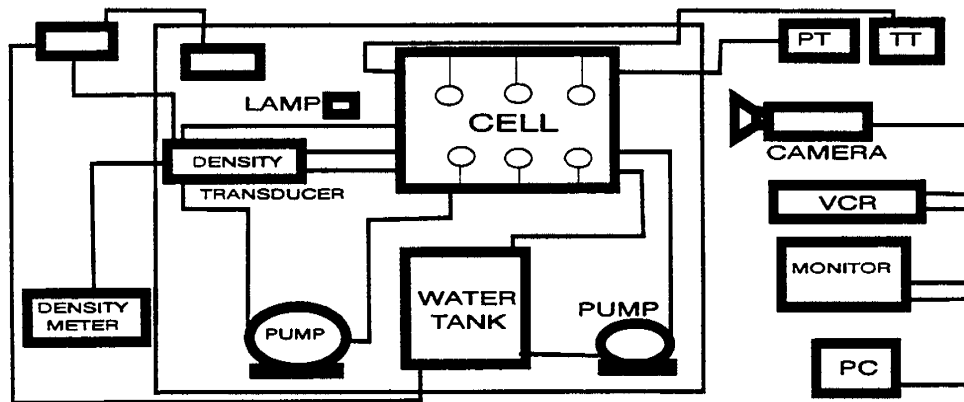


Fig. 2.8 - Diagram of experimental set-up for IFT measurements

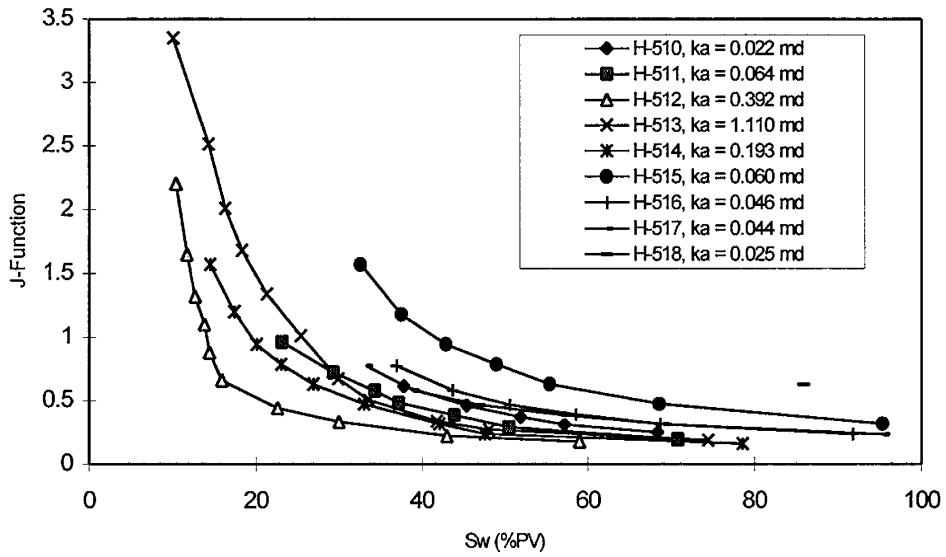


Fig. 2.9 - J-function calculated from mercury injection capillary pressure data, cores from Shackelford #1-38A

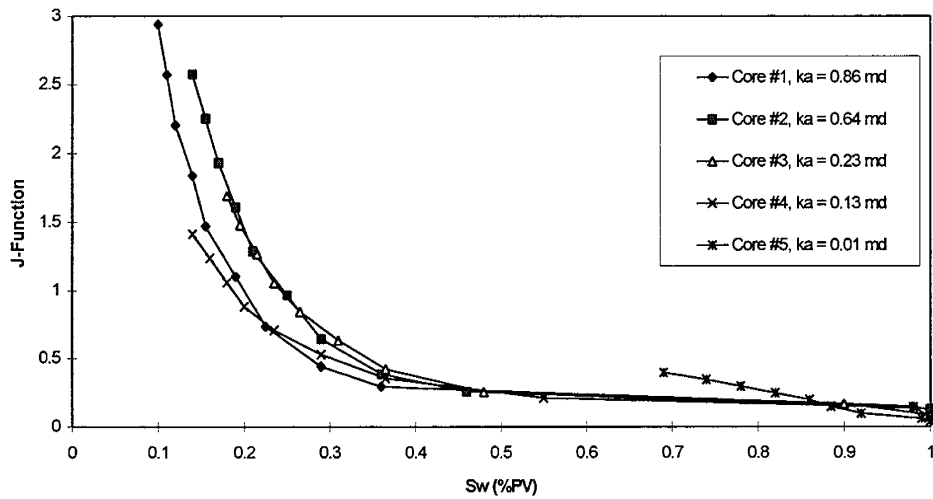


Fig. 2.10 - J-function calculated from mercury injection capillary pressure data, cores from Judkins A#5

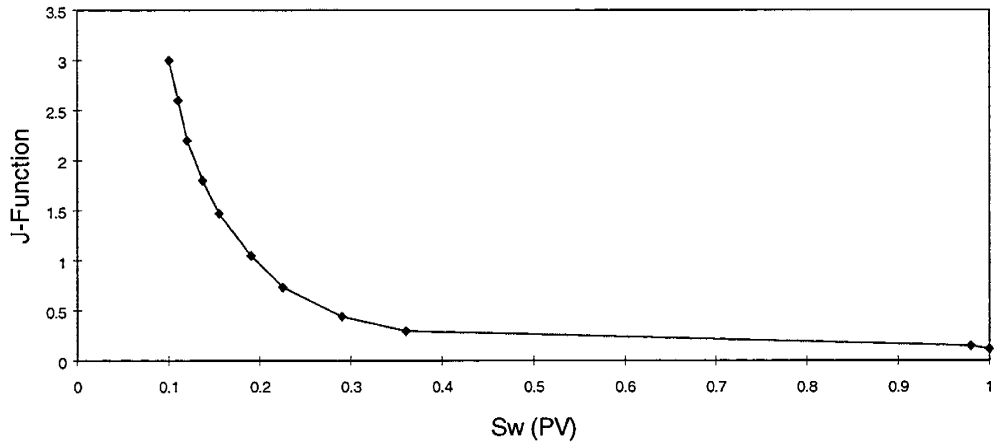


Fig. 2.11 - J-Function calculated from mercury injection capillary pressure data, cores from wells Judkins A#5 and Shackelford #1-38A

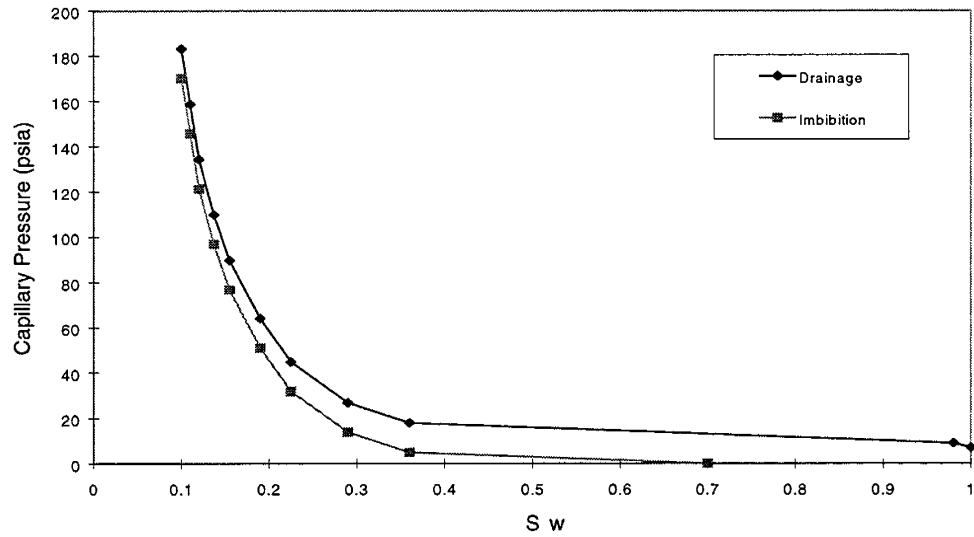


Fig. 2.12 - Estimated water-oil capillary pressure in Spraberry sand, permeability = 0.5 md, porosity = 0.10, water-oil IFT = 42 mN/m, contact angle = 45 degrees. Imbibition capillary pressure curve is positioned based on Amott wettability index (I_w) evaluated from imbibition and coreflood tests

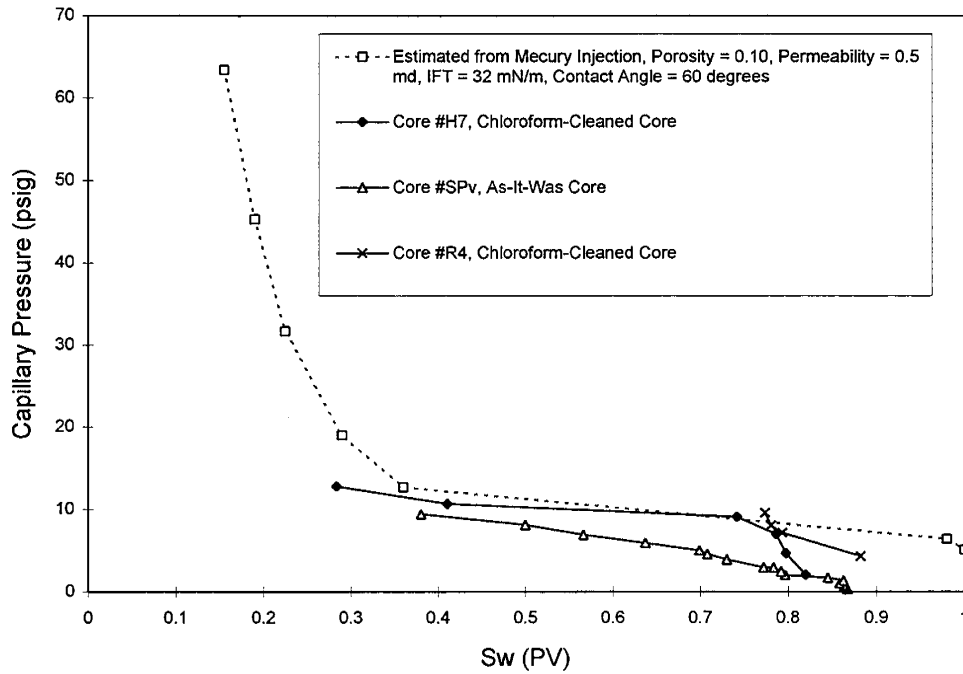


Fig. 2.13 - Measured and estimated (from mercury injection pressure data) drainage water-oil capillary pressure in Spraberry 1U and 5U pay sand

3. RESERVOIR PERFORMANCE

3.1 Scaling Analysis of Water Imbibition Results

Introduction

In order to understand the interaction between rock, crude oil and brine in Spraberry Trend Area reservoirs, water imbibition experiments have been performed using Spraberry oil, synthetic Spraberry reservoir brine, and Spraberry reservoir rock under ambient conditions. Macroscopic displacement efficiency of water to oil in core samples due to capillary forces has been determined by spontaneous imbibition tests. Wettability of Spraberry cores taken from the Spraberry Shackelford #1-38A and E.T. O'Daniel #37 has been estimated based on spontaneous water and oil imbibition tests. It is found that Spraberry reservoir rock is weakly water-wet with mixed wetting behavior. The Amott Wettability index to water (I_w) has been determined to be on average about 0.55, based on 29 imbibition tests. The macroscopic displacement efficiency during spontaneous water imbibition is on the order of 50%. Using 50% for the maximum recoverable oil, scaling from core geometry to matrix block geometry (assuming a fracture spacing of 4 feet) in the 5U Unit of the Upper Spraberry zone resulted in oil recovery after 44 years of waterflood of between 8% and 15.5% depending upon sand permeability. Integration of the recovery profile along the depth of the pay zone resulted in an estimate of imbibition oil recovery from the 5U zone to be about 11%. This is higher than the observed 5-9% of waterflood oil recovery from the Upper Spraberry sand. One of the reasons for overestimation is believed to be wettability alteration of the sand under reservoir conditions. It has been observed that the oil recovery process is slower in our on-going imbibition experiments at reservoir temperature. When the effective oil permeability is used in the scaling equation, scaling from core geometry to matrix block geometry in the 5U Unit of the Upper Spraberry zone resulted in oil recovery after 44 years of waterflood of between 5.5% and 11% with an average of 7.7%, which is close to the observed 5-9% of waterflood oil recovery from the Upper Spraberry sand. However, it is unclear if the effective oil permeability should be used in the scaling equation because the scaling equation was derived on the basis of absolute permeability.

Experimental Results

Experimental procedure and results for imbibition experiments have been presented in the Section II of this report¹. Results from 9 complete runs are plotted in Fig. 3.1 in dimensionless form. The dimensionless time (t_D) is defined by Ma et al. as²

$$t_D = t (k/\phi)^{0.5} \sigma/\mu_g L_c^2 \quad (1)$$

where t is the imbibition time, k is the permeability, ϕ is the porosity, σ is the interfacial tension, μ_g is the geometric mean of water and oil viscosities, and L_c is the characteristic

length defined by Ma et al.² Also plotted in Fig. 1 is the scaled oil recovery curve established by Ma et al.² using Berea cores under varying conditions. It is seen from Fig. 3.1 that although the recovery data are plotted against dimensionless time, they still do not collapse in a narrow band as do recovery curves obtained using Berea cores.²

Scaling Equation

In order to apply experimental imbibition data to reservoir development, it is desirable to develop an simple equation relating experimental oil recovery through core geometry to matrix geometry in fractured reservoirs. Such an equation can be established based on Gupta and Civan's work³ and Eq. (1). Assuming that the mass transfer rate is proportional to the available mass of oil in place, the following governing equation is formulated:

$$dV/dt = -\lambda V^\alpha \quad (2)$$

where V is the volume of oil in place to be recovered by imbibition, t is the time, λ is a proportionality coefficient, and α is an empirical exponent. If an initial condition of $V=V_o$ at $t=0$ is used, where V_o is the volume of recoverable oil by imbibition, the following two solutions to Eq. (2) can be obtained:

$$V = V_o e^{-\lambda t} \quad (3)$$

for $\alpha = 1$, and

$$V = [V_o^{1-\alpha} - \lambda(1-\alpha) t]^{1/(1-\alpha)} \quad (4)$$

for α not equal to unity. Dimensionless oil recovery due to imbibition is defined as

$$R_{im} = (V_o - V)/V_o \quad (5)$$

Substitutions of Eqs. (3) and (4) into Eq. (5) result in

$$R_{im} = 1 - e^{-\lambda t} \quad (6)$$

for $\alpha = 1$, and

$$R_{im} = 1 - [1 - \lambda(1-\alpha) t / V_o^{1-\alpha}]^{1/(1-\alpha)} \quad (7)$$

for α not equal to unity, respectively.

Equation (6) was assumed by Aronofsky *et al.*⁴¹ in 1958 without derivation.

For the purpose of simplicity, Eq. (6) is used for analyzing imbibition data from Spraberry cores. A curve fit of Eq. (6) to the experimental data shown in Fig. 3.1 is obtained when the following relation is used:

$$\lambda t = 0.0001 t_D \quad (8)$$

Substituting Eq. (8) into Eq. (6) yields:

$$R_{im} = 1 - e^{-0.0001 t_D} \quad (9)$$

Fig. 3.2 shows that the shape of the recovery curve given by Eq. (8) for the Spraberry cores is similar to the recovery curve established for Berea cores as established by Ma et al.²

Application

Eq. (9) may be utilized for analyzing 44-years of waterflood performance in the Spraberry Trend Area. Assuming fracture spacing of 4 feet, imbibition oil recoveries from the two pay sands have been calculated using Eq. (9) and the absolute permeability. The result is plotted in Fig. 3.3 which indicates that permeability is one of the key factors affecting imbibition oil recovery. Using log-derived porosity and absolute permeability,⁴ an oil recovery profile in the 5U Unit of the Upper Spraberry zone has been estimated and found to be between 8% and 15.5% as shown in Fig. 3.4. Integration of the recovery profile along the depth of the pay zone resulted in an estimate of imbibition oil recovery from the 5U zone to be about 11%. This is higher than the observed⁶ 5-9% waterflood oil recovery from the Upper Spraberry sand. One of the reasons for the overestimation is believed to be wettability alteration of the sand under reservoir conditions. It has been observed that the oil recovery process is slower in our on-going imbibition experiment at reservoir temperature. Another reason may be the significant difference between the absolute permeability and the effective permeability for the very tight Spraberry sand. Yet another reason for the discrepancy may be the experimental conditions are not representative of reservoir conditions.

The oil-water relative permeability for cores taken from the Tippett #5 was utilized in this analysis.⁵ Relative permeability data has been correlated to the reduced water saturation as shown in Fig. 3.5. Empirical equations for relative permeability to water (k_{rw}) and relative permeability to oil (k_{ro}) are expressed in this study as follows:

$$k_{rw} = S_{wD}^{3.5} \quad (10)$$

and

$$k_{ro} = 0.71 (1-S_{wD})^9 \quad (11)$$

where the reduced water saturation (S_{wD}) is defined as

$$S_{wD} = S_w - S_{wi} \quad (12)$$

where S_w and S_{wi} are water saturation and initial water saturation, respectively. With known relative permeabilities, effective permeability to each phase (oil and water) can be estimated because the absolute permeability of the sand is known from core analysis and well logs. Using the effective oil permeability in the scaling equation, the result is shown in Fig. 3.6. It is indicated by Fig. 3.6 that oil recovery after 44 years of waterflood in the 5U Unit of the Upper Spraberry zone should be between 5.5% and 11% with an average of 7.7%. This value is close to, but still a little higher than the observed recovery (5-9%) from the Upper Spraberry.⁶ However, it is unclear if the effective oil permeability should be used in the scaling equation because the scaling equation was derived on the basis of absolute permeability.

Summary

Imbibition experiments conducted under ambient conditions suggest that the maximum recoverable oil by water imbibition is about 50% of original oil in place. The experimental imbibition data has been scaled to reservoir dimensions using the absolute and effective oil permeabilities respectively. Analysis for the 5U Unit of the Upper Spraberry zone indicates that the scaling result using the absolute permeability is higher than the observed oil recovery, while a good match between the scaled oil recovery and the field observed oil recovery was obtained using the effective oil permeability. More experiments are being conducted to verify the validity of our wettability determination procedures.

References

1. "Advanced Reservoir Characterization and Evaluation of CO₂ Gravity Drainage in the Naturally Fractured Spraberry Reservoir," PRRC Report No. 96-18, Quarterly Technical Report to DOE, DOE Contract No. DE-FC22-95BC14942. 1996
2. Ma, S., Zhang, X., and Morrow, N.R.: "Influence of Fluid Viscosity on Mass Transfer between Rock Matrix and Fractures," paper CIM 95-94, presented at the 46th Annual Technical Meeting of the Petroleum Society of CIM held in Banff, Alberta, Canada, May 14-17, 1995.
3. Gupta, A. and Civans, F.: "Correlation of the Imbibition Drive Matrix-to-Fracture Oil Transfer," paper SPE 28929.
4. Banik, A.K. and Schechter, D.S.: "Characterization of the Naturally Fractured Spraberry Trend Shaly Sands Based on Core and Log Data," paper SPE 35224 presented at the SPE Permian Basin Oil & Gas Recovery Conference held in Midland, Texas, 27-29 March, 1996.
5. Humble Oil & Refining Company: "Analysis of Cores from Well Tippet #5," Core Analysis Data Report 431, August 12, 1963, PRRC Spraberry Database.
6. Epic Consulting Services Limited: "Reasons for the Relatively Low Recovery of the

- Spraberry Waterfloods,” PRRC Spraberry Database, 1996.
7. Buckley, J.S., Bousseau, C., and Liu, Y.: “Wetting Alteration by Brine and Crude Oil: From Contact Angles to Cores,” paper SPE 30765 presented at the Ann. Tech. Conf. and Exhib., Dallas, Oct. 22-25, 1995.

3.2 Analysis of Inflow Performance of Spraberry Trend Area Wells

Introduction

A model study of a waterflooding pilot in Spraberry Trend Area indicated a NE-SW trend of the major fractures.¹ A contrast of 144/1 was required for the major/minor fracture trend permeability to match the pilot response. This strong anisotropic effective permeability implies the existence of well inter-connected, long natural fractures in the Spraberry reservoir. A characteristic of flow in long natural fractures is the pressure variation along the fracture should be significantly higher compared to that in a hydraulic fracture or a short natural fracture. Unfortunately, a method for analyzing flow behavior in reservoirs with long fractures is not readily available from the literature. This section presents a more rigorous analysis on productivity of wells intersecting long fractures. Equations presented in this paper are general and useful for estimating inflow performance relationship (IPR) of vertical and horizontal wells intersecting long fractures.

Several analytical solutions have been presented for transient flow in fractured reservoirs.²⁻⁸ Numerical models have also been developed for simulating fluid flow in fractured reservoirs.^{9,10} However, it is still customary for reservoir engineers to use equations derived for steady flow conditions. This is not only because the analytical transient-flow solutions and numerical simulators are not convenient to use in construction of IPR, but also because steady or pseudo-steady flow prevails as the dominating flow mechanism in the lifetime of most oil wells. Therefore, steady flow equations are more attractive rather than transient flow equations and numerical models for productivity analysis.

The first mathematical model for analyzing productivity of horizontal wells intersecting fractures was presented by Giger et al.^{11,12} Two solutions were proposed for short horizontal wells and long horizontal wells respectively. For both cases, flow in the rock matrix and flow in the fractures were formulated separately, and then combined to obtain an equation for flow in both regimes (from external boundary to wellbore). Radial flow was assumed in the fracture for both short and long well cases. For the case of a short horizontal well, they employed a radial flow equation presented by Muskat¹³ for matrix flow from external boundary to a small fracture. For the long horizontal well case, a flow equation developed by Houpeurt¹⁴ for flow in matrix from external boundary to an extended fracture was utilized. The drawback of Giger’s approach is that the equations for flow from external boundaries to the fractures were derived based on the assumption that the pressure in the fracture is uniform (invariant along the fracture length and height). Karcher et al.⁹ calculated productivity increase of fractured horizontal wells over fractured vertical wells using equations presented by Giger.¹² Consistent results were obtained. They also investigated issues of increasing

productivity, reducing coning, and improved sweep efficiency by multi-fractured horizontal wells using their numerical simulation for infinite conductivity fractures. Joshi¹⁵ proposed a steady state flow equation for analyzing productivity of horizontal wells. His equation for flow in the matrix was also derived based on the assumption of constant pressure in the fracture (infinite conductivity fracture). Joshi¹⁶ presented a review of horizontal well technology. He pointed out that in most fracture jobs it is difficult to obtain infinite conductivity and, moreover, fracture conductivity decreases over time. Mukherjee and Economides¹⁷ developed a simplified steady-state approach to calculate the number of infinite conductivity fractures equivalent to a drainhole. Their model was developed on the basis of the inflow performance relationship suggested by Joshi¹⁵ with Prats'¹⁸ correlation of dimensionless wellbore radius. Economides et al.¹⁰ performed a comprehensive simulation of horizontal-well performance. Their results agree well with Joshi's¹⁵ equation. Raghavan and Joshi¹⁹ presented a steady flow solution based on uniform flux along the fracture length. This solution was presented as valid for finite-conductivity fractures with a specific dimensionless fracture conductivity value of $C_{fD}=4.4$. Guo and Evans²⁰ performed analyses similar to that of Giger's¹² except that direct flow from matrix to wellbore, reservoir anisotropy, and multi-phase flow were included in the mathematical models. Like Giger's¹² model, Guo and Evans'²⁰ models were also derived assuming uniform pressure in the fracture when the flow in matrix was formulated using Darcy's law. Recently, Li et al.²¹ presented an approximate formula for predicting performance of fractured horizontal wells. It was assumed that oil first flows linearly from the external reservoir boundary to the vicinity of a vertical fracture, then turns 90 degrees and flows linearly to the fracture face while pressure in the fracture is equal at all points. Flow in the fracture was assumed to be linear away from the wellbore and radial near the wellbore. The drawback of their formulation is similar to that of Giger's and Guo and Evans'.

In summary, most steady flow equations presented by previous investigators for productivity analysis of fractured horizontal wells rely on the assumption of infinite conductivity fractures (invariant pressure in the fracture) when the flow from external boundary to the fracture was formulated. While the mathematical problems were very much simplified by using this assumption, reliability of the solutions is questionable. Only one analytical solution dealing with horizontal wells in finite-conductivity fractures was reported in the literature.¹⁹ This solution is applicable to fractured reservoirs where fractures have dimensionless conductivity of 4.4 and the flux in the fractures is uniform, which may not occur in practice.

This paper presents a simple and more rigorous mathematical model for predicting performance of vertical and horizontal wells intersecting fractures fully penetrating reservoir sections. An important feature of the new model is that it was derived by rigorous coupling of flow in the matrix and flow in the fracture, where a unique pressure distribution was consistently used both for flow in the matrix and for flow in the fracture. Another feature of the new model is simplicity of use by reservoir engineers. This is because the equations in the model are closed and in a very simple form. However, this model was derived for wells intersecting long fractures where 1-dimensional flow to the fracture face dominates in the matrix. Care needs to be taken when this model is used for estimating performance of wells

intersecting short, highly conductive fractures where significant 2-dimensional (in x and y directions as discussed in Appendix A) flow may exist in the matrix. It is probable that both long and relatively short fractures contribute in Spraberry.

This mathematical model has been utilized for analyzing performance of wells intersecting natural fractures in the Spraberry Trend Area, West Texas. Use of the model to match production data aided in the understanding of the unusual primary behavior of Spraberry Trend Area reservoirs.

Mathematical Model

A simple and more rigorous mathematical model has been derived in this study for estimating productivity of vertical and horizontal wells intersecting long fractures, where pressure variation in the fracture is of significance. While derivation of the model is presented in detail in Appendix A, resultant equations for flow of an incompressible fluid in a fracture wing are summarized in this section.

Pressure in a Fracture

Pressure distribution in a fracture may be estimated using Eq. (1):

$$p_f(x) = p_e - (p_e - p_w)e^{\sqrt{c}(x-x_f)} \quad (1)$$

where x is the distance from the fracture tip, $p_f(x)$ is fracture pressure at point x, p_e is the pressure at the drainage boundary, p_w is the flowing bottom hole pressure, x_f is the length of a fracture wing (from fracture tip to wellbore), and c is defined as a group of variables:

$$c = \frac{2k_z}{z_e w k_f} \quad (2)$$

where k_z is the permeability of the rock matrix in the direction perpendicular to the fracture face, z_e is the distance from the fracture to the drainage boundary of the fracture, w is the average fracture width (aperture), and k_f is the fracture permeability. Consistent units should be used in Eqs. (1) and (2) so that the exponential function is dimensionless.

Inflow Performance Relationship (IPR)

Production rate Q from a fracture wing is given by Eq. (3) in field units:

$$Q = \frac{0.00254k_z h}{B_o \mu z_e \sqrt{c}} (p_e - p_w)(1 - e^{-\sqrt{c}x_f}) \quad (3)$$

where h is the fracture height, B_o and μ are formation volume factor and viscosity of oil, respectively. Productivity index PI for the fracture wing is given by

$$PI = \frac{Q}{p_e - p_w} = \frac{0.00254k_z h}{B_o \mu z_e \sqrt{c}} (1 - e^{-\sqrt{c}x_f}) \quad (4)$$

It must be noted that these inflow equations were derived assuming that one-dimensional flow dominates the flow from the drainage boundary to the fracture face in the rock matrix. This is an ideal situation where the fracture extends to no-flow boundaries. If the fracture is not long enough to reach no-flow boundaries, pressure drawdown at the fracture tip may not be negligible compared to drawdown in the wellbore, and significant two-dimensional flow may exist near the fracture tip. In such cases, results from this mathematical model may be erroneous. To ensure the applicability of the mathematical model to a given fractured reservoir, the minimum fracture length should be checked before using the equations. This is discussed as follows. A conservative estimation of the minimum length of the fracture above which this model is applicable can be determined using Eq. (1). The relative pressure drawdown at the fracture tip ($x=0$) can be determined from Eq. (1) to be

$$\frac{p_e - p_{x_f}}{p_e - p_w} = e^{-\sqrt{c}x_f} \quad (5)$$

where p_{x_f} is the pressure at the fracture tip. The fracture half length x_f can be solved from Eq. (5):

$$x_f = -\frac{1}{\sqrt{c}} \ln \frac{p_e - p_{x_f}}{p_e - p_w} \quad (6)$$

Eq. (6) can be utilized to estimate the minimum required fracture length for a given relative pressure drawdown ($p_e - p_{x_f}$)/ ($p_e - p_w$) at the fracture tip. For example, if the maximum allowable relative pressure drawdown at the fracture tip is 5% , the drainage boundary for the fracture is 2 feet, matrix permeability is 0.5 md, fracture width and permeability are 0.002 inch and 20 Darcies respectively, the minimum required length of the fracture wing is calculated to be 7.74 feet.

Relation between Fracture Width and Permeability

Application of the new mathematical model requires information regarding fracture width w and fracture permeability k_f . However, these two parameters should not be used independently because they are closely related. Similar to the cubic law²² which describes the relationship between fracture width and fracture conductivity, a simple relation between fracture width and fracture permeability is derived analytically in Appendix B and summarized as follows:

$$k_f = \frac{\phi_f^3 w^2}{12} \quad (7)$$

where ϕ_f is the fracture porosity accounting for volume of minerals, crushed rock, and proppant introduced during hydraulic fracturing operations. If the fracture porosity and permeability are known, fracture width can be estimated using Eq. (8):

$$w = \sqrt{\frac{12k_f}{\phi_f^3}} \quad (8)$$

Stress-Sensitive Fractures

It has been reported that productivity of some wells intersecting naturally fractured reservoirs decline rapidly as wellbore/reservoir pressure declines.²³ It has been postulated that partial closure of fractures is responsible for this behavior. As the pressure in the fracture decreases, fracture aperture could conceivably decrease and effective stress at the fracture face would thus increase to support the matrix. The partially closed fracture should have a much lower conductivity resulting in lower productivity of the well. Walsh's model²⁴ for conductivity in a fracture is frequently employed for correlating both laboratory and field data.²³ Since conductivity and permeability are equivalent, both representing flow resistance of the medium for given fluid properties, the following simplified relation similar to Walsh's model may be utilized for fracture permeability analysis:

$$k_f^n = A + B \ln(\sigma - \alpha p) \quad (9)$$

where k_f is fracture permeability, A and B are constants, σ is the confining stress, p is the pore pressure, α is the poroelastic parameter defining the effective-stress law, and the exponent n is 1/3 according to Walsh. The $(\sigma - \alpha p)$ term represents the effective stress. Assuming that the fracture permeability is k_{fo} at unit effective stress, the constant A can be determined to be k_{fo}^n , and Eq. (9) becomes

$$k_f^n = k_{fo}^n + B \ln(\sigma - \alpha p) \quad (10)$$

Substituting of Eq. (10) into Eq. (8) yields

$$w = \sqrt{\frac{12}{\phi_f^3} [k_{fo}^n + B \ln(\sigma - \alpha p)]^{\frac{1}{2n}}} \quad (11)$$

Combination of Eqs. (10) and (11) gives the following expression for the product of fracture width and fracture permeability that appears in Eq. (2):

$$wk_f = \sqrt{\frac{12}{\phi_f^3} [k_{fo}^n + B \ln(\sigma - \alpha p)]^{\frac{3}{2n}}} \quad (12)$$

If the fracture width and porosity at unit effective stress are denoted by w_o and ϕ_{fo} , Eq. (12) can be simplified as

$$wk_f = w_o k_{fo} [1 - D \ln(\sigma - \alpha p)]^{\frac{3}{2n}} \quad (13)$$

where D is a constant and its value reflects sensitivity of fracture conductivity to the effective stress.

It can be shown that if the cubic law²² for a fracture, rather than Eq. (7), is used in the derivation, the exponent $3/2n$ in Eq. (13) is 4. This exponent is 4.5 if Walsh's $n=1/3$ is used. Warpinski and Teufel showed that the value of n varies for different rocks and an n value of 0.515 for chalk was reported. This corresponds to an exponent $3/2n$ of 2.91 for chalk.²³

Applications

The newly developed mathematical model can be used for analyzing and understanding the unusual behavior of Spraberry Trend Area reservoirs. The Spraberry Field of West Texas was discovered in 1949 and was considered the largest field in the world. The Spraberry encompasses a productive area greater than 2,500 square miles and consists of a 1,000-ft section of sandstones, shales and limestones. The productive sands are relatively thin as was demonstrated in Section 1. All sands have matrix permeabilities of 1 md or less and porosities of 8-15 per cent. Initial water saturation varies from 0.25 to 0.60 in productive sands. Initial reservoir pressures were approximately 2,300 psi in the Upper Spraberry. Bubble point pressure of Spraberry oil is about 1,900 psi.²⁶ Oil viscosity at the saturation pressure is about 0.71 cp.²⁷ Spraberry wells typically produced 100-400 bopd initially after hydraulic fracture treatment. Primary oil recovery by solution gas drive is less than 10 per cent of oil in place. Waterflooding in the Spraberry was initiated after two pilot tests conducted by Atlantic and Humble.²⁸ While the unconfined Atlantic pilot was disappointing, the Humble pilot was promising. Oil production of the center well increased from 50 bopd to 256 bopd in four months. A model study of the Humble pilot indicated a NE-SW (N50°E) trend for the major fractures.²⁷ A major/minor fracture trend permeability contrast of 144/1 was required to match the pilot response.

The Spraberry Field presents unusual problems for both primary production and waterflooding. After more than 40 years of waterflooding, the current oil recovery is still less than 15 per cent. The reasons for the low productivity of Spraberry wells and disappointing imbibition waterflooding remain a mystery to this day. Various hypotheses have been proposed to explain the poor behavior of waterflooding. These hypotheses include: lack of pattern confinement and injection well density, incorrect well pattern alignment, weak wettability to water of the reservoir rock and fracture mineralization which could restrict crossflow,²⁸ and low permeability to oil after waterflooding of the gas-saturated reservoir, etc.²⁹ The new mathematical model presented in the previous section is used here for analyzing performance of Spraberry wells. This analysis may be helpful for understanding Spraberry reservoir performance.

According to interpretations of a tracer test,³⁰ fracture lengths in Spraberry are probably less than the interwell distance (<1,800 feet). Schechter et al.²⁸ found that the fractures vanish at

shale-sand interface. It may be a good assumption that the fracture height is equal to the thickness of the pay zone. Elkins²⁷ summarized fracture analyses and reported that fracture spacing varies from a few inches to a few feet. Schechter et al.²⁸ estimated that fracture spacing in the 1U Unit of the Upper Spraberry is about 4 feet. Based on 111 measurements of fracture openings, Elkins²⁷ reported that the fracture width ranged up to 0.013 inch and averaged 0.002 inch. This number agrees with Christie's²⁶ estimation of fracture width of 0.002-0.004 inch based on flow rates and measurement of the fractures in cores. Brownscombe and Dyes³¹ reported 0.002-0.003 inch fracture width and 3-4 foot fracture spacing. All of these numbers are applied with caution since there was no distinction between coring induced and natural fractures when all of this data was accumulated. The in-situ fracture width in the reservoir may be estimated based on well tests. Well testing^{32,33} has not shown dual porosity pressure transient behavior. This indicates that the fracture volume is less than 1/1000 of the matrix volume.²⁸ Assuming that matrix volume is on the order of 8,000 bbl/acre then the fracture volume should be less than 8 bbl/acre, or 45 cubic feet in a square area of 209 ft by 209 ft assuming a 10-foot-thick pay zone. If a fracture spacing of 4 feet is assumed in the area, at most 52 fractures exist in the area. The maximum fracture width can then be estimated to be 0.005 inch. However, if the fracture spacing is 2 feet in the area, the maximum fracture width should then be about 0.0025 inch.

Primary Production

Initial Production: The mechanism of primary oil production in the Spraberry Trend Area is believed to be dominated by solution gas drive.²⁷ Initial potential of wells was estimated to be 5 to 10 bopd before hydraulic fracture treatment. Eq. (3) has been used to calculate productivity of a Spraberry well under primary production. Data used in the calculations are presented in Table 3.1. This table shows that Eq. (3) gives a capacity of 5.01 bopd from each fracture. Comparison of this oil rate with actual production rate indicates that the wellbore might intersect one or two natural fractures due to extension of drilling induced fractures.

Hydraulically Fractured Well: Initial potential of a typical Spraberry well was 100 to 400 bopd after hydraulic fracture treatment. Table 1 also shows calculated production rate of a hydraulically fractured well using Eq. (3). The calculated production rate from each fracture is 31.45 bopd. Comparison with actual production rate of 100-400 bopd indicates that the hydraulic treatment might intersect 3 to 13 natural fractures depending upon the scale of the treatment. It appears that hydraulic fracturing probably caused more natural fractures to become connected to the wellbore, rather than opening and extending an existing natural fracture.

Productivity Decline: Eqs. (3) and (13) have been used for matching the production data from a 1951 shut-in test in the X.B. Cox A-4 in the Driver Unit of the Spraberry Trend Area. Based on a micro-fracture test in the E.T. O'Daniel #37,³⁴ the minimum horizontal stress in the Upper Spraberry formation is about 3200 psi (0.447 psi/ft). Rapid productivity decline of the well could not be matched by the equations when this minimum stress was utilized. However, when the drawdown, instead of the effective stress, was used in Eq. (13), a match

to the production data was achieved. The stress sensitivity factor (D in Eq. (13)) has been determined to be about 0.1. Table 3.2 shows data used for matching. Matched production rate and productivity index is plotted in Fig. 3.7. The matched parameters have been used for estimation of productivity of 5 shut-in tests in the Driver Unit. Figures 3.8 through 3.12 show the comparison between the calculated oil production rates and actual oil production rates observed from the 5 shut-in wells. These figures indicate that calculated and actual oil rate match well at most points except at the point corresponding to the time of April 1952. The reason for the discrepancy is not clear. Fig. 3.13 shows a comparison between the calculated oil production rates and actual oil production rates observed from 6 regularly producing wells. Consistency between calculated and actual productivity index of the 6 wells is also observed as shown in Fig. 3.14. However, direct application of the stress sensitivity factor of 0.1 to some of the regularly producing wells under-estimated decline of productivity. The result in Figs. 3.13 and 3.14 was obtained assuming that stress-sensitivity factor increases with time slightly. For example, to match data from the Davenport B-14, the stress-sensitivity factor D was increased from 0.1 to 0.105 for a three month time.

Waterflooding

Unusual Behavior: Large scale waterflooding in the Driver Unit was initiated in July, 1960. It was found that oil production rate was very sensitive to whether the water injection wells were shut-in or not.^{25,35} Oil rate was low during water injection and high when injection wells were shut-in. Consequently, a high-rate cyclic waterflooding (pressure pulsing) scheme was adopted in the Sohio-operated Driver Unit. This production scheme was very successful in the beginning. However, after three cycles of water injection, it was found long-term performance of the cyclic waterflood to be no better than that achieved with much slower steady water injection in a Mobil cooperative waterflood.³⁶ The interpretation of the mechanism of cyclic water injection has never been satisfactory. Elikins and Skov²⁵ presented a hypothesis for explaining the behavior of the reservoir subjected to cyclic water injection. It was written in their paper that “over-injection might have been responsible for the absence of waterflood oil at water breakthrough. It appeared that cessation of water injection to permit capillary forces to become dominant and expansion of the rock and its contained fluids during pressure reduction might aid in expulsion of oil from the rock matrix into the fractures.” It is possible that the sensitivity of fracture conductivity to effective stress in the fracture dominates the mechanism of cyclic water injection. Fig. 3.15 shows calculated pressure distributions along a stress-insensitive fracture. It is seen that if the fracture width is 0.015 inch, the drainage distance in the fracture may be up to 300 feet from the wellbore. Fig. 3.16 shows calculated pressure distributions along a stress-sensitive fracture. The stress sensitivity factor used in the calculation is 0.1. It is seen from Fig. 3.16 that if the fracture width is 0.015 inch, the drainage distance in the fracture may be only 30 feet from the wellbore, which is 10 times less than 300 feet. This concept of stress-sensitivity may be used to explain cyclic waterflooding behavior. Consider a wellbore intersecting several natural fractures after hydraulic fracture treatment. Let us divide these fractures into two groups: group A and group B. Let fractures in group A represent fractures situated near the line

between an injection well and a production well, and let fractures in group B represent fractures located far from the line between the injection well and the production well, as depicted in Fig. 3.17. Obviously, the flow resistance from the injection well to the production well through fractures in group A is less than that through fractures in group B. This is because the flow path in group B fractures is longer than that in the group A fractures. During high-rate water injection, fractures in both group A and group B should open, and a higher proportion of water flows from the injector to the producer through path A rather than through path B. Since path A contains less oil expelled from the rock by capillary pressure than path B, high water cut is expected from the producer. However, when the injector is shut-in, the pressure in path A should drop faster than the pressure in path B. As a result, fractures in path A close (to some degree) faster than that in path B. Since path B contains more oil, lower water-cut is expected at the producer. After resumption of water injection, more water should enter path B because some of the fractures near the injector in group B should still be open, and low water cut production is expected to remain for a certain time before path A opens for water influx. This phenomenon was observed from all the three cycles of water injection in the Driver Unit (see Figure 4 in reference 35). As the number of cycles increase, oil supply from path B decreases due to low rate of water imbibition. Oil production rate should also decrease, and eventually, the cyclic water injection scheme should be no better than steady low rate water injection scheme. This was also observed from the Driver Unit waterflood.

Productivity: After three cycles of waterflooding, productivity in the Driver Unit declined to a level equivalent to low rate waterflooding. Since then low rate waterflooding has been carried out over many years. Well performance has been poor although pattern injections are sparse. Large volume hydraulic fracturing treatments were conducted on several wells.³⁵ The results were unsatisfactory as large-scale treatments improve productivity only very little.

Table 3.3 shows a comparison between actual production rate and calculated production rate for three wells before and after hydraulic treatments. Results indicate that the calculated pre-fracture oil rates match the actual pre-fracture oil rates when tight natural fractures are assumed, indicating that compacted natural fractures exist in the reservoir under high drawdown conditions. Table 3.3 also indicates that calculated post-fracturing oil rates match the actual post-fracturing oil rates if improvement in fracture conductivity is poor. This may be an indication that proppant was pumped into existing natural fractures rather than hydraulically induced fractures. This is evident based on Ogden and Locke's³⁷ analysis indicating that the high leakoff encountered is unlikely to be a result of the matrix permeability. If this is true, proppant in the natural fractures may have been crushed during production because of a low concentration in the fractures. As a result, well productivity has remained low. This hypothesis is also consistent with the observation by Barba et al.³⁸ It was written in their paper that "although it is apparent that the natural fractures were open during drilling, logging, and stimulation operations, they were clearly no longer open when normal reservoir condition were restored." However, to what degree the fractures are open needs further investigation.

Possible Solutions: Tremendous oil reserves in the Spraberry reservoir keeps operators searching for better methods of producing oil. The above analysis implies that probably there is no proppant that is strong enough to withstand the stress in the fracture under low reservoir pressure conditions because of low proppant concentration. However, several possible solutions to the low productivity problem in the Spraberry reservoir exist. Schechter and Guo³⁹ have demonstrated that CO₂ gravity drainage may be a promising method to recover oil from the Spraberry reservoir. The second solution might be acidizing fractures while waterflooding. Significant mineralization has been found on fracture surfaces in core taken from the Spraberry. Saleta et al.⁴⁰ found that the composition of the minerals on the fracture surface is primarily calcite or barite. Thin section analysis indicates that it is impossible for water to imbibe into the rock across layers of minerals on the surface of the fractures. If a large portion of natural fractures are found to be mineralized, acidizing fractures while waterflooding should be investigated. Another possible solution is to fracture hydraulically the pay zones with porous cement which should be stronger than low concentration proppant to keep fractures open, at least around wellbore. The combination of the three measures may lead to performance enhancement.

Conclusions

1. A simple and more rigorous mathematical model has been developed for estimating productivity of wells intersecting long fractures. The model reveals that pressure variation is significant in tight fractures.
2. This model helps to understand the unusual performance of Spraberry reservoirs. Matching of the new model to production data indicates that:
 - i) During primary production, a Spraberry wellbore interconnected 1 to 2 natural fractures due to extension of drilling induced fractures before hydraulic treatment.
 - ii) A Spraberry wellbore interconnects several natural fractures after hydraulic fracture stimulation.
 - iii) Stress-sensitive fracture conductivity may be partially responsible for the decline of well productivity in the Spraberry Trend Area. However, other factors, such as gas saturation, can similarly affect the decline of well productivity in the area. Further investigations need to be conducted.
 - vi) Currently natural and hydraulic fractures in the Spraberry reservoir may, or may not, be closed depending upon local pore pressures in the fractures. Fractures near high-drawdown wellbores may be compacted and closed to some degree.
 - v) Large scale hydraulic fracturing treatments were not helpful probably due to low concentration of proppant spread in a large volume of natural fractures. Horizontal

wells may not provide significant help if a high pressure drawdown is utilized during oil production.

3. Cyclic waterflood performance in the Spraberry can be interpreted based on the theory of stress-sensitive fracture conductivity.
4. Integration of CO₂ flooding, fracture acidizing and utilization of porous cement as a fracturing fluid may be potential measures for improving well productivity in the Spraberry Trend Area.

Nomenclature

A	=	constant in Walsh's equation.
B	=	constant in Walsh's equation
B _o	=	formation volume factor of oil
c	=	a group of variables defined by Eq. (2)
c ₁	=	integration constant
c ₂	=	integration constant
C _{FD}	=	specific dimensionless fracture conductivity
D	=	stress-sensitivity factor
f	=	friction factor
h	=	fracture height
k _f	=	permeability of fracture
k _{fo}	=	permeability of fracture at unity effective stress
k _z	=	permeability of matrix in z-direction
L	=	fracture length
n	=	conductivity exponent
p	=	pore pressure
p _d	=	pressure drawdown in fracture
p _d *	=	pressure drawdown in wellbore
p _d '	=	derivative of pressure drawdown with respect to distance
p _e	=	pressure at drainage boundary
p _f (x)	=	fracture pressure at point x
PI	=	productivity index
p _w	=	flowing bottom hole pressure
p _{xf}	=	fracture pressure at point x=x _f
Q	=	total oil flow rate from one wing of fracture
Q(x)	=	flow rate in fracture at point x
R _e	=	Reynold's number
v	=	interstitial velocity
v _D	=	Darcy velocity
v _z	=	velocity in z-direction

w	=	fracture width (aperture)
w_o	=	fracture width (aperture) at unity effective stress
x	=	distance from fracture tip
x_f	=	length of a fracture wing
y	=	vertical distance
z	=	distance in the direction perpendicular to fracture face
z_e	=	distance between fracture and drainage boundary
α	=	poroelastic parameter defining effective stress law
Δp	=	pressure drop across fracture length L
μ	=	oil viscosity
ρ	=	oil density
σ	=	confining stress
ϕ_f	=	fracture porosity
ϕ_{fo}	=	fracture porosity at unity effective stress

References

1. Barfield, E.C., Jordan, J.K. and Moore, W.D.: "An Analysis of Large-Scale Flooding in the Fractured Spraberry Trend Area Reservoir," *J. Pet. Tech.* (April 1959) 15-19.
2. Soliman, M. Y., Hunt, J.L., and El Rabaa, W.: "Fracturing Aspects of Horizontal Wells," *JPT* (Aug. 1990) 966-73.
3. Chen, C.C., Ozkan, E., and Raghavan, R.: "A Study of Fractured Wells in Bounded Reservoirs," paper SPE 22717 presented at the 1991 SPE Annual Technical Conference and Exhibition held in Dallas, Texas, Oct. 6-9, 1991.
4. Cinco-L., H., Samaniego-V., F., and Dominguez-A., N.: "Transient Pressure Behavior for a Well with a Finite-Conductivity Vertical Fracture," *SPEJ* (Aug. 1978) 253-64.
5. Ozkan, E., and Raghavan, R.: "New Solutions for Well-Test-Analysis Problems: Part 1 - Analytical Considerations," *SPEFE* (Sept. 1991) 359-65.
6. Chu, W., and Shank, G.D.: "A New Model for a Fractured Well in a Radial, Composite Reservoir," *SPEFE* (Sept. 1993) 225-32.
7. Beier, R.A.: "Pressure-Transient Model for a Vertically Fractured Well in a Fractal Reservoir," *SPEFE* (June 1994) 122-28.
8. Chen, C., and Raghavan, R.: "Modeling a Fractured Well in a Composite Reservoir," *SPEFE* (Dec. 1995) 241-46.
9. Karcher, B.J., Giger, F.M., and Combe, J.: "Some Practical Formulas to Predict Horizontal Well Behavior," paper SPE 15430, presented at the 1986 SPE Annual Technical Conference and Exhibition held in New Orleans, Louisiana, Oct. 5-8, 1986.
10. Economides, M.J., Delmbacher, F.X., Brand, C.W., and Heinemann, Z.E.: "Comprehensive Simulation of Horizontal-Well Performance," *SPEFE* (Dec. 1991) 418-26.

11. Giger, F.M., Reiss, L.H., and Jourdan, A.P.: "The Reservoir Engineering Aspect of Horizontal Drilling," paper SPE 13024 presented at the 1984 SPE Annual Technical Conference and Exhibition in Houston, Texas, Sept. 16-19, 1984.
12. Giger, F.M.: "Horizontal Wells Production Techniques in Heterogeneous Reservoirs," paper SPE 13710, presented at the SPE 1985 Middle East Oil Technical Conference and Exhibition held in Bahrain, March 11-14, 1985.
13. Muskat, M.: *The Flow of Homogeneous Fluids through Porous Media*, I.H.R.D.C., Boston, 1982.
14. Houpeurt, A: *Elements de mecanique des fluides dans les milieux poreux*, Editions Technip, Paris, 1975.
15. Joshi, S.D.: "Augmentation of Well Productivity with Slant and Horizontal Wells," SPE 15375, 1986; *JPT* (June 1988) 729-39; *Trans. AIME*, **285**.
16. Joshi, S.D.: "A Review of Horizontal Well and Drainhole Technology," paper SPE 16868, presented at the 1987 SPE Annual Technical Conference and Exhibition held in Dallas, Texas, Sept. 27-30, 1987.
17. Mukherjee, H., and Economides, M.J.: "A Parametric Comparison of Horizontal and Vertical Well Performance," *SPEFE* (June 1991) 209-16.
18. Prats, M.: "Effect of Vertical Fractures on Reservoir Behavior -- Incompressible Fluid Case," *SPEJ* (June 1961) 105-16; *Trans. AIME*, **222**.
19. Raghavan, R., and Joshi, S.D.: "Productivity of Multiple Drainholes or Fractured Horizontal Wells," *SPEFE* (March 1993) 11-16.
20. Guo, G., and Evans, R.D.: "Inflow Performance of a Horizontal Well Intersecting Natural Fractures," paper SPE 25501, presented at the SPE Production Operations Symposium held in Oklahoma City, Oklahoma, March 21-23, 1993.
21. Li, H., Jia, Z., and Wei, Z.: "A New Method to Predict Performance of Fractured Horizontal Wells," paper SPE 37051, presented at the 1996 SPE International Conference on Horizontal Well Technology held in Calgary, Canada, November 18-20, 1996.
22. Van Golf-Racht, D.T.: *Fundamentals of Fractured Reservoir Engineering*, Elsevier Scientific Publishing Co., New York, 1982.
23. Warpinski, N.R., and Teufel, L.W.: "Effect of Stress and Pressure on Gas Flow Through Natural Fractures," paper SPE 22666, presented at the 1991 SPE Annual Technical Conference and Exhibition held in Dallas, Texas, Oct. 6-9, 1991.
24. Walsh, J.B.: "Effect of Pore Pressure and Confining Pressure on Fracture Permeability," *Int. J. Rock Mech., Min. Sci. & Geomech. Abstr.*, **18**, 1981, 429-35.
25. Elkins, L.F., and Skov, A.M.: "Cyclic Water Flooding the Spraberry Utilizes 'End Effects' to Increase Oil Production Rate," *JPT* (Aug. 1963) 877-84.
26. Christie, R.S., and Blackwood, J.C.: "Production Performance in Spraberry," *Oil & Gas Journal* (April 7, 1952) 107-15.
27. Elkins, L.F.: "Reservoir Performance and Well Spacing, Spraberry Trend Area Field of West Texas," *Trans. AIME*, **198**, (1953) 177-96.
28. Schechter, D.S., McDonald, P., Sheffield, T., and Baker, R.: "Reservoir Characterization and CO₂ Pilot Design in the Naturally Fractured Spraberry Trend Area," paper SPE

- 35469, presented at the SPE Permian Basin Oil & Gas Recovery Conference held in Midland, Texas, 27-29, March 1996.
29. Epic Consulting Services Limited: "Reasons for the Relatively Low Recovery of the Spraberry Waterfloods," (July 1996) PRRC Spraberry Database.
 30. Howell, W.D., Armstrong, F.E., and Watkins, J.W.: "Radioactive Gas Tracer Survey Aids Waterflood Planning," *World Oil* (Feb. 1961).
 31. Brownscombe, E.R. and Dyes, A.B.: "Water Imbibition Displacement - Can It Release Reluctant Spraberry Oil?" *Oil & Gas Journal* (November 3 1952) 264-65.
 32. Baker, R.: "Pressure Test Analysis for Midkiff 25-08 ," (April 1994) PRRC Spraberry Database.
 33. Baker, R.: "Vertical Pulse Test Analysis of Shackelford 1-38A," (April 1994) PRRC Spraberry Database.
 34. Pedersen, S.H.: "In-Situ Stress Evaluation in the Spraberry Trend," presentation at the Naturally Fractured Reservoir Forum held 19 April 1995 in Socorro, New Mexico. PRRC Spraberry Database.
 35. Elkins, L.F., Skov, A.M., and Gould, R.C.: "Progress Report on Spraberry Waterflood Reservoir Performance, Well Stimulation and Water Treating and Handling," *JPT* (Sept. 1968) 1039-49.
 36. Guidroz, G.M.: "E.T. O'Daniel Project -- A Successful Spraberry Flood," *JPT* (Sept. 1967) 1137-40.
 37. Ogden, V. and Locke, J.: "What Are the Facts and Figures for Spraberry Trend Core Analysis," *Oil & Gas Journal* (Jan. 14, 1952) 97-99.
 38. Barba, R.E. Jr., and Cutia, A.S.: "Evaluating Horizontal Well Potential in the Spraberry Trend," paper SPE 23949, presented at the SPE Permian Basin Oil & Gas Recovery Conference held in Midland, Texas, 18-20, March 1992.
 39. Schechter, D.S., and Guo, B.: "Mathematical Modeling of Gravity Drainage After Gas Injection into Fractured Reservoirs," paper SPE 35170, presented at the SPE Improved Oil Recovery Symposium held in Tulsa, Oklahoma, 22-24 April, 1996.
 40. Saleta, C.J., Banik, A.K., Cather, M.E., and Schechter, D.S.: "Application of Analytical Techniques to Evaluate the Heterogeneities of the Upper Spraberry Formation (Permian) and Its Influence on the Quality of the Midland Basin Reservoir in West Texas," SPE 35225, presented in the poster session at the SPE Permian Basin Oil & Gas Recovery Conference held in Midland, Texas, 27-29, March 1996.
 41. Aronofsky, J.S., Masse, L., and Natanson, S.G.: "A Model for the Mechanism of Oil Recovery from the Porous Matrix due to Water Invasion in Fractured Reservoirs," *Trans. AIME*, **213**, (1958) 17-19.

Table 3.1 - Well Productivity Before and After Hydraulic Fracturing Treatment for Primary Production

	Before Treatment	After Treatment
Matrix permeability, md	0.8	0.8
Water saturation	0.38	0.38
Residual oil saturation	0.15	0.15
Oil viscosity, cp	0.71	0.71
Formation volume factor	1.385	
Fracture spacing, ft	3	3
Fracture length, ft	200	600
Fracture height, ft	15	15
Initial fracture width, in	0.002	0.007
Initial fracture porosity	0.56	0.58
Reservoir pressure, psig	2400	2400
Flowing bottom hole pressure, psig	1900	1900
Stress sensitivity factor	0.1	0.1
Calculated oil production rate per fracture, bopd	5.01	31.45
Typical oil production rate per well, ²⁵ bopd	5 - 10	100 - 400

Table 3.2 - Data Used for Matching Productivity Decline of X. B. Cox A-4

Month during 1952	March	April	May	June
Matrix permeability, md	0.8	0.8	0.8	0.8
Water saturation	0.38	0.38	0.38	0.38
Residual oil saturation	0.15	0.15	0.15	0.15
Oil viscosity, cp	0.90	0.95	1.0	1.0
Formation volume factor, v/v	1.310	1.295	1.285	1.285
Fracture spacing, feet	3	3	3	3
Fracture length, feet	600	600	600	600
Fracture height, feet	15	15	15	15
Initial fracture width, inch	0.005	0.005	0.005	0.005
Initial fracture porosity	0.6	0.6	0.6	0.6
Number of fractures	5	5	5	5
Reservoir pressure, psig	1650	1600	1500	1400
Flowing bottom hole pressure, psig	1000	1000	800	750
Stress sensitivity factor	0.1	0.1	0.1	0.1
Calculated oil production rate, bopd	101	89	84	75
Actual oil production rate, bopd	100	85	80	75
Calculated productivity index, B/D/psi	0.156	0.149	0.119	0.115
Actual productivity index, B/D/psi	0.160	0.140	0.099	0.087

Table 3.3 - Productivity of Depleted Wells in Driver Unit Before and After Large Scale Hydraulic Treatment

	Well 385		Well 389		Well 397	
	Pre-Frac.	Post-Frac.	Pre-Frac.	Post-Frac.	Pre-Frac.	Post-Frac.
Matrix permeability, md	0.8	0.8	0.8	0.8	0.8	0.8
Initial water saturation	0.38	0.38	0.38	0.38	0.38	0.38
Water saturation	0.50	0.50	0.50	0.50	0.50	0.50
Residual oil saturation	0.20	0.20	0.20	0.20	0.20	0.20
Oil viscosity, cp	1.5	1.3	1.5	1.3	1.7	1.6
Formation volume factor	1.18	1.22	1.18	1.22	1.16	1.16
Fracture spacing, feet	3	3	3	3	3	3
Fracture length, feet	600	600	600	600	600	600
Fracture height, feet	15	15	15	15	15	15
Initial fracture width, inch	0.003	0.005	0.003	0.004	0.002	0.0025
Initial fracture porosity	0.60	0.63	0.59	0.57	0.45	0.49
Number of fractures	4	4	3	3	4	4
Reservoir pressure, psig	1575	1480	1725	1565	1885	1635
Flowing bottom hole pressure, psig	370	530	350	505	180	190
Stress sensitivity factor	0.1	0.1	0.1	0.1	0.1	0.1
Calculated oil production rate, bopd	16	39	11	17	7	10
Actual oil production rate, bopd	15	39	11	17	7	10

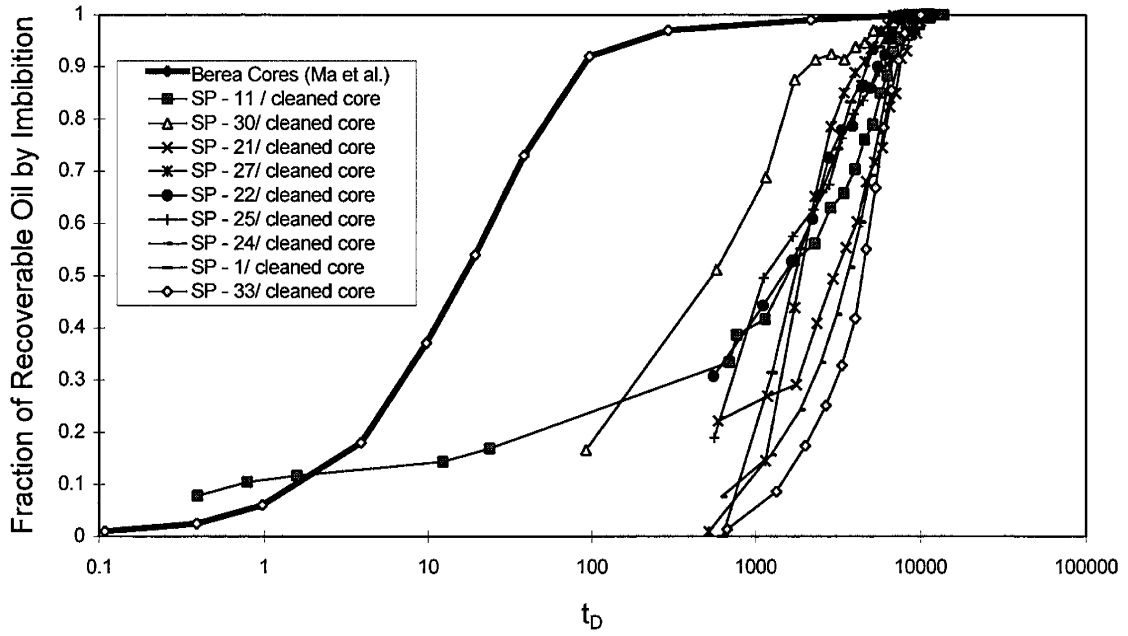


Fig. 3.1 - Imbibition oil recovery from cleaned Spraberry cores compared with scaling curve for Berea presented by Ma *et al.*

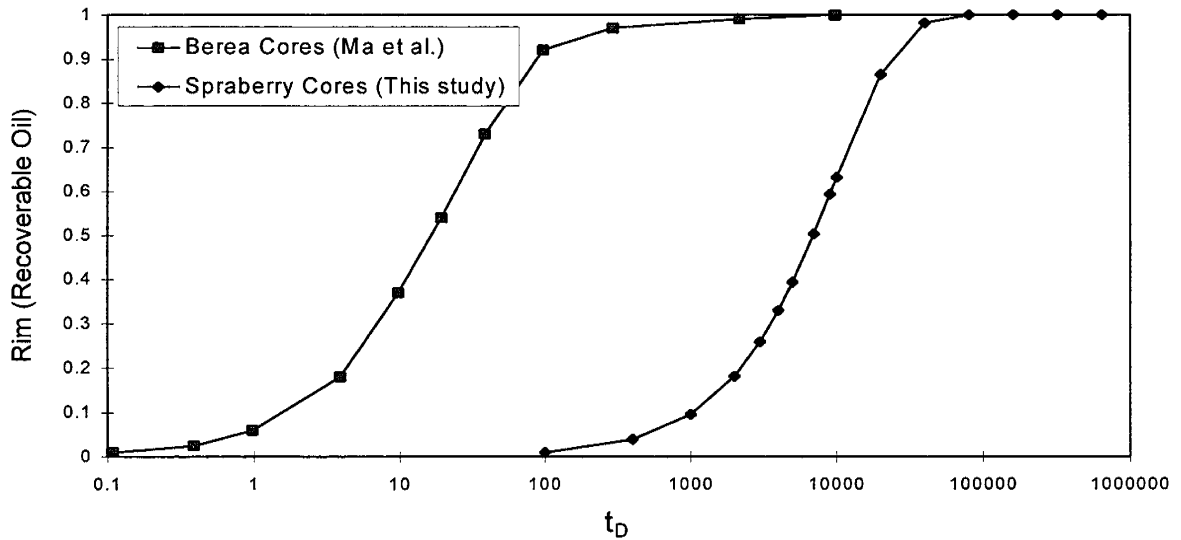


Fig. 3.2 - Dimensionless imbibition oil recovery curves from Ma *et al.* compared with Spraberry data

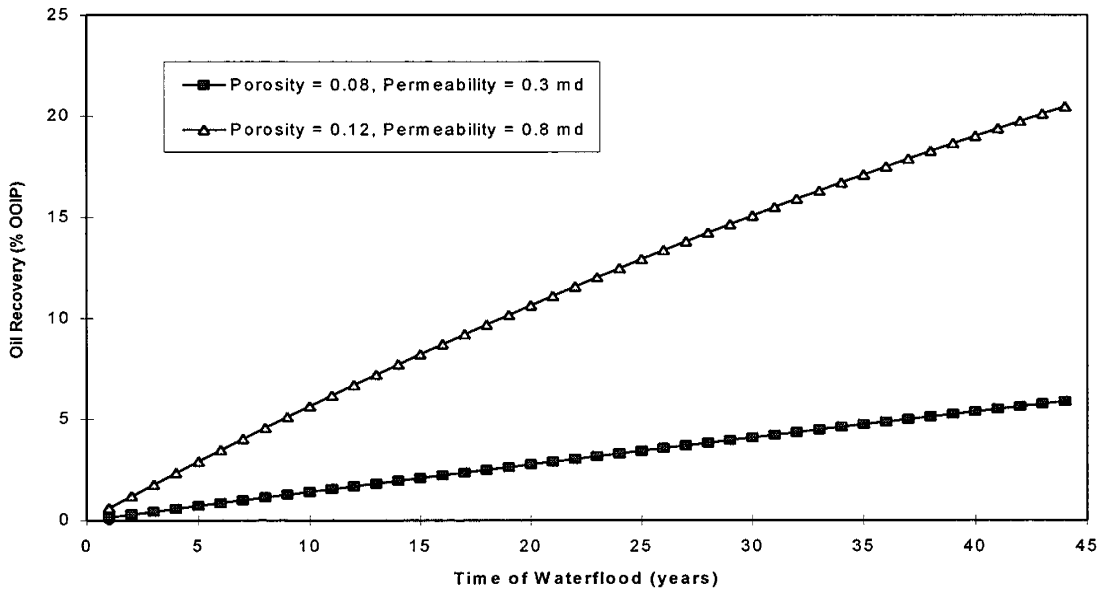


Fig. 3.3 - Calculated imbibition oil recovery from Spraberry reservoir based on scaling of experimental data and fracture spacing 4 feet

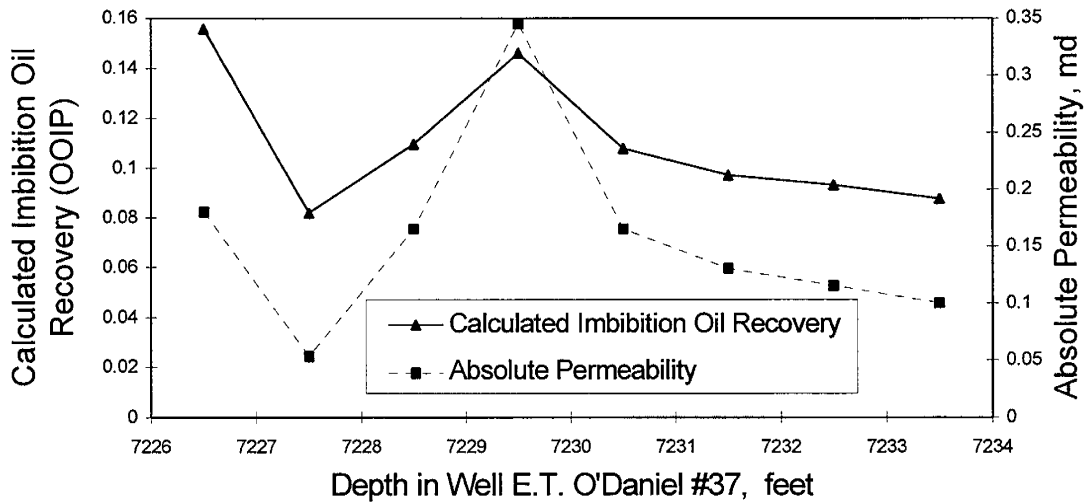


Fig. 3.4 - Calculated imbibition oil recovery from the 5U Unit, Upper Spraberry based on absolute permeability

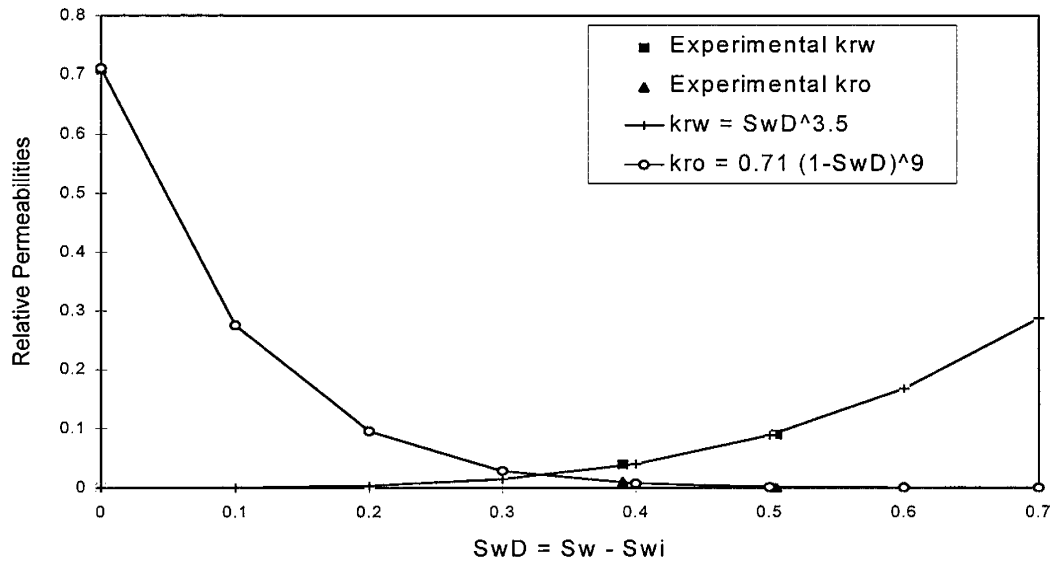


Fig. 3.5 - Oil water relative permeability curves for Spraberry sand

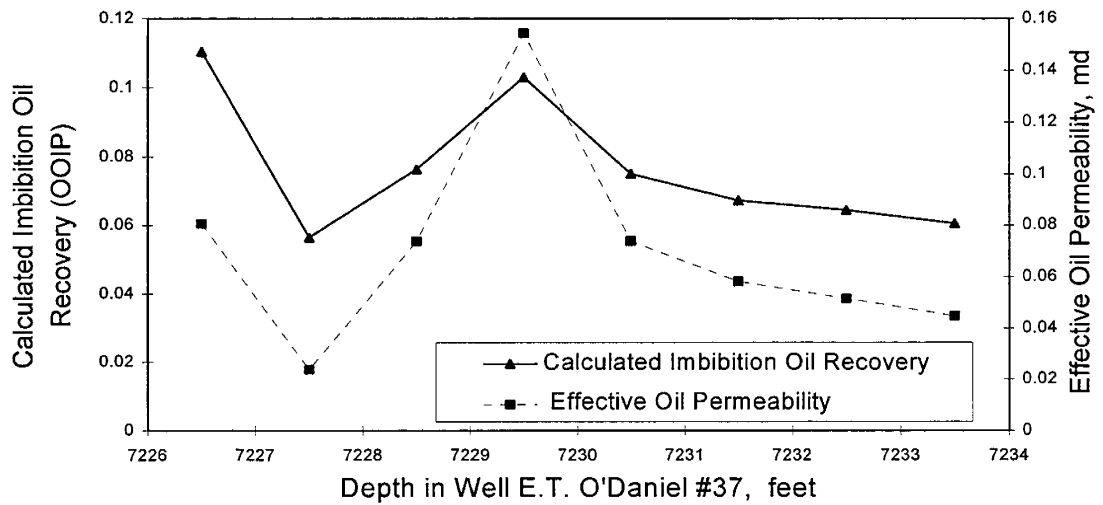


Fig. 3.6 - Calculated imbibition oil recovery from the 5U Unit, Upper Spraberry based on effective oil permeability

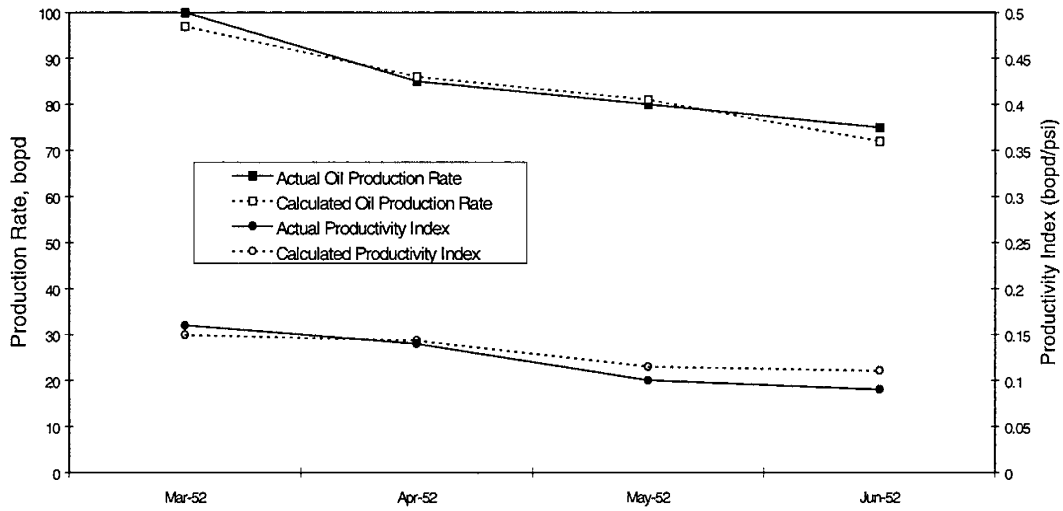


Fig. 3.7 - Match for calculated and actual productivity for X.B. Cox A-4 (Driver Unit)

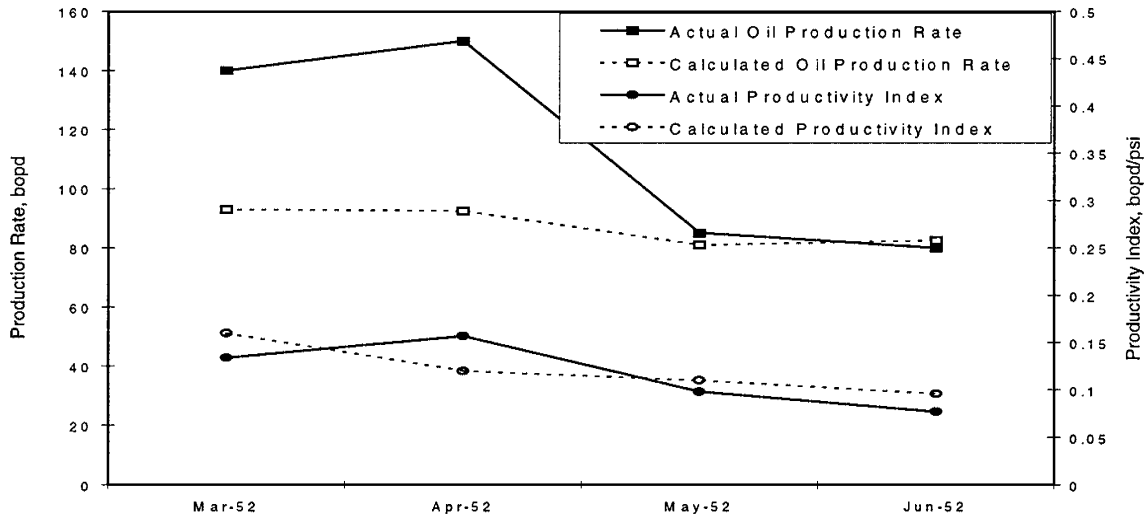


Fig. 3.8- Comparison between calculated and actual productivity for Davenport B-5

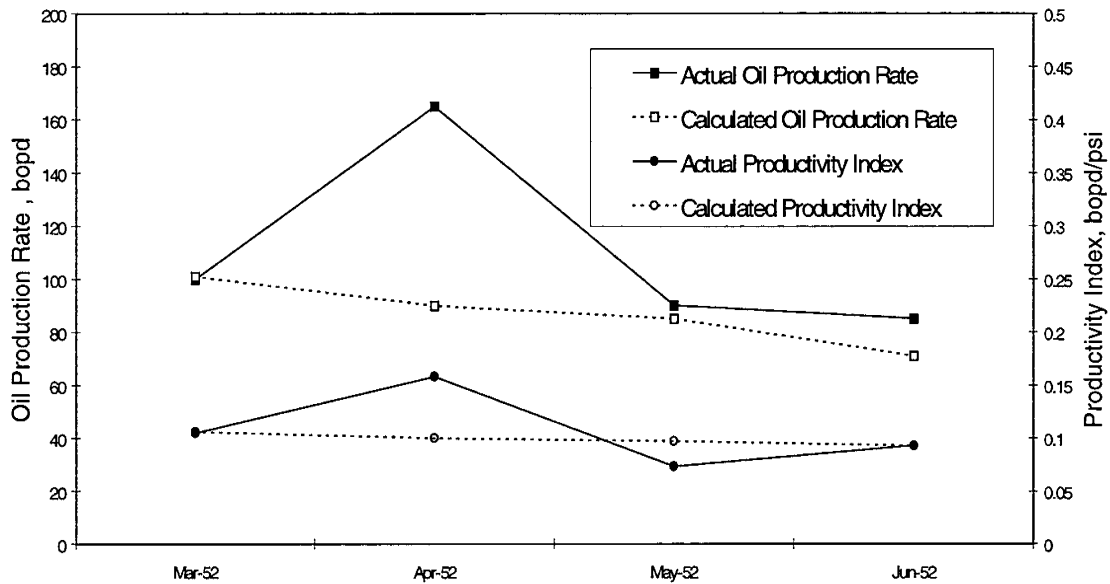


Fig. 3.9 - Comparison between calculated and actual productivity for Davenport B-7

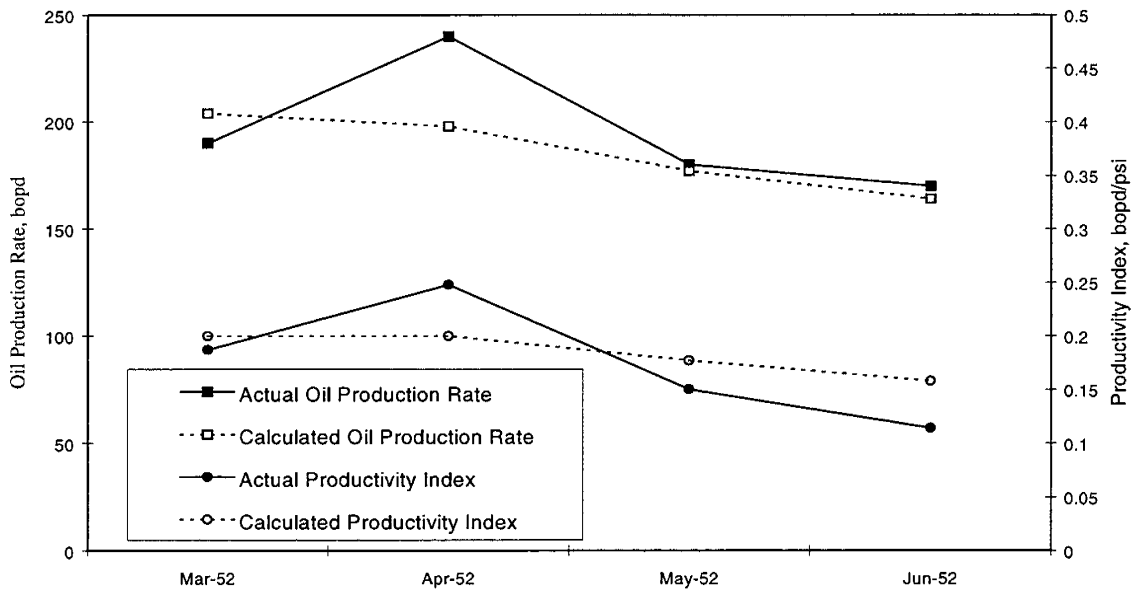


Fig. 3.10 - Comparison between calculated and actual productivity for Davenport C-6

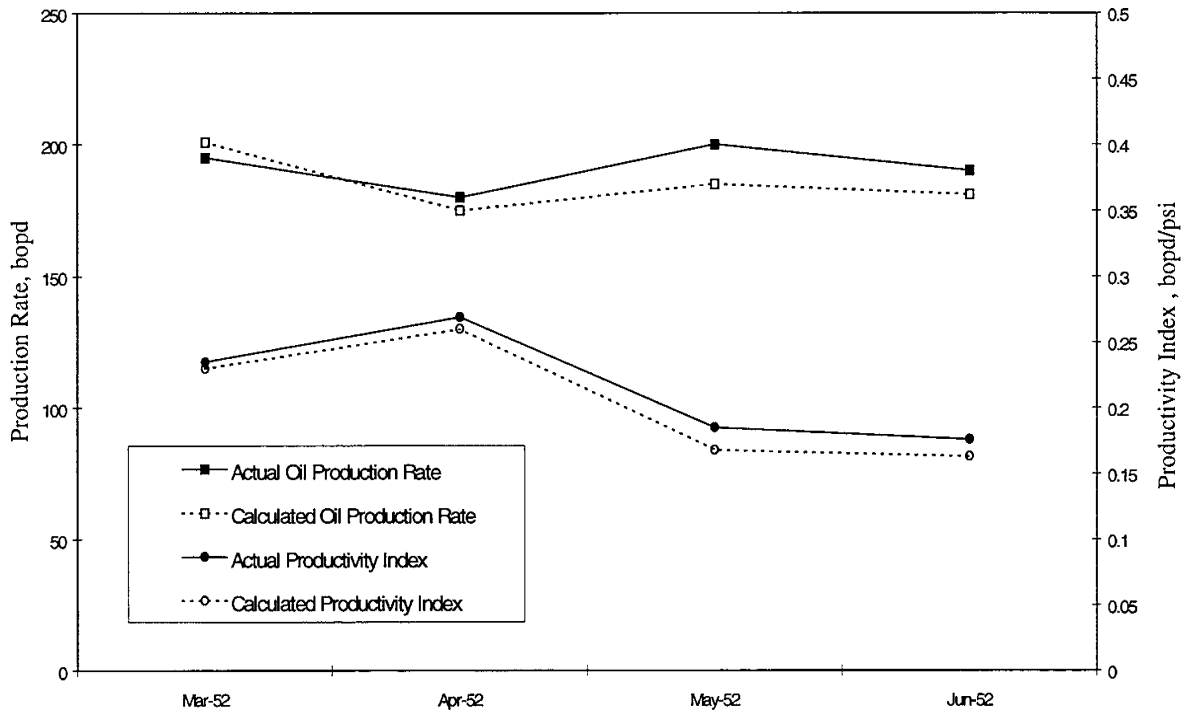


Fig. 3.11 - Comparison between calculated and actual productivity for Davenport C-8

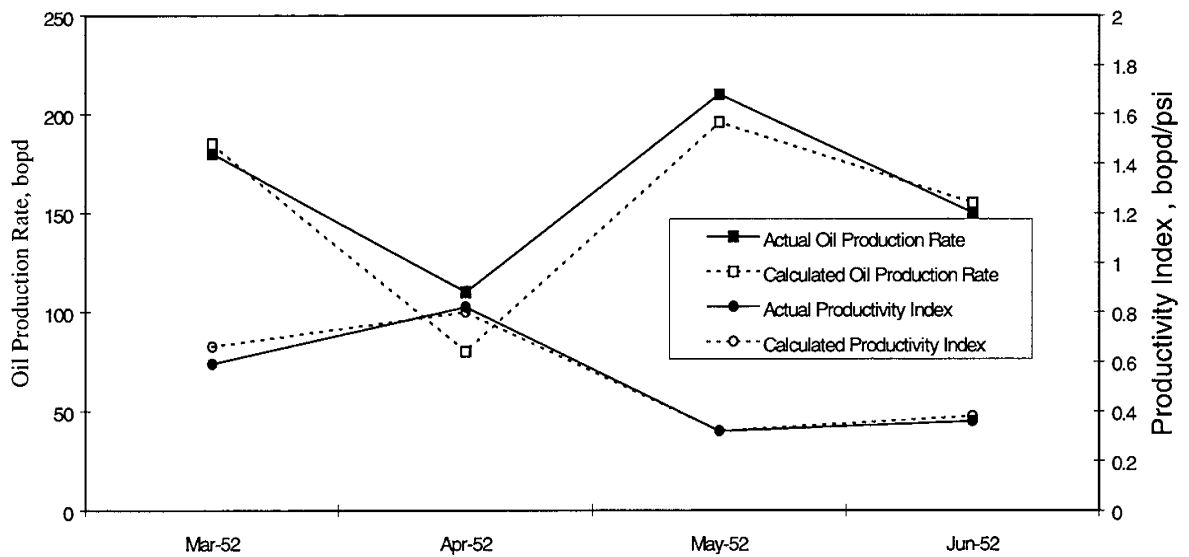


Fig. 3.12 - Comparison between calculated and actual productivity for Bryans A-2

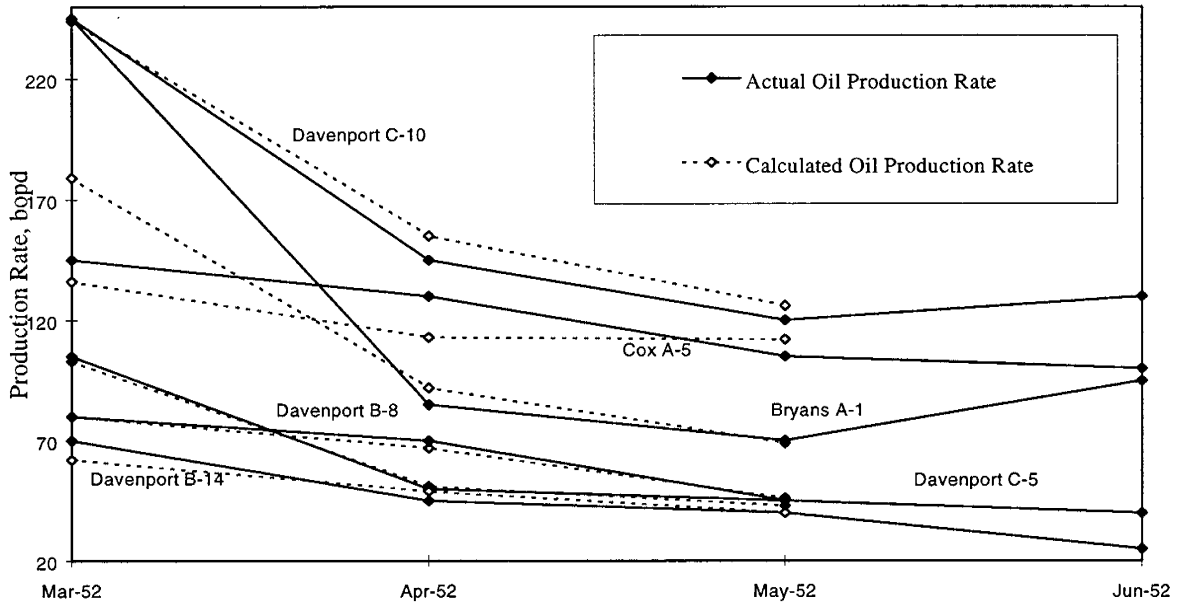


Fig. 3.13 - Comparison between calculated and actual oil production rates in Driver Unit waterflood

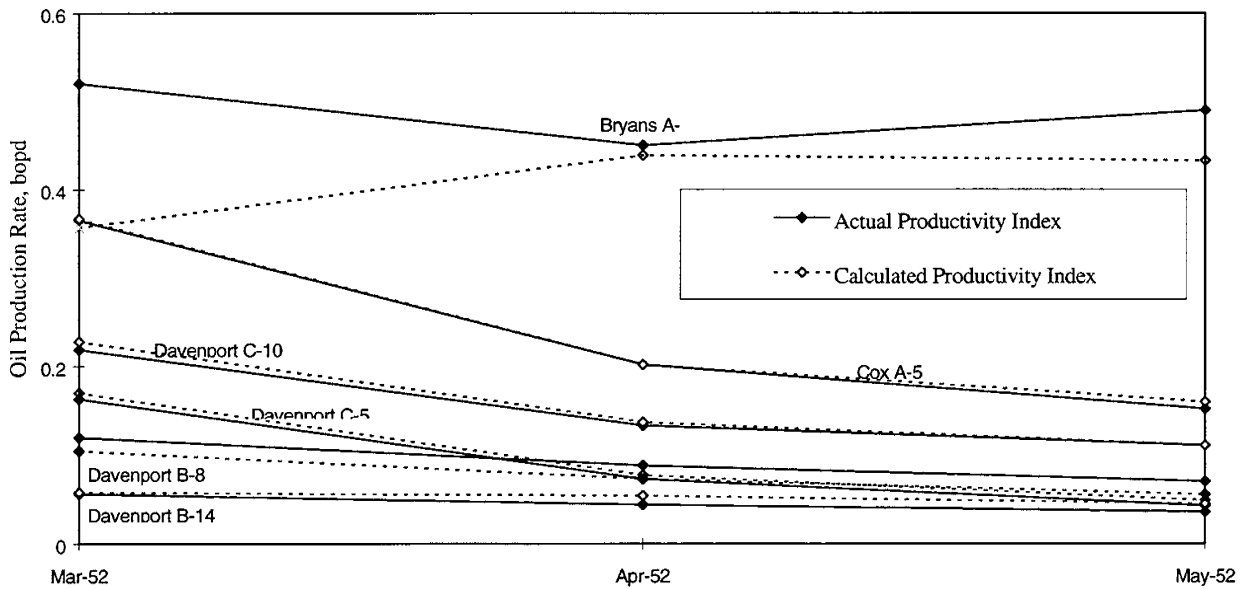


Fig. 3.14 - Comparison between calculated and actual productivity indices

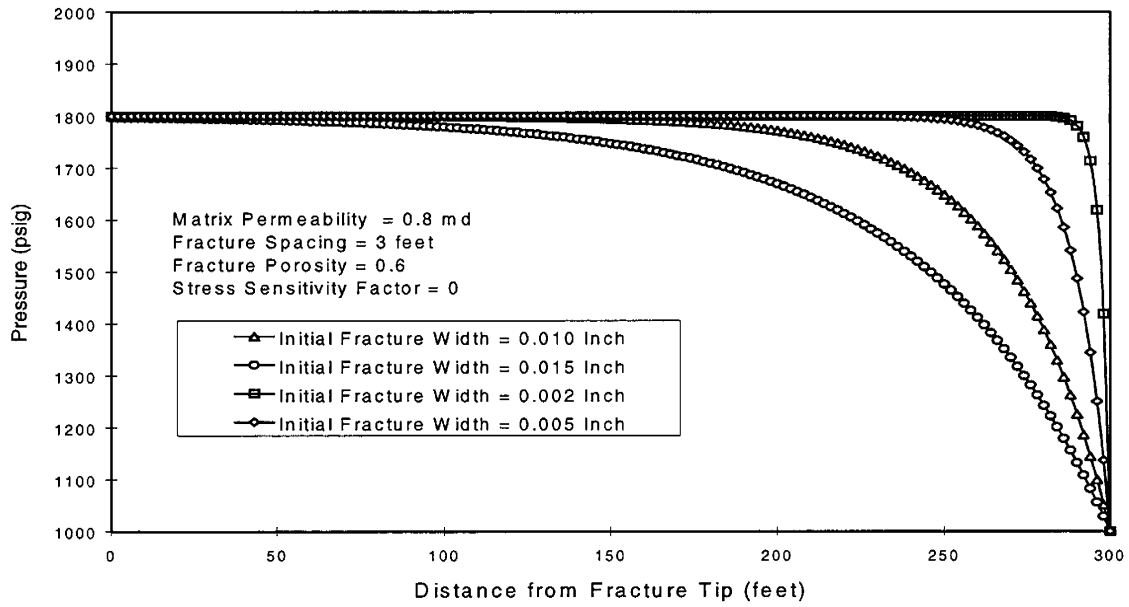


Fig. 3.15 - Calculated pressure distribution along a stress-insensitive fracture

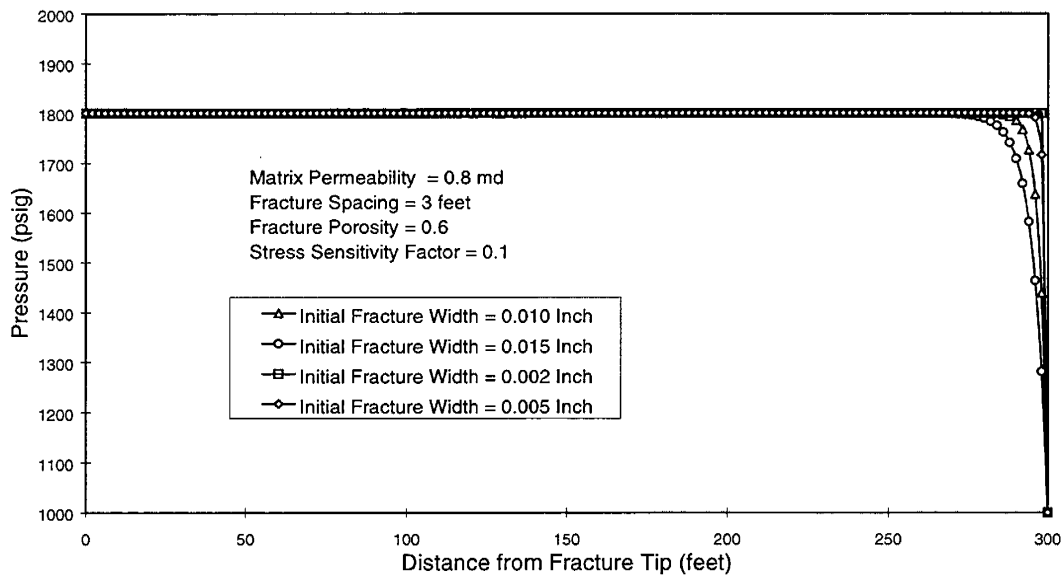


Fig. 3.16 - Calculated pressure distribution along a stress-sensitive fracture

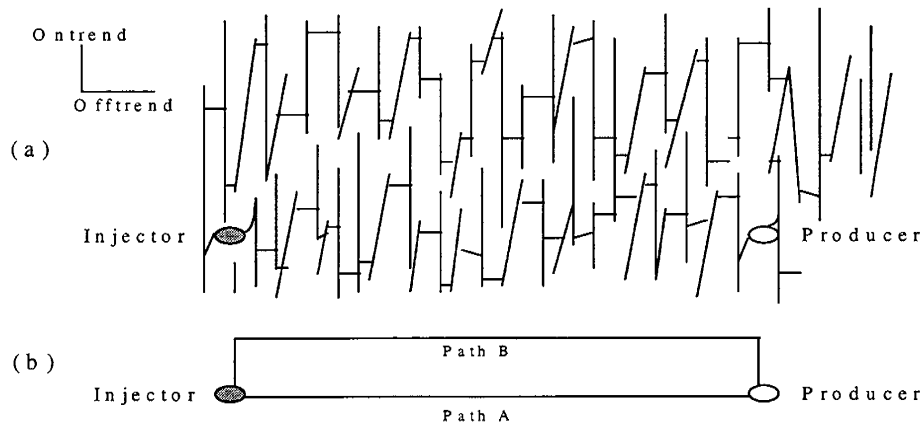


Fig. 3.17 - A model to interpret cyclic waterflooding performance

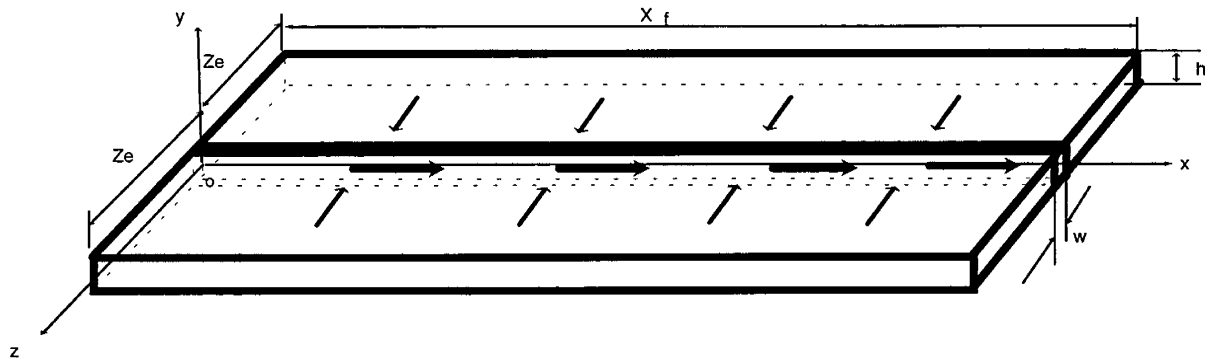


Fig. 3.18 - Geometry of a reservoir drained by a wing of a fracture

Appendix III.A - Matrix-to-Fracture Cross Flow in Fractured Oil Reservoirs

Assumptions

A major assumption in this analysis is that the fracture is long enough to reach no-flow boundaries in the drainage area. Such no-flow boundaries exist at the borders of drainage areas of production wells. Oil flow in the neighborhood of such a long fracture may be analyzed with the following assumptions:

1. One-dimensional flow in the matrix.
2. One-dimensional flow in the fracture.
3. Pseudo steady flow prevails.
4. Oil is treated as an incompressible fluid.
5. Darcy flow dominates.

Governing Equation

The geometry of a reservoir section drained by a fracture wing is depicted in Fig. 3.18. Oil flows within the drainage boundaries ($z = \pm z_e$) to the fracture face in z-direction. Darcy velocity of oil in the matrix can be described by Darcy's law :

$$v_z(x) = \frac{k_z}{\mu z_e} [p_e - p_f(x)] \quad (\text{A.1})$$

where $v_z(x)$ is Darcy velocity in z-direction at lateral distance x from the fracture tip, k_z is matrix permeability in z-direction, μ is oil viscosity, z_e is drainage distance of the fracture, p_e is the pressure at the drainage boundary, and $p_f(x)$ is the pressure in the fracture at the point x . The volumetric flow rate of oil in the fracture at point x can be determined based on $v_z(x)$:

$$Q(x) = 2h \int_0^x v_z(x) dx \quad (\text{A.2})$$

where $Q(x)$ is the volumetric flow rate in the fracture at point x , h is the height of the fracture which is assumed to be equal to reservoir thickness. Substituting Eq. (A.1) into Eq. (A.2) gives:

$$Q(x) = \frac{2hk_z}{\mu z_e} \int_0^x [p_e - p_f(x)] dx \quad (\text{A.3})$$

If the average width (aperture) of the fracture is w , Darcy velocity in the fracture $v_f(x)$ can be obtained by dividing Eq. (A.3) by the cross sectional area of the fracture:

$$v_f(x) = \frac{Q(x)}{hw} = \frac{2k_z}{\mu w z_e} \int_0^x [p_e - p_f(x)] dx \quad (\text{A.4})$$

Application of Darcy's law in the fracture gives:

$$\frac{dp_f(x)}{dx} = -\frac{\mu}{k_f} v_f(x) \quad (\text{A.5})$$

where k_f is the permeability of the fracture when it is treated as a porous medium. Substituting of Eq. (A.4) into Eq. (A.5) yields:

$$\frac{dp_f(x)}{dx} = -\frac{2k_z}{w z_e k_f} \int_0^x [p_e - p_f(x)] dx \quad (\text{A.6})$$

Differentiation of Eq. (A.6) with respect to x gives:

$$\frac{d^2 p_f(x)}{dx^2} = -\frac{2k_z}{w z_e k_f} [p_e - p_f(x)] \quad (\text{A.7})$$

which is the governing equation for the fracture pressure function $p_f(x)$. This equation can be further simplified using the definitions

$$p_d = p_e - p_f(x) \quad (\text{A.8})$$

and

$$c = \frac{2k_z}{w z_e k_f} \quad (\text{A.9})$$

where p_d is pressure drawdown in the fracture at point x , and c is a dimensionless variable describing the contrast between matrix and fracture conductivities. Substituting Eqs. (A.8) and (A.9) into Eq. (A.7) results in:

$$\frac{d^2 p_d}{dx^2} = c p_d \quad (\text{A.10})$$

Boundary Conditions

The first boundary condition for Eq. (A.10) assumes that at any point where the drawdown is zero, the variation of the drawdown with respect to distance is negligible. This boundary condition is expressed as

$$\left(\frac{dp_d}{dx}\right)_{p_d=0} = 0 \quad (\text{A.11})$$

The second boundary condition is that the drawdown at the exit of the fracture wing is equal to drawdown in the wellbore, or

$$p_d = p_d^* = p_e - p_w \quad (\text{A.12})$$

Pressure distribution in a fracture may be estimated using Eq. (1):

Solution

Let

$$p_d' = \frac{dp_d}{dx} \quad (\text{A.13})$$

then

$$\frac{d^2 p_d}{dx^2} = \frac{dp_d'}{dx} = \frac{dp_d'}{dp_d} \frac{dp_d}{dx} = p_d' \frac{dp_d'}{dp_d} \quad (\text{A.14})$$

Substituting Eq. (A.14) into Eq. (A.10) yields:

$$p_d' \frac{dp_d'}{dp_d} = c p_d \quad (\text{A.15})$$

By separation of variables, a solution to Eq. (A.15) is obtained:

$$\frac{1}{2} p_d'^2 = \frac{1}{2} c p_d^2 + c_1 \quad (\text{A.16})$$

where c_1 is an integration constant and can be determined using the boundary condition expressed by Eq. (A.11) as

$$c_1 = 0. \quad (\text{A.17})$$

Substituting $c_1 = 0$ into Eq. (A.16) and rearranging the latter yield:

$$p_d' = \sqrt{c} p_d \quad (\text{A.18})$$

Substituting of Eq. (A.13) into Eq. (A.18) gives:

$$\frac{dp_d}{dx} = \sqrt{c} p_d \quad (\text{A.19})$$

which has a solution of

$$\ln(p_d) = \sqrt{c}x + c_2 \quad (\text{A.20})$$

The integration constant c_2 can be determined using boundary condition Eq. (A.12) to be

$$c_2 = \ln(p_d^*) - \sqrt{c}x_f \quad (\text{A.21})$$

Substituting Eq. (A.21) into Eq. (A.20) and rearranging the latter yield:

$$\ln\left(\frac{p_d}{p_d^*}\right) = \sqrt{c}(x - x_f) \quad (\text{A.22})$$

or

$$p_d = p_d^* e^{\sqrt{c}(x-x_f)} \quad (\text{A.23})$$

Substitution of Eqs. (A.8) and (A.12) into Eq. (A.23) result in an equation for pressure drawdown distribution in the fracture:

$$p_e - p_f(x) = (p_e - p_w) e^{\sqrt{c}(x-x_f)} \quad (\text{A.24})$$

The equation for pressure distribution in the fracture is then:

$$p_f(x) = p_e - (p_e - p_w) e^{\sqrt{c}(x-x_f)} \quad (\text{A.25})$$

Based on Eq. (A.3), the oil flow rate at the exit of the fracture wing can be expressed as

$$Q = \frac{2hk_z}{\mu z_e} \int_0^{x_f} [p_e - p_f(x)] dx \quad (\text{A.26})$$

Substituting Eq. (A.24) into Eq. (A.26) yields:

$$Q = \frac{2hk_z}{\mu z_e} \int_0^{x_f} (p_e - p_w) e^{\sqrt{c}(x-x_f)} dx \quad (\text{A.27})$$

which can be integrated resulting in the following inflow performance relationship:

$$Q = \frac{2hk_z}{\mu z_e \sqrt{c}} (p_e - p_w) (1 - e^{-\sqrt{c}x_f}) \quad (\text{A.28})$$

The productivity index for the fracture wing is then

$$PI = \frac{Q}{p_e - p_w} = \frac{2hk_z}{\mu z_e \sqrt{c}} (1 - e^{-\sqrt{c}x_f}) \quad (\text{A.29})$$

If field units are used, Eqs. (A.28) and (A.29) take the following form:

$$Q = \frac{0.00254k_z h}{B_o \mu z_e \sqrt{c}} (p_e - p_w)(1 - e^{-\sqrt{c}x_f}) \quad (\text{A.30})$$

and

$$PI = \frac{Q}{p_e - p_w} = \frac{0.00254k_z h}{B_o \mu z_e \sqrt{c}} (1 - e^{-\sqrt{c}x_f}) \quad (\text{A.31})$$

where B_o is the formation volume factor of oil.

Appendix III.B - Relationship between Fracture Width and Permeability

Application of the mathematical model derived in Appendix A requires information concerning the fracture width w and fracture permeability k_f . However, these two parameters should not be used independently because they are closely related. Similar to the cubic law²² for the relationship between fracture width and fracture conductivity, a simple relation between fracture width and fracture permeability is derived analytically in this section.

For flow of a liquid in a fracture at a practical rate encountered in petroleum reservoirs, laminar flow should prevail. Pressure drop (Δp) across a fracture length (L) can be written as²³

$$\Delta p = \frac{f \rho v^2 L}{w \phi_f} \quad (\text{B.1})$$

where f is the friction factor, ρ is the fluid density, v is fluid velocity, and ϕ_f is fracture porosity. The fracture porosity characterizes volume of solid materials including minerals, crushed and uncrushed rock within the fracture aperture. The friction factor for laminar flow in a fracture can be expressed as²³

$$f = \frac{24}{R_e} \quad (\text{B.2})$$

where R_e is the Reynold's number and is expressed as²³

$$R_e = \frac{2 \rho v w \phi_f}{\mu} \quad (\text{B.3})$$

where μ is fluid viscosity. Substituting Eqs. (B.2) and (B.3) into Eq. (B.1) yields:

$$\Delta p = \frac{12\mu v L}{w^2 \phi_f^2} \quad (\text{B.4})$$

If the fracture is treated as a porous medium, the pressure drop can also be expressed in Darcy equation:

$$\Delta p = \frac{\mu v_D L}{k_f} \quad (\text{B.5})$$

where v_D is Darcy velocity and is related to interstitial velocity (v) through fracture porosity (ϕ_f):

$$v_D = \phi_f v \quad (\text{B.6})$$

Equating the right-hand-side of Eqs. (B.4) and (B.5) gives the interrelationship of fracture width, fracture porosity and fracture permeability as

$$k_f = \frac{\phi_f^3 w^2}{12} \quad (\text{B.7})$$

3.3 Simulation of a Spraberry Waterflood Pilot

Abstract

The Spraberry Trend Area in West Texas, although one of the largest oil fields in the world, has always been marginally profitable. Spraberry reservoirs present unusual problems for both primary production and waterflooding. Primary production under solution gas drive recovered less than 10 per cent of the oil in place. After more than 40 years of waterflooding, the current oil recovery is still not much greater than 10 per cent. The reasons for low productivity and disappointing waterflood performance are still not clearly understood.

This paper focuses on analysis and simulation of a waterflood pilot test in order to understand reservoir performance. This pilot was conducted by Humble Oil & Refining Company in March 1955 in the Midkiff Unit of the Spraberry Trend Area.

A pilot model was constructed using a three-phase, three-dimensional, dual porosity simulator (VIP-Western Atlas). A large pilot area, 13,642 ft x 10,052 ft with 2700 total number of gridblocks was developed for simulation of the pilot.

The effect of varying the fracture and matrix parameters; such as fracture spacing, capillary pressure, permeability and relative permeability to history match the pilot response was simulated in detail. The analysis may be helpful for understanding reservoir behavior and reducing uncertainty in future process options such as horizontal wells and CO₂ injection.

Introduction

The Spraberry Trend Area was discovered in January 1949. Location of the field is shown in Fig. 3.19. In addition to being one of the world's largest fields in areal extent, the Spraberry Trend was considered one of the richest oil provinces in the world. However, well productivity declined rapidly after the fracture system was depleted. Along with rapid decline of well productivity, the GOR increased rapidly since primary recovery was dominated by solution gas drive. Primary recovery produced less than 10 % of the oil in place. Due to low oil recovery and favorable results from laboratory imbibition experiments, Atlantic performed an unconfined five-spot pilot in 1954. The results were not encouraging enough for full-scale waterflooding in Spraberry. However, displacement of oil by waterflooding proved to be very successful in a pilot performed by Humble Oil & Refining Company in 1955.

From the results of this pilot, large scale waterflooding was initiated in the Spraberry Trend. After more than 40 years of waterflooding, the current oil recovery is still not much greater than 10 per cent. The low productivity of Spraberry wells may be caused by several reasons, such as poor understanding of reservoir performance, incorrect well pattern alignment poor

understanding of fracture system (fracture orientation and fracture density), and poor understanding of water imbibition, capillary pressure and wettability of the rock matrix. The purpose of this study is to simulate the Humble pilot waterflood performed in the Spraberry Trend Area in 1955 and reduce the number of unknown parameters for application in other Spraberry fields.

The Humble pilot has an extensive data set available on a well by well basis which is uncommon for the Spraberry Trend. The existence of this data therefore, allows us to apply modern simulation techniques to evaluate the performance of this 40 year old pilot.

The reservoir model for Humble pilot area was developed based on the assumption that oil production was largely controlled by natural fractures in homogeneous, sheetlike reservoirs. The reservoir model was created using 3-phase, 3-D and dual porosity option in VIP. Reservoir parameters such as fracture orientation, fracture and matrix permeabilities, fracture spacing, fracture and matrix capillary pressure, etc. were altered until the best matches were achieved. The variable parameters are confined by the data available in the Spraberry data set. We continue to perform laboratory experiments to narrow parameter adjustment.

From interpretation of this pilot flood, understanding of Spraberry Trend Area reservoir performance will aid in current plans for expanded process options. This pilot model can also be used in the future to simulate horizontal wells and CO₂ injection and combinations of these technologies.

Characterization of the Spraberry Trend

The Spraberry Trend which covers approximately 400,000 acres in Midland Basin (Fig. 3.19) has a stratigraphy mainly composed of sandstone, shales, siltstone and limestone^{1,2,3}. The mass of rock is divided into three distinct units: the Upper Spraberry, sandy zone; Middle Spraberry, a zone of shales and limestones; and Lower Spraberry, a sandy zone.

The Spraberry Trend was proven productive in February 1949 and produced predominantly from the Upper Spraberry. The Upper Spraberry is found at average depth of 7000 ft has a gross thickness of approximately 220 ft and is composed of six stacked units (1U-6U)¹¹. The individual beds rarely exceed 15 feet in thickness. Reservoir characterization presented in Section I has demonstrated the productive oil sands in the Upper Spraberry to consist of two thin intervals, the 1U and 5U.

Core analysis and well logging show that the reservoir rock are characterized by both low porosity and low permeability^{6,7,10}. Matrix permeabilities are on the order of 1 mD or less with porosities ranging from 7 to 14 per cent^{2,4,19}. The pay zones are cut by an extensive system of vertical fractures. The values of matrix permeability would not be commercial if not for a system of interconnected vertical fractures which allow flow of oil from the matrix

through the fractures and to the production well. However, most of the oil is stored in the matrix since fracture porosity is on the order of 1 per cent or less.

The fracture trend orientation varies from area to area from N36° E to N76° E and the ratio of permeabilities along the fracture trend to that perpendicular to the trend varies from area to area from about 6:1 to 144:1 or higher⁵. These results are in good agreement with fluid injection tests and pressure analysis. The orientation of this fracture system is of primary importance in selecting a flood development pattern. Fracture spacing varies from a few inches up to several feet⁷. The effective permeability of the reservoir as determined by pressure build-up tests ranges from 2 to 18 mD⁴.

Reservoir Performance and the Humble Waterflood Pilot

The original pressure measured in different parts of the field varied between 2300 and 2400 psia⁹. Spraberry wells typically produced 100-400 bopd initially after hydraulic fracturing. Pressure declined rapidly with production as the field was produced under solution gas drive. In a matter of months, the pressure declined below the bubble point which resulted in high GOR⁸. Partial closure of the fractures with declining reservoir pressure may have contributed to this behavior as was demonstrated in Section 3.2.

Due to low oil recovery, in 1952, Atlantic Refining Co. conducted a series of laboratory experiments to displace oil in Spraberry core by utilizing the principle of water imbibition. Results from this study led to an unconfined 80 acre five spot pilot waterflood test. The results, although favorable, did not demonstrate the economic feasibility of waterflooding in the Spraberry. Another pilot test was initiated by Humble Oil & Refining Company March 8, 1955. The pilot flood was performed in an 80-acre five spot in the North Pembroke area, Section 16, (now the Midkiff Unit) with one central producing well and 4 injection wells, all drilled on 40-acre spacing as shown in Fig. 3.20.

Water was injected into the Sh. B-2 and Sh. B-6 continuously for 2.9 years after commencement of injection. From the middle of 1956 to July 1957, water was injected into Sh. B-4 and Sh. B-10 only a portion of the time; these wells were shut-in for several months as shown in Fig. 3.21. As of February 1, 1958, approximately 3.7 MMbbls of water had been injected into the pilot waterflood area. The high water injection rates of 1500 bopd/well were used to restore the reservoir pressure and to reopen fractures near the central production well. This resulted in a significant production rate increase as is shown in Fig. 3.22. Before the pilot was initiated, the Sh. B-9 was producing 70 bopd. At the height of waterflood response, this well was producing 256 bopd. The center well produced 117 Mbbl of oil during the test. Fig. 3.22 shows the effect of injection wells on the performance of the central production well in the pilot area.

Humble Pilot Waterflood Model

Characterization of the Humble pilot and corresponding input was performed using the 3D, 3-phase dual porosity option in VIP. The dual porosity model was used since the Spraberry formation is very tight and no significant fluid flow in the matrix can be assumed. The main flow occurs through exchange of fluid from the matrix to the fractures and the fractures towards the production wells. The matrix size and shape varies considerably depending on the fracture system thus making the network difficult to characterize. Therefore, for simplicity, a sheet model was assumed (Fig. 2.23). The dimension of the matrix block are specified by arrays LX,LY,LZ which correspond to fracture spacing in the x-, y- and the z-direction respectively. Since regional fractures are primarily oriented in one direction, LY is set 3 ft and no fractures are assumed in the other directions, LY and LZ are set to the size of the grid model.

The pilot area simulated is 13,642 ft x 10,052 ft with 450 grid blocks in the horizontal direction and 3 grid blocks in the vertical direction. A total number of 2700 grid blocks were used to simulate the pilot. The total number of grid blocks becomes twice that of a single porosity realization since the simulator generates one set of grid blocks for matrix parameters and one set for the fracture parameters. The wells were aligned parallel with the major fracture system with an orientation of N50°E.

Fig. 3.24 shows the grid model for the five spot after orientation with the major fracture system. The virgin reservoir properties are shown in Table 3.4. The reservoir fluid analysis report (PVT analysis) was conducted by Magnolia Petroleum Co¹². The report is displayed in Table 3.5. The fluid samples were recombined and flashed to reservoir conditions at a temperature of 140° F. It was found that the saturation pressure was 1840 psia, 460 psia below the estimated original reservoir pressure of 2300 psi.

The two main zones, the 1U and 5U, were modeled with one large intervening shale layer. An assumption was made that there is no vertical communication in the matrix between the two different sand zones, by setting transmissibilities in the intervening shale to be zero.

The five spot with one producer (Sh. B-9) and four injectors (Sh. B-2, Sh. B-4, Sh. B-6 and Sh. B-10) were modeled in the simulation. In addition to the five spot wells, five observation wells; Sh. B-1, Sh. B-5, Sh. B-7, Sh. B-11 and T-1 were included to provide information on the changes in reservoir pressure and production rates which helps in tracing the response of the flood outside the pattern.

Sensitivity Parameters

In order to reduce the number of parameters that determined pilot performance, the unknown parameters were altered to match the observed data. The known properties were input in the model as fixed parameters.

These are the sensitivity parameters investigated in this simulation study:

- a. Fracture spacing
- b. Matrix and fracture permeability
- c. Matrix and fracture relative permeability
- d. Capillary pressure
- e. Matrix and fracture porosity
- f. Fracture orientation.

a. Fracture Spacing

The pilot model was set up with extensive vertical fractures having the same spacing in all zones, including the shale layer. An assumption was made that there is no vertical communication between the two sand units (1U and 5U). This was accounted for by setting the matrix transmissibility in the shale to be zero. No cross fractures were input physically in the model, but the value of fracture permeability in the y-direction (off-trend) can be accounted for with a higher permeability than the matrix permeability in y-direction (Fig. 3.23). Matrix permeability in y-direction should be set different than the fracture permeability in the y-direction, in order to represent different values of fracture spacing.

A fracture spacing of 3-ft was used to history match the observed field data performance. Lowering the fracture spacing will increase oil and gas production, decrease water rate and increase bottom hole pressure.

Results of a recent outcrop study in the Bone Springs, a Spraberry equivalent outcrop show that 3-ft fracture spacing dominates in the outcrop. This fracture spacing also closely matches with 4-ft spacing estimated by Schechter *et al.*¹⁴ and 5-ft spacing simulated by Kindem.¹³

b. Matrix and Fracture Permeability

The reservoir permeability in the pilot area was much greater in the direction of the major fracture trend than in the minor direction. A permeability ratio of 144 : 1 parallel to the fracture trend was used. If the same value of matrix and fracture permeability in the y-direction is used, water will not be produced at all. We input a different value for matrix and fracture permeability in y-direction to account for cross fractures. Water can be produced

from the middle producer (Sh. B-9) under these conditions. The fracture permeability ratio used in this study is based on summary given by Barfield *et al.*²¹ for the Humble Pilot. This ratio is also supported by Wolf.²⁰

The permeability ratio was kept constant, starting from 144:1 until the best match was achieved. The best match was a ratio of 100:0.694. Beside constraining the production rate and bottom hole pressure, cumulative water injection was also used as one of the constraints for this match.

Using a permeability ratio of 144:1, the results showed that oil, gas and water can be matched but this leads to difficulty matching the bottom hole pressure. The simulated data for bottom hole pressure showed very high pressure averaging 8000 psia while the observed data of bottom hole pressure was only around 1500 psia. Using the ratio of 100:0.694, the bottom hole pressure can be decreased significantly until it reflects the observed data yet we are still having difficulty matching BHP in the latter stage of the pilot. Also, the production rates matched well with the observed data.

c. Matrix and Fracture Relative Permeability

Relative permeability curves for the matrix were obtained from several unfractured core reports¹⁰ taken from a well close to the pilot area as discussed in Section 3.4. The permeability in the matrix for water-oil was restricted to the mobile saturation range from $S_w = 0.3$ to $S_w = 0.7$.

It is very difficult to measure accurately fracture permeability curves for a reservoir. Assumptions are that both phases are equally mobile for the entire range of saturations in the fractures (Fig. 3.25). Several curves were used to match the observed data, however, it was observed that alteration of relative permeability curves in the fracture system does not significantly change the results.

d. Capillary Pressure

The capillary pressure is an important parameter in the water imbibition process. When water comes in contact with the oil zone via the fracture, water may imbibe into the matrix blocks to displace oil.

Gilman and Kazemi¹⁶ suggested that the matrix capillary pressure should be set much greater than the fracture capillary pressure to imbibe water in the matrix more easily. The fracture capillary pressure is set up to be near zero for most water-saturation values. The maximum capillary pressure in the fracture is set equal to the matrix and declines rapidly with increasing water saturation. The capillary-pressure end points in both the fracture and matrix

are set to the same value to maintain static equilibrium (gravity/capillary equilibrium) for saturation and pressure distribution.^{16,17}

The imbibition capillary pressure curves were generated since there is currently no data available. Various curves were used in the model to investigate the effect of water imbibition (Fig. 3.26). Lowering capillary pressure increases water production, decreases oil and gas production and bottom hole pressure, and yields a better history match. However, it was found that the simulation results are not sensitive to the capillary pressure. Therefore, a low value of imbibition capillary pressure was used to achieve the best match of the observed data.

e. Matrix and Fracture Porosity

A fracture porosity of 0.1 % was used in the model. This value will depend on the fracture spacing and width of the fractures. Width is not an input parameter in this model, however fracture spacing is given independent of fracture porosity. Fracture permeability could be dependent on spacing, since a more dense system of fractures should give better overall permeability. The fact that these various parameters are given individually in the model, although they are dependent on each other, might cause some confusion. However, if the width is not a constant parameter, the fracture porosity will be an indicator of fluid storage. The fracture spacing will account for matrix surface area in contact with the injected water and would then alter the effectiveness of the imbibition process. The fracture permeability should be a value that represents the productivity of the field. Using a fracture porosity value lower than 0.1%, will increase computer time more than 10 times as opposed to using a fracture porosity equal to 0.1% while the result was almost the same. Increasing the fracture porosity will increase bottom hole pressure, oil and gas production and decrease water production. The matrix porosity was kept constant at 10 %. However if we change this parameter, the effect will be the same as changing the fracture porosity. A fracture porosity of 0.1 % matches with Elkins⁷ estimation as well as Baker and Spenceley's analysis based on a tracer study.¹⁸

f. Orientation of the Major Fracture Trend

Several sources of data, such as interference tests, core analysis, etc., have been conducted to determine the orientation of the major fracture system. From the map of the pilot area (Fig. 3.20) and the flood fronts shown in Fig. 3.27, it is clear that there is a distinct northeast-southwest fracture permeability direction that is oriented approximately N50°E. Two additional simulations were conducted to investigate the effects of rotation of the major fracture orientation. The orientations simulated were N60°E and N85°E. Both these simulations resulted in too high water production in the middle producer, since the production well at these orientations was aligned with east and west water injectors.

A simulation was performed with the dual porosity/dual permeability option, but no significant differences in the results were observed between dual porosity/single permeability. Since the Spraberry formation is very tight, we can assume no significant fluid flow occurs in the matrix rock. The main flow occurs through exchange of fluid from the matrix to the fractures.

Matched Parameters

Production rates and pressure data for the five observation wells around the pilot area were input into the model in addition to the middle producer. From the map shown in Fig. 3.27, Sh. B-7 and Sh. B-11 did not produce any water after water injection and it appears that these wells continued to produce under primary depletion. Water did not flow off-trend to these wells. From observation data and simulation results, it is seen that the Sh. B-9 was the first well to experience water breakthrough, closely followed by Sh. B-1, Sh. B-5 and T-1 (Fig. 3.28). A total of 3.7 MMbbls of water was injected into the model and matched with observed injection data (Fig.3.29).

From the parameters listed in Table 3.6 and Table 3.7, an attempt was made to match the observed data for the middle producer, Sh. B-9.

The simulation of oil production rate matches the observed data (Fig 3.30 and 3.31). Gas production has approximately the same trend as the observed data, but the first peak in gas production observed in the field upon initiation of water injection is not obtained in the simulated results (Fig. 3.32). The trend of oil and gas rates should be the same since a straight line relative permeability curve in the fracture was used. Since the first peak in gas production cannot be matched, the first peak in gas-oil ratio also can not be matched with the observed data (Fig. 3.33).

The water production did not give an accurate match with the observed data, but the cumulative water production can be matched. (Fig. 3.34 and 3.35). Water oil ratio and water cut also matched the observed data (Fig. 3.36 and 3.37). The water cut curve for Sh.B-9 showed that the breakthrough time can be matched.

The bottom hole pressure for the middle producer is strongly dependent on the rates of surrounding observation wells. After injected water fills up the confined pilot area, the simulated bottom hole pressure increases to value greater than observed data at the end of the pilot, as can be seen in Fig. 3.38. Work is in progress to improve the BHP match.

Conclusions

From the interpretation of the Humble pilot using a dual porosity simulator, the following conclusion can be drawn :

1. A dual porosity model was used for this simulation since this method gave the same results as dual porosity/dual permeability model. This indicates that there is negligible fluid flow in tight matrix rock and that main flow occurs within the fractures with local exchange of fluids between the fracture system and matrix blocks.
2. A low value of capillary pressure was used to achieve the best history match of the observed water production and bottom hole pressure data from the Humble pilot waterflood which could indicate that the reservoir rock is weakly water-wet. This correlates well with lab observation of weakly water-wet behavior.
3. The constant fracture spacing of the major fracture trend is determined to be approximately 3.0 ft, and any cross fractures are accounted for using a value of fracture permeability higher than the matrix permeability in that direction.
4. A fracture orientation of N50°E best matches the movement of water observed during the Humble pilot test.
5. A ratio of permeability parallel and perpendicular to the major fracture trend of 100:0.694 was one of the parameters that gave the best match of observed data. This compares reasonably well with the original 144/1 determined by Barfield *et al.*²¹

References

1. Wilkinson, W.M., "Fracturing in Spraberry Reservoir, West Texas," American Association of Petroleum Geologists Bulletin, Vol.37, No.2, p. 250-265, Feb. 1953.
2. Warn, G.W. and Sidwell, R., "Petrology of The Spraberry Sands of West Texas," Journal of Sedimentary Petrology, Vol.23, No. 2, p. 67-74, June 1953.
3. Stanley, T.B., et al., "Geology Investigation of The Spraberry, Midland Basin, West Texas," Humble Oil & Refining Co., PRRC Spraberry Database, Dec.1951.
4. Dyes, A.B. and Johnston, O.C., "Spraberry Permeability from Build-Up Curve Analyses," Trans., AIME, Oct., Vol.198, 1953.
5. Elkins, L.F., "Determination of Fracture Orientation from Pressure Interference," Trans., AIME, Vol. 219, Oct.1960.
6. Lytle, W. J. And Rieke, R.R., "Well Logging in The Spraberry," Oil and Gas Journal, Vol. 50, No.32, P. 92-96 and 105, Dec. 13, 1951.
7. Elkins, L.F., "Reservoir Performance and Well Spacing, Spraberry Trend Area Field of West Texas," Trans., AIME, Vol. 198, Feb. 1953.
8. Elkins, L.F., "Cyclic Water Flooding the Spraberry Utilizes "End Effect" to Increase Oil Production Rate," JPT, May 1963.

9. Christie, R.S. and Blackwood, J.C., "Production Performance in Spraberry," Oil and Gas Journal, April 7, 1952.
10. Humble Oil & Refining Co., Core Analysis Report 431, PRRC Spraberry Database, July 12, 1963.
11. Guevara, E.H., Geology Characterization of Permian Submarine Fan Reservoirs of the Driver Waterflood Unit, Spraberry Trend, Midland Basin, Texas, Report of Investigations No. 172, Bureau of Economic Geology, The University at Austin, 1988.
12. Petroleum Production Laboratories Inc., PVT Analysis Report, Louise Shackelford No. 1, Spraberry Reservoir, Tex Harvey Field, PRRC Spraberry Database, May 30, 1952.
13. Kindem, E., "Characterization and Reservoir Simulation of a Waterflood Pilot in The Naturally Fractured Spraberry Trend," MS-Thesis, NMIMT, Socorro, NM, PRRC Spraberry Database, May 1996.
14. Schechter, D.S., McDonald, P., Sheffield, T., Baker, R., "Reservoir Characterization and CO₂ Pilot Design in The Naturally Fractured Spraberry Trend Area," SPE 35469 presented at the SPE Permian Basin Oil & Gas Recover Conference held in Midland, TX, on March 27-29, 1996.
15. Guo, B., Schechter, D.S., "An Analysis on Productivity of Spraberry Trend Wells," PRRC Spraberry Database.
16. Gilman, J.R., Kazemi, H., "Improvements in Simulation of Naturally Fractured Reservoirs," SPEJ (Aug. 1983), 695-707.
17. Coats, K.H., "Implicit Compositional Simulation of Single-Porosity and Dual-Porosity Reservoirs," paper SPE 18427 presented at the SPE Symposium on Reservoir Simulation held in Houston, Texas, Feb.6-8, 1989.
18. Baker, R., and Spenceley, N., "Analysis of Tracer Study at The Midkiff Unit Upper Spraberry Formation," Epic Consulting Ltd ., Calgary, Canada, PRRC Spraberry Database, Aug. 1996.
19. Banik, A.K, Schechter, D.S., "Characterization of the Naturally Fractured Spraberry Trend Shaly Sands Based on Core and Log Data," SPE 35224 presented at the SPE Permian Basin Oil & Gas Recover Conference held in Midland, TX, on March 27-29, 1996.
20. Wolff, M., Miller, M.A., and Lake, L.W., "Oil Recovery From Geologically Based Fracture Networks," *In Situ* (1990), 14(4), 407-427.
21. Barfield, E.C., Jordan, J.K. and Moore, W.D.: "An Analysis of Large-Scale Flooding in the Fractured Spraberry Trend Area Reservoir," *J. Pet. Tech.* (April 1959) 15-19.

Table 3.4. Reservoir Properties for the Humble Pilot Flood¹³

Original Reservoir Pressure, psia	2300
Saturation Pressure, psia	1840
Reservoir Temperature, °F	140
Initial Water Saturation, %	30-35
Initial Oil Saturation, %	65-70
Matrix Porosity, %	6 - 18
Effective Permeability, mD	2.0-183.0
Matrix Permeability; mD;	
Area	0.1 - 0.5
Vertical	0.05-0.25
Pore Compressibility, psi ⁻¹	4.00E-6

Table 3.5. Reservoir Fluid Properties¹³

Oil Formation Volume Factor, g/cc	1.385
Density of Residual Oil, g/cc	0.851
Molecular Weight of Residual oil	217
Stock Tank Oil Gravity, °API	37.8
Gas Specific Gravity	0.932
Density of Stock Tank Water, g/cc	1.010
Water Formation Volume Factor, rb/STB	1.003
Water Viscosity, cp	1.2486
Water Compressibility, psi ⁻¹	3.00E-6

Table 3.6. - Matched Parameters for Matrix Rock

Property	Symbol	Value
Porosity	ϕ_m	10.0 %
Permeability in the x-direction	K_x	0.01 md
Permeability in the y-direction	K_y	0.01 md
Permeability in the z-direction	K_z	0.01 md

Table 3.7. - Matched Parameters for Fractures

Property	Symbol	Value
Porosity	ϕ_f	0.1 %
Permeability Ratio	k_x/k_y	100/0.694
Permeability in the z-direction	k_z	100.0 md
Fracture Spacing	L_y	3.0 ft
Major Fracture Orientation	-	N50°E

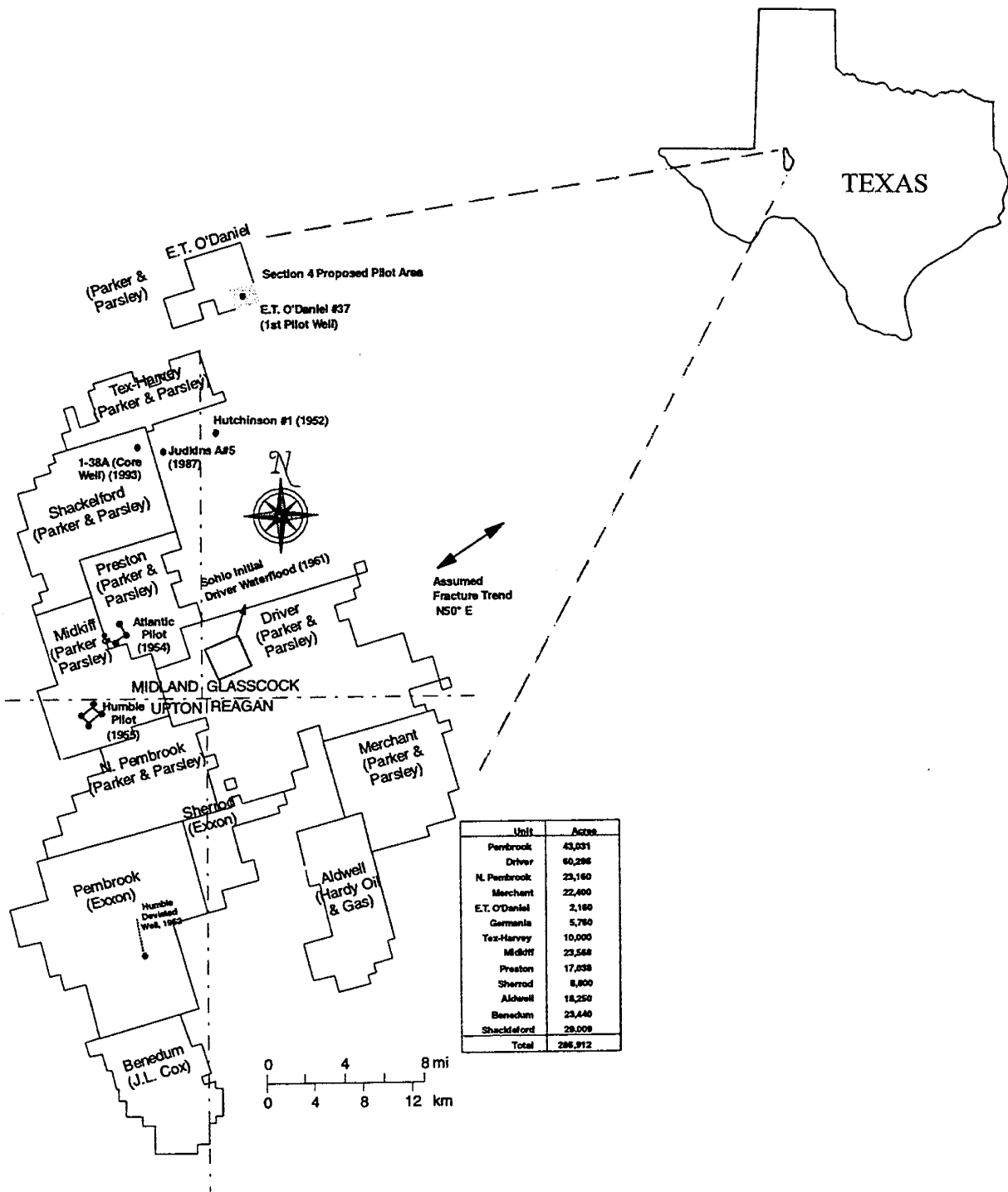
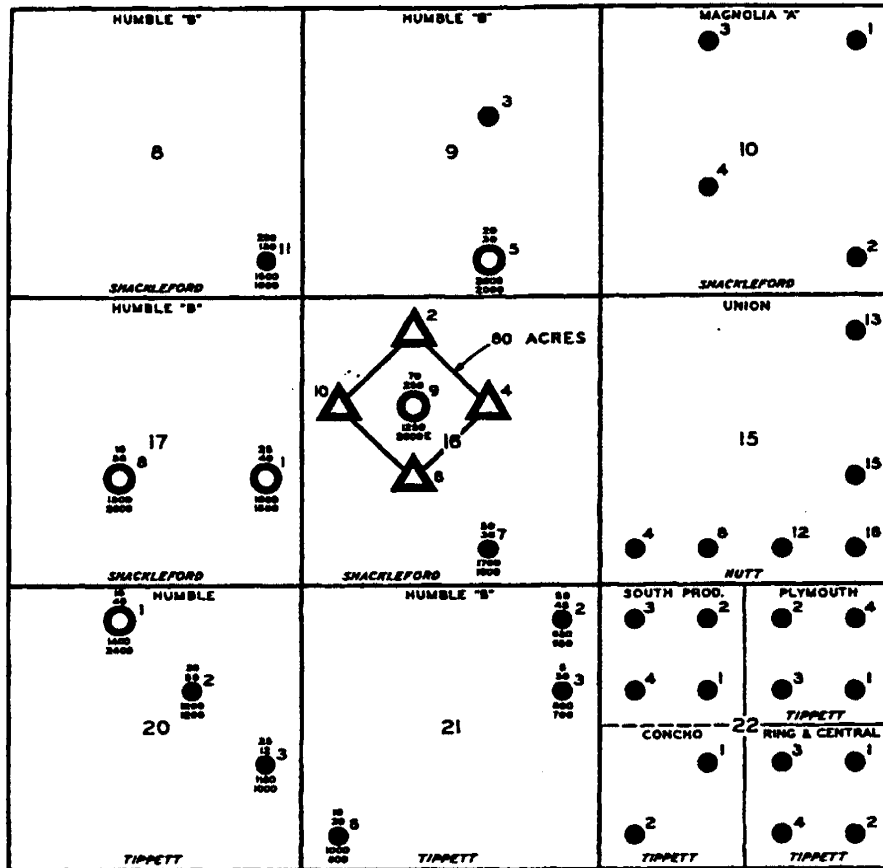


Fig. 3.19- The unitized portion of the Spraberry Trend Area, showing location of Humble pilot area



HUMBLE WATER FLOOD TEST

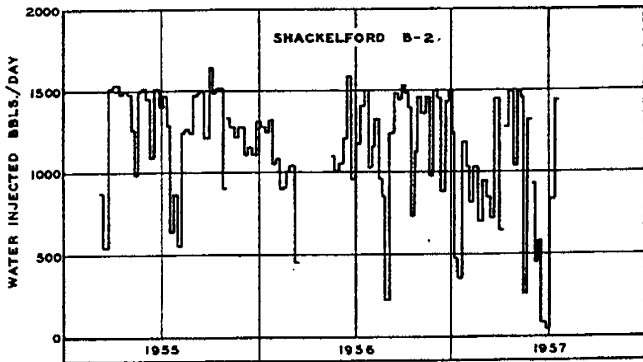
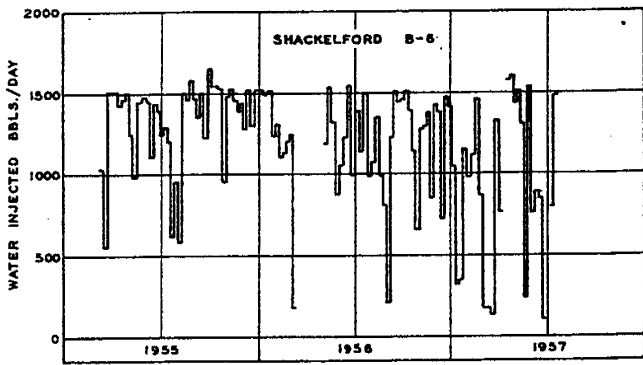
- WATER INJECTION WELL
- INJECTED WATER IN PRODUCTION

- 25 PRODUCTION TEST WHEN WATER INJECTION STARTED - BOPD
- 40 PRODUCTION TEST FALL 1955 - SPRING 1956 - BOPD
- RESERVOIR PRESSURE WHEN WATER INJECTION STARTED - PSI
- RESERVOIR PRESSURE FALL 1955 - SPRING 1956 - PSI (SONIC MEASUREMENTS)



Fig. 3.20 - Humble pilot test showing increase in center production well over 250 bopd after waterflooding. Also the wells in the outside of the pattern influenced by injected water from the pilot wells can be seen to occur along the fracture trend.

WATER INJECTION HISTORY
NORTH-SOUTH INJECTION WELLS
HUMBLE WATER FLOOD TEST



WATER INJECTION HISTORY
EAST-WEST INJECTION WELLS
HUMBLE WATER FLOOD TEST

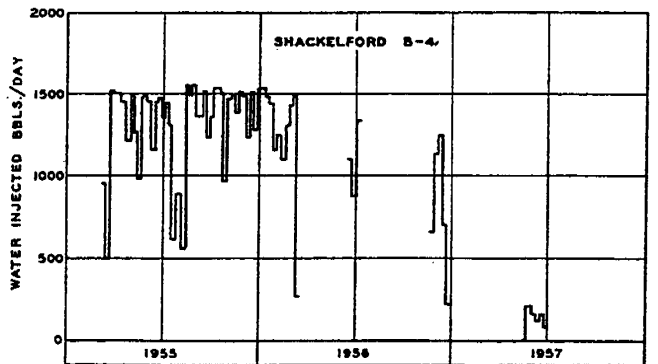
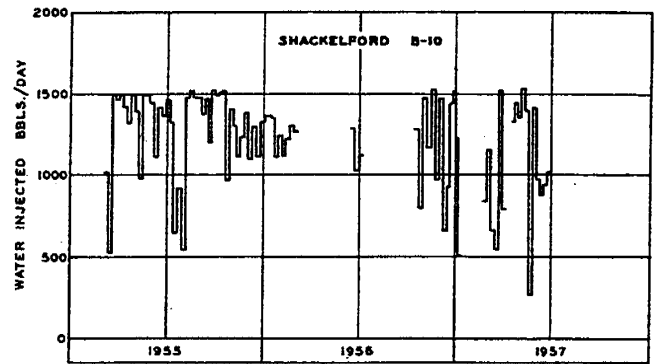


Fig. 3.21 - High water injection rates were used to reopen the fractures and increase well productivity.

WATER FLOOD PERFORMANCE - HUMBLE TEST
PRODUCTION WELL - SHACKELFORD B-9
INJECTION WELLS SHACKELFORD B-2, B-4, B-6, & B-10

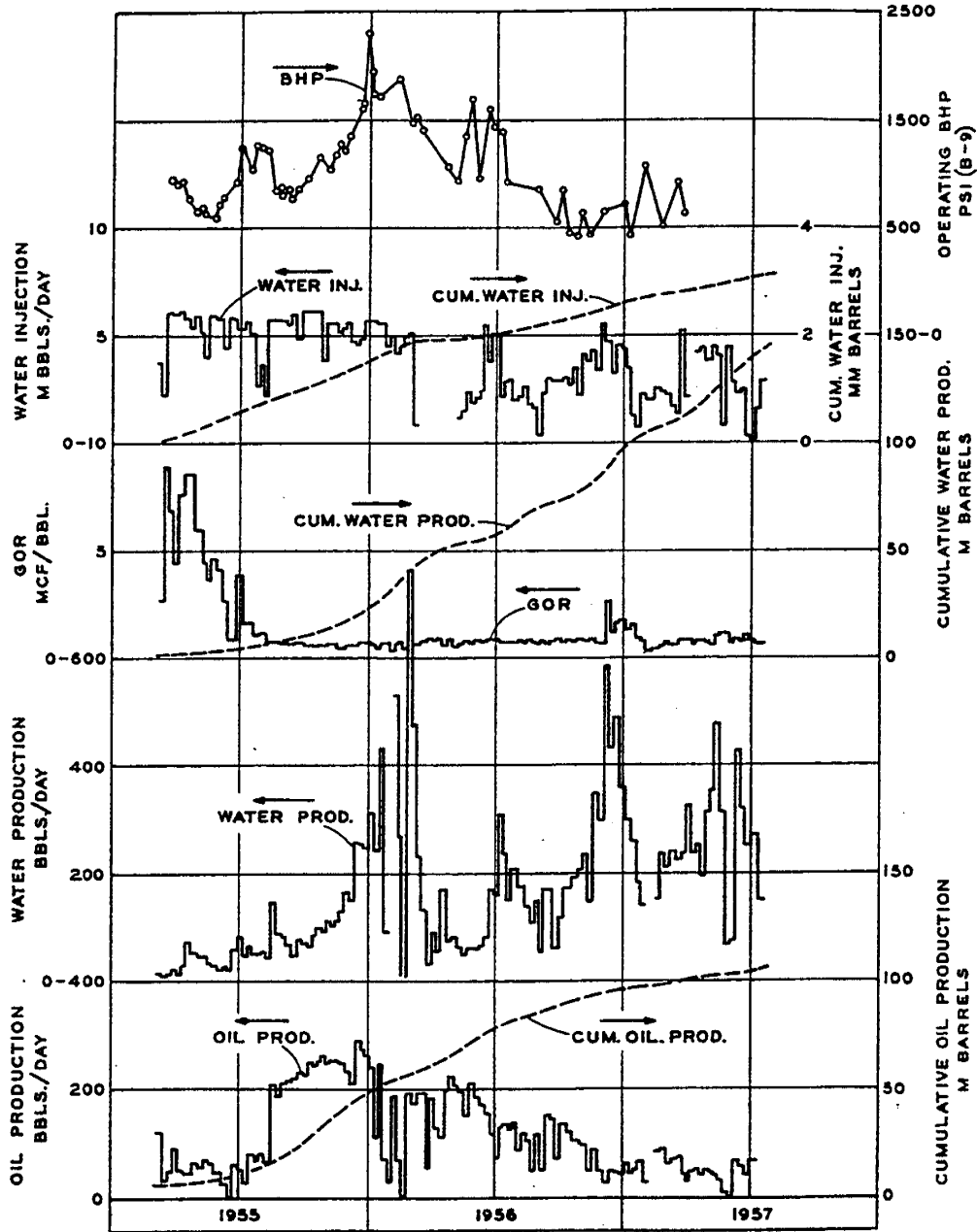


Fig. 3.22 - Three years performance of the Humble Pilot waterflood.

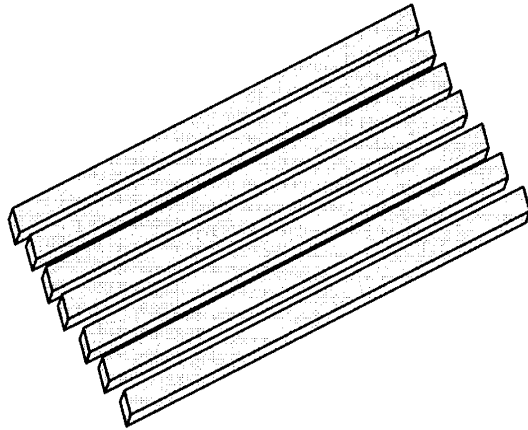


Fig. 3.23 - Sheet model for fractured reservoirs

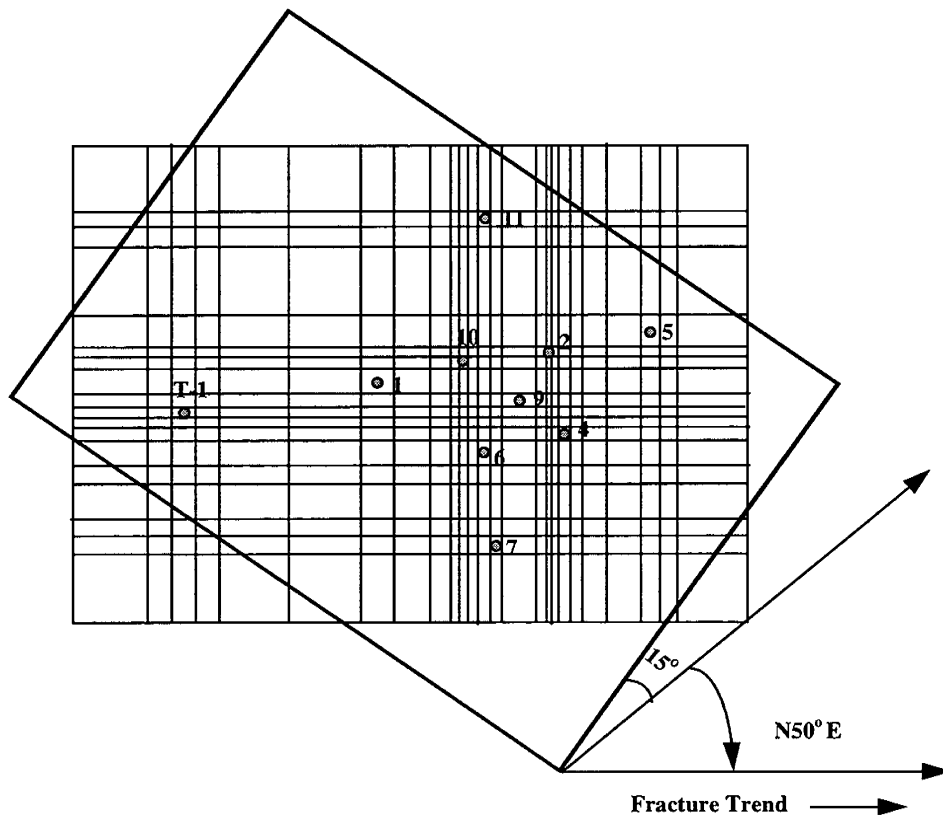


Fig. 3.24 -Grid model after orientation to N50°E along the major fracture system

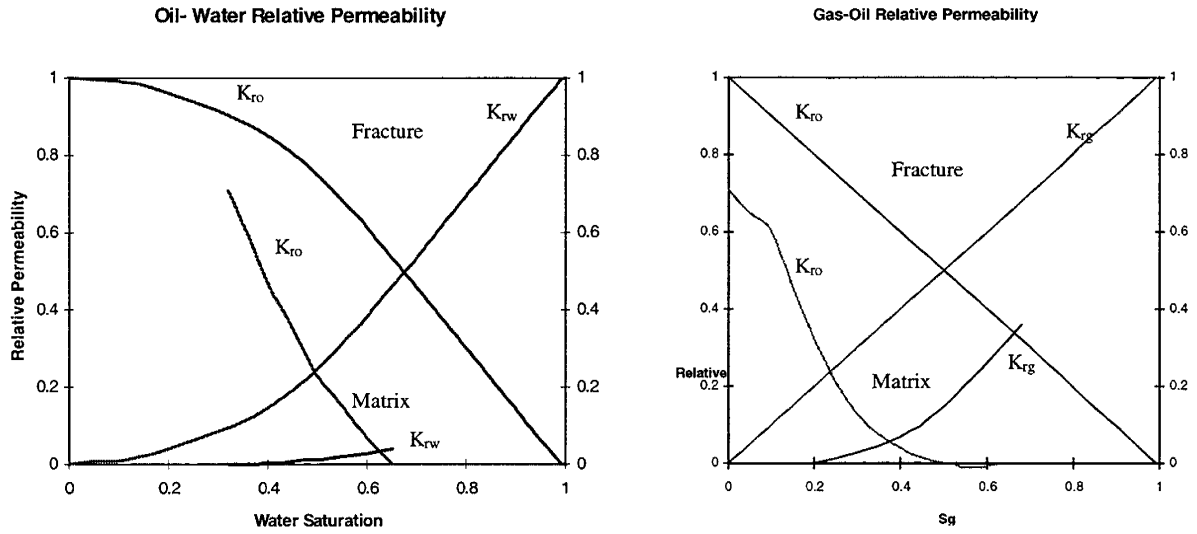


Fig. 3.25 -Matrix and fracture relative permeabilities

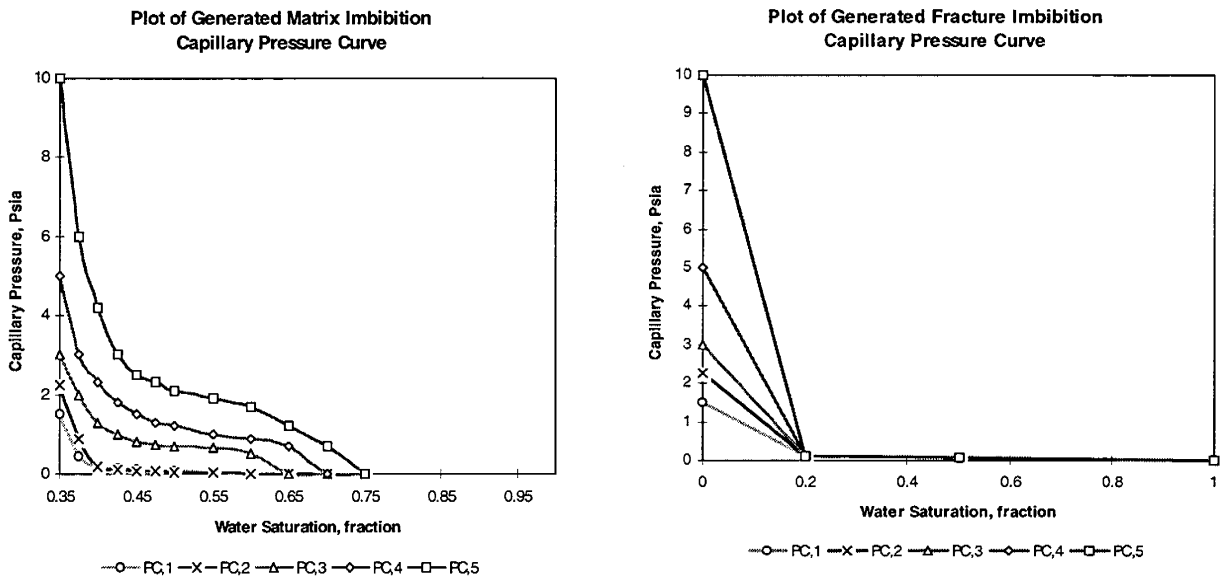


Fig. 3.26 -Plot of generated matrix and fracture imbibition capillary pressure showing the maximum capillary pressure is assumed equal to maintain static equilibrium.

Calculated Position of Flood Front as of March, 1957.

(E. C. Barfield *et al*, 1959)

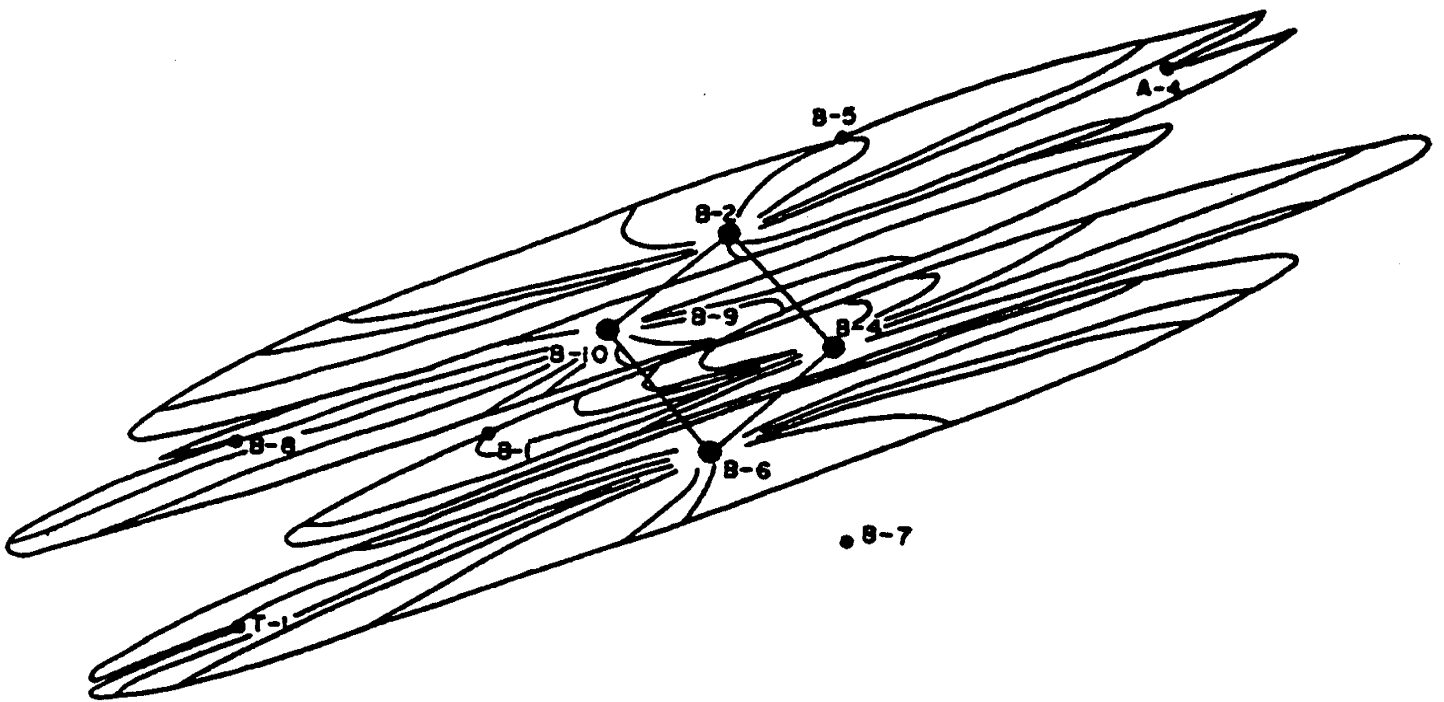


Fig. 3.27 -The flood fronts as of Feb 1, 1958 showing Sh. B-7 and Sh. B-11 did not produce any water after water injection.

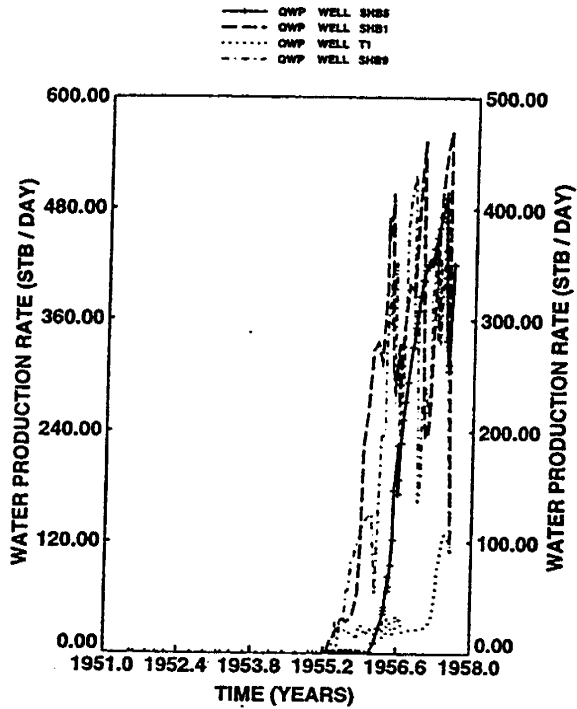


Fig. 3.28 - Water production after water flooding from the middle producer (Sh. B-9) and the wells outside the pattern. Note the Sh. B-9 had water breakthrough first.

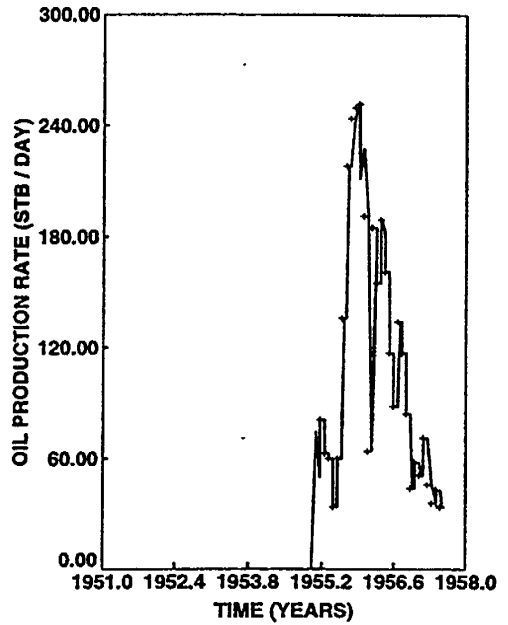


Fig. 3.30 - Match of observed and simulated data for oil production rate in central production well (Sh. B-9).

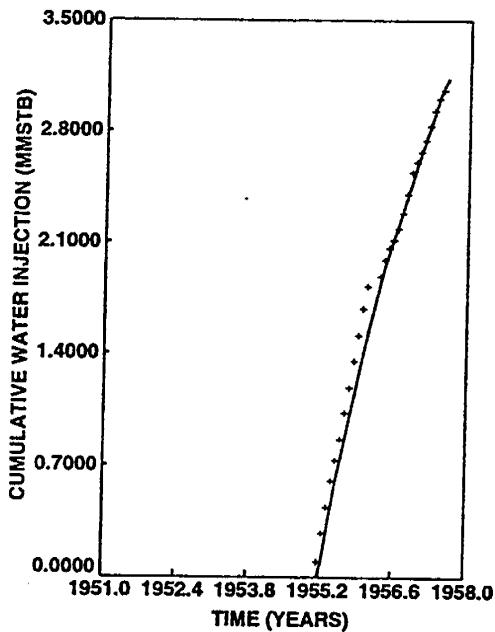


Fig. 3.29-Match of observed and simulated data for cumulative water injection.

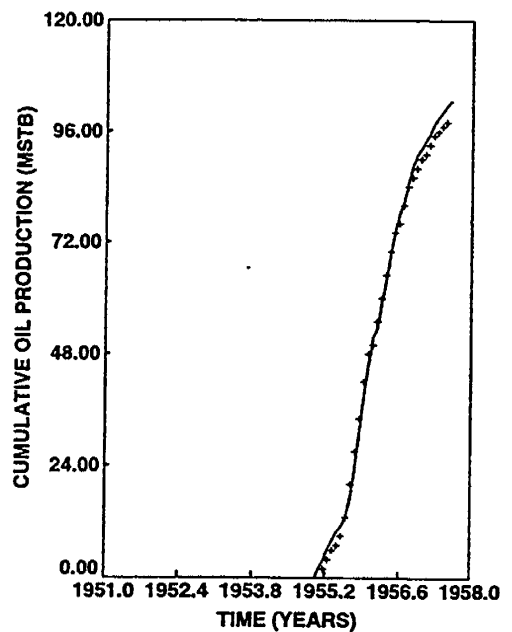


Fig. 3.31 - Match of observed and simulated data for cumulative oil production.

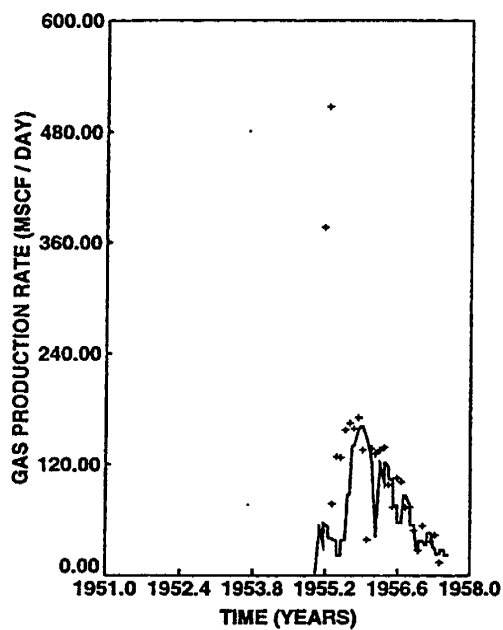


Fig. 3.32 - Match of observed and simulated data for gas production rate.

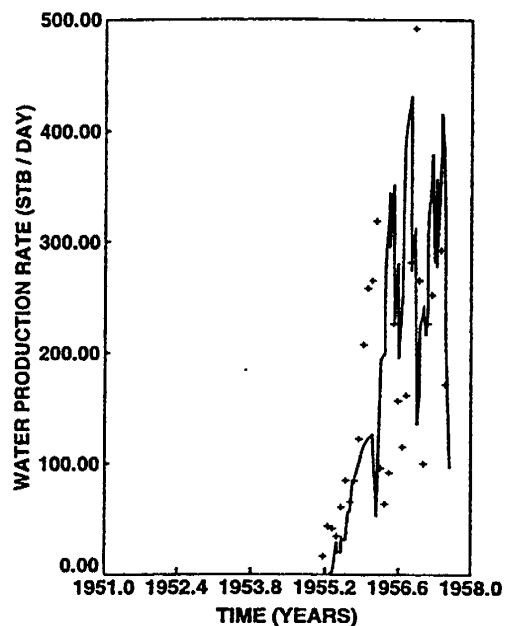


Fig. 3.34 - Match of observed and simulated data for water production rate.

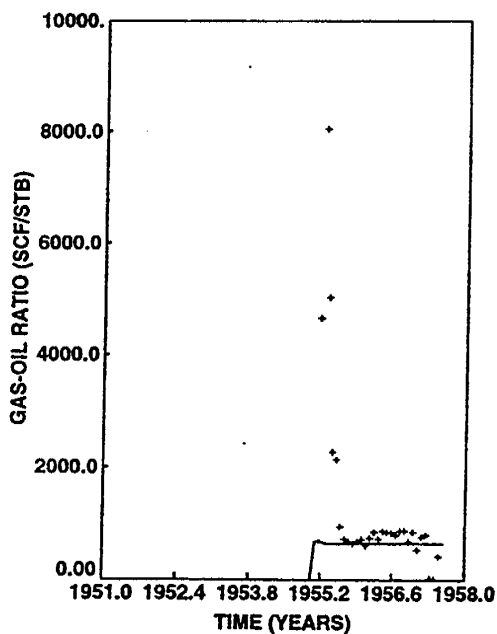


Fig. 3.33 - Match of observed and simulated data for gas-oil ratio.

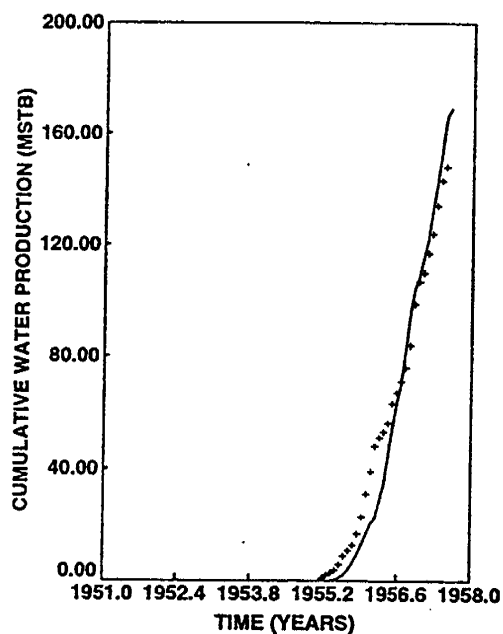


Fig. 3.35 - Match of observed and simulated data for cumulative water production.

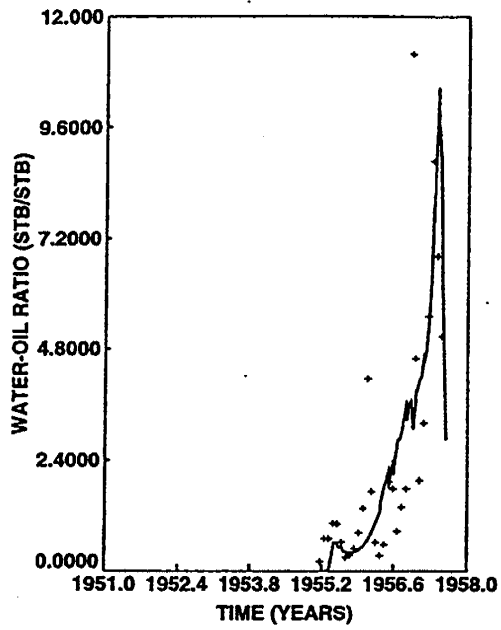


Fig. 3.36 - Match of observed and simulated data for water-oil ratio.

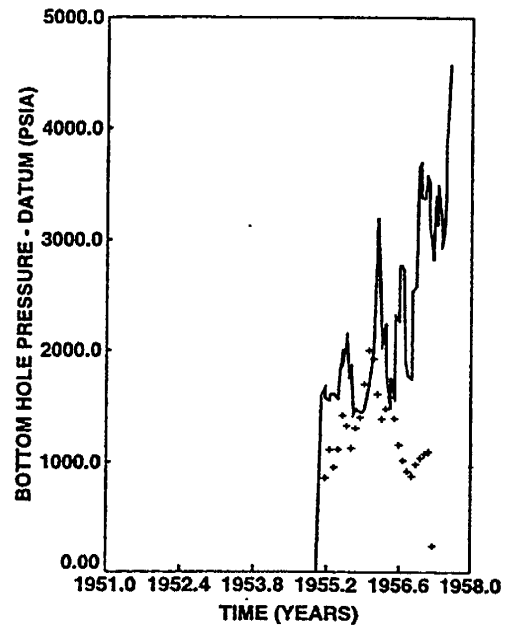


Fig. 3.38 - Match of observed and simulated data for bottom hole pressure.

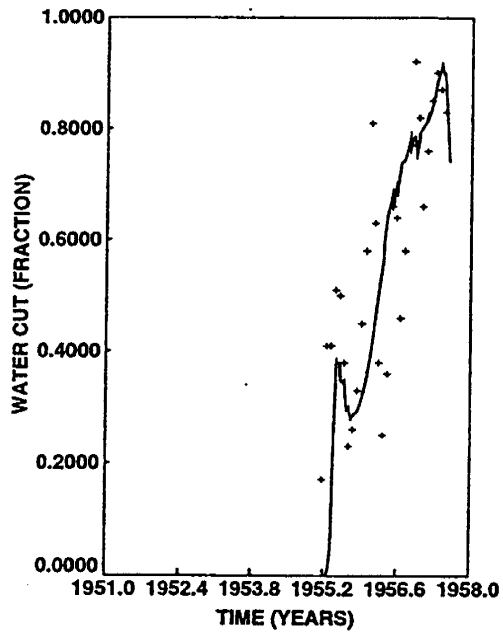


Fig. 3.37 - Match of observed and simulated data for water cut.

4. INVESTIGATION OF CO₂/CRUDE OIL PHASE BEHAVIOR AND RECOVERY MECHANISM BY CO₂ INJECTION IN FRACTURED SYSTEMS

4.1 Minimum Miscibility Pressure (MMP)

We have measured the MMP of Spraberry separator oil in our laboratory. Figure 4.1 shows oil recovery versus pressure. The MMP is estimated to be about 1,550 psig. The interstitial velocity in our slim tube was calculated to be 0.094 cm/s. Viscosity of CO₂ was estimated to be 0.03 cp under experimental conditions. IFT was estimated using the Peng-Robinson Equation of State (PREOS) to be about 1.8 mN/m, which is consistent with recently measured values near 2 mN/m (shown in the next section). The MMP value of 1,550 psig corresponds to a capillary number of 5.5×10^{-5} .

4.2 Interfacial Tension Measurements

Interfacial tension (IFT) of two CO₂/crude oil systems were measured versus pressure at 138 °F using the pendant drop apparatus in our laboratory. The first sample investigated was Spraberry separator oil which was tested to have a Minimum Miscibility Pressure (MMP) of about 1,550 psig. The second sample was recombined Spraberry reservoir oil with an MMP of about 1,565 psig which is within experimental variation of the separator oil. Phase densities of the two systems were also measured versus pressure. Fig. 4.2 shows measured density data for the two systems. This figure demonstrates that the presence of light components in the recombined reservoir oil causes the density of the liquid and gaseous phases of the recombined oil to be lower than that of the separator oil. Measured first-contact IFT data are plotted against pressure in Fig. 4.3. A composite plot of density difference against IFT is illustrated in Fig. 4.4 for the two systems.

It can be seen from Fig. 4.3 that the IFT of the CO₂/separator oil declines rapidly with pressure until about 1,550 psig which is close to the MMP. At pressures above the 1,550 psig, the IFT drops slowly with pressure. The CO₂/recombined oil demonstrates a similar trend with IFT declining rapidly with pressure before 2,000 psig is reached. This was higher than the measured MMP of 1,565 psig.

Although Fig. 4.2 and Fig. 4.3 demonstrate significant difference in IFT and density between the two systems, Fig. 4.4 clearly indicates that their first-contact IFT's have the same density-dependent behavior as they follow the same trend in the plot. However, as shown in Fig. 4.4, the slope deviates from the slope of 3.88 especially at high pressures. The 3.88 slope is defined by critical scaling law for pure substances³⁷, rather than for multi-component systems. However, it should be noted that the measured IFT are for first-contact fluids and this may not reflect the IFT during the multi-contact process.

4.3 Vaporization of Oil Fractions into CO₂

To test the extent of vaporization of oil into CO₂ in the core and diffusion of such a fraction out of the core in the gaseous phase, we are conducting an experiment on CO₂ extraction of Spraberry separator oil used in the gravity drainage experiment. 290 cc of the oil was injected into a 1 liter container which was placed in a 138°F air bath. CO₂ was then injected into the container to a pressure of 2000 psig. The container was occasionally agitated to accelerate thermodynamic equilibrium. After 24 hours, the gaseous phase was vented through a condenser. The temperature of the water input to the condenser was 0 °C. The temperature of the water flowing out of the condenser was 2.5 °C. Due to the Joule-Thomson cooling effect, the temperature of the expanding gaseous phase was believed to be below 0 °C because the formation of ice was observed at the surface of the still hose which delivers the gaseous phase to the condenser. The produced oil from the container was in liquid form as observed at the outlet of the condenser. The liquid was collected with a test tube standing in an ice-packed beaker under atmospheric conditions. After depletion of the gaseous phase pressure to atmospheric pressure, 0.15 cc of oil was observed in the test tube. The color of the oil is lighter than any oil produced during the CO₂ gravity drainage experiment. After gas depletion, the container was recharged with CO₂ to 1700 psig and the same mixing procedure was followed. The gaseous phase was vented to the condenser on the fourth day of experiment, 1.7 cc of oil was recovered from the gaseous phase. Again the collected oil was almost colorless. The container was recharged again with CO₂ to 2000 psig and the same mixing procedure was followed. Ten days later gaseous phase was vented to the condenser and no liquid oil was recovered from the gaseous phase.

Although it is difficult to quantify the efficiency of the oil recovery from the gaseous phase, judging from the color of the recovered oil, it is evident that only very light components of the Spraberry separator oil vaporized into the CO₂ phase. The composition of the recovered oil and comparison to the CO₂ gravity drainage experiment are under investigation.

4.4 Investigation of CO₂ Gravity Drainage

Laboratory Experiments

Laboratory experiments were conducted to simulate vertical free-fall gravity drainage from a matrix block in a naturally fractured reservoir. Core samples were first saturated with synthetic reservoir brine. The brine was then horizontally displaced by separator oil to S_{wi} . The oil saturated core was transferred to a vertical core holder with an inner diameter 0.2 cm greater than the core diameter. During the experiment, CO₂ was continuously injected into the 0.1-centimeter wide annulus (simulating a fracture) between the core sample and core holder at reservoir pressure and temperature. Oil recovered from the core sample was collected at ambient pressure. The key parameter of interest is the oil recovery as a function of time.

Core Samples. Two Berea cores with high and low permeabilities and one whole reservoir core from the Spraberry Trend Area in West Texas (Shackelford 1-38 A) were tested. The high permeability Berea core is 55.25 cm long, 10.16 cm in diameter, 18.7% porosity, 500 md absolute permeability, and 35% residual brine saturation after oil displacement. The low permeability Berea core is 55.25 cm long, 10.16 cm in diameter, 13% porosity, 50 md absolute permeability, and 29.4% residual brine saturation after oil displacement. The Spraberry core is 55 cm long, 10.16 cm in diameter, 10% porosity, 0.01 md vertical permeability to brine, and 38.6% residual brine saturation after oil displacement.

Oil. Separator oil produced from the Spraberry Trend Area was used in the experiments. Composition of the oil was obtained from GC analysis. Composition and average molecular weight of the oil are shown in Table 4.1. The oil sample was tested at 100 °F and 1000 psig. The density was 0.8329 g/cc and the viscosity was equal to 2.956 cp. Density of the oil at 138 °F and various pressures are presented in Fig. 4.2. The MMP of the oil was measured and found to be 1550 psig using slim tube at the reservoir temperature of 138 °F.

Results

The experiment with the high permeability Berea core was carried out under pressure of 1450 psig and temperature of 138°F. The experiment was terminated at six days. The produced oil looks similar to original separator oil. Experimental oil recovery data is plotted in Fig. 4.5. The experiment with the low permeability Berea core was carried out under pressures ranging from 1,700 psig to 2,000 and temperature of 138°F. The experiment was terminated at 220 days. The produced oil are black, brown, and yellow in color. Experimental oil recovery data is plotted in Fig. 4.6. The experiment with the Spraberry reservoir core was also performed at a temperature of 138 °F. Pressure started at about 2,000 psig and eventually dropped to 1,500 psig as shown in Fig. 4.7. The produced oils are yellow, light brown, and brown in color. Composition of the yellow and brown oils are also shown in Table 4.1. Density and viscosity of the yellow oil are measured at 60°C and atmospheric pressure. They are 0.82 g/cc and 2.1 cp, respectively. Experimental oil recovery data are plotted in Fig. 4.8.

Discussion

Figure 4.5 indicates fast drainage of oil from the high permeability Berea core during CO₂ injection into the core holder annulus. This is expected because the capillary pressure is already low in the high permeability Berea core and a slight decrease in IFT can reduce capillary pressure to less than the gravitational force. The black color of the produced oil confirms that oil drained before much of CO₂ diffused into the oil bank. However, Figs. 4.6 and 4.8 indicate slow oil recovery from very low permeability reservoir core. This is again expected because of high capillary pressure in the low permeability cores. The light color of the produced oil from the low permeability Berea core and the Spraberry core seems to indicate the formation of a “gas”-rich liquid phase in the pore space of the cores. Comparison of compositions of injected separator oil and produced yellow and blown oils

(see Table 4.1) clearly shows that the produced oil contains much less heavy hydrocarbons than separator oil does. This comparison also shows that some light hydrocarbons were lost during collection of the recovered oil. This is because the oil was collected under atmospheric pressure and, more importantly, elevated temperature that is close to reservoir temperature. Under this condition, some light components should escape with CO₂ in the gaseous state. Material balance calculations indicate that up to 70 % volume of oil was lost with the produced CO₂ stream. By considering the lost volume of produced oil not captured, recovery data is corrected and plotted in Fig. 4.9 for the Spraberry core experiment.

4.5 Mathematical Modeling of CO₂ Gravity Drainage

Introduction

Because fractures are highly conductive to gas and gas is the non-wetting phase in the rock matrix, gas injection into fractured reservoirs has been traditionally considered as an inefficient method for enhancing oil recovery from fractured reservoirs. However, the Midale Pilot¹ indicated that the efficiency of CO₂ injection into fractured reservoirs is not as low as expected. The only explanation is that when a non-equilibrium gas is injected into the fractured system at elevated pressure, compositional effects become active between the gas in the fractures and oil in the matrix. Due to multi-contact mechanism, light hydrocarbons in the oil can be extracted from the virgin oil bank forming a "gas"-rich light liquid phase and an oil-rich heavy liquid phase. This kind of phase split has been reported by several investigators including Lansangan and Smith². The interfacial tension (IFT) between phases is low compared to that between virgin oil phase and gas phase. Therefore, the capillary pressure threshold may be overcome by gravity resulting in gravity drainage of oil from the matrix blocks. In order to understand the mechanism of gravity drainage and predict the response of fractured reservoirs to gas injection, a mathematical model of the process is desirable.

Equilibrium Gravity Drainage. Studies on gravity drainage were conducted a century ago when King³ investigated the principles and conditions of aquifer motion. Investigations of gravity drainage of oil in oil reservoirs were initiated in early 40's of this century. Leverett⁴ and Katz⁵ presented data and discussed the theory relating capillary and gravitational forces acting on liquids contained in a sand body. Stahl *et al.*⁶ conducted experiments to investigate behavior of free-fall gravity drainage of water and oil in an unconsolidated sand. Elkins *et al.*⁷ presented a simplified theory of regional drainage of oil from an up-structure location to a down-structure location due to gravity assuming zero capillary pressure gradient. Cardwell and Parsons⁸ presented a governing equation for the free-fall gravity drainage process. They could not solve the equation because of its non-linearity. By neglecting the term involving the product of permeability and variation of capillary pressure with saturation, they derived a solution for the simplified cases using the concept of a demarcator. Terwilliger *et al.*⁹ conducted experimental and theoretical investigations on gravity drainage performance under

controlled flow rates. Their theory was based on a Buckley and Leverett¹⁰ approach. Nenniger and Storrow¹¹ presented an approximate series solution for free-fall gravity drainage based on film flow theory. The results accurately matched experimental data obtained from a highly permeable pack of glass beads. Essley *et al.*¹² analyzed the gravity drainage process and final oil recovery in a steeply dipping reservoir. Templeton and Nielsen¹³ experimentally investigated the counterflow segregation of fluids under gravitational force field using glass beads. Dumore and Schols¹⁴ performed experimental studies of free-fall gravity drainage of oil in the laboratory and developed a drainage capillary pressure function. Dykstra¹⁵ generalized the approximate theory presented by Cardwell and Parsons. His mathematical model matched some experimental data with assumed permeability values. Hagoort¹⁶ theoretically analyzed vertical displacement efficiencies of forced and free-fall gravity drainage processes. He derived a governing equation for saturation during free-fall gravity drainage, which is identical to that given by Cardwell and Parsons except that he used the Leverett J -function for expressing capillary pressure. He again did not solve the saturation equation because of its non-linearity. Haldorson *et al.*¹⁷ evaluated the gravity drainage mechanism in an oil field using compensated neutron logs, centrifugal displacements and an analytical stochastic approach. Nectoux¹⁸ investigated the velocity influence on sweep efficiency in oil drainage experiments. Compositional effects were also discussed in his paper. Jacquin *et al.*¹⁹ investigated gravity drainage with fluids not in equilibrium. Their laboratory experiments show that the oil recovery by gravity drainage increases if the content of intermediate components in the gas or in the liquid phase increases.

Low IFT and Non-equilibrium Gravity Drainage. Pavone *et al.*²⁰ conducted experiments to investigate free-fall gravity drainage at low IFT. The IFT of the C_1/C_7 mixture utilized in their experiments was 0.53 dyne/cm. They found that a drainage process can be divided into two phases. During the first phase, almost 50% of the oil in place was produced. The second phase began suddenly at a breakpoint or smoothly on the semilog plot. The second-phase production rate was low but led to more than 20 % additional oil production. They also presented a non-linear governing equation for gas saturation during drainage. Their governing equation is similar to the one given by Cardwell and Parsons. They linearized the governing equation by assuming straight-line permeability curve and logarithmic capillary pressure curve. They solved the linearized governing equation analytically assuming that the minimum gas saturation is always at the outlet of the core (the demarcator is always at the bottom of the core). They matched some experimental data by dual use of the analytical solution, i.e., the analytical solution was used twice for early and later times, respectively, to match the same set of experimental data. Stensen *et al.*²¹ performed experiments for analyzing the effect of IFT on gravity drainage. They employed brine and a $C_1/n-C_7$ mixture having IFT ranging from 76 (reported in the paper) to 0.5 dyne/cm. Suffridge and Renner²² investigated gravity drainage experimentally under constant and varying IFT in fractured and non-fractured cores. The varying IFT was obtained by first placing C_{10} in the core, and then letting C_1 to diffuse into the core. Vilva and Meyer²³ presented a formulation for oil desaturation curves used for reservoir simulation. Schechter *et al.*²⁴ reported experimental results of investigations on low IFT imbibition and drainage. They utilized brine/IPA/ $i-C_8$

systems with IFT's of 0.1, 1.07, and 38.1 dynes/cm and density differences of 0.11, 0.21, and 0.33 g/cc, respectively. They also presented analyses of imbibition and drainage mechanisms. It was concluded that gravity drainage of wetting phase from fully saturated vertical cores occurs for inverse Bond numbers less than 1. Luan²⁵ discussed theoretical aspects of free-fall gravity drainage in naturally fractured reservoirs. He solved the governing equation given by Hagoort¹⁶ analytically and numerically. However, he used the same boundary condition as that utilized by Pavone *et al.*, that is, the demarcator is assumed to be always at the bottom of the core. Espie *et al.*²⁶ investigated gravity drainage/waterflood interaction in the laboratory. They found that injection of water into a gravity drained oil column with high gas saturations improves the mobilization of a dry oil bank. Catalan *et al.*²⁷ reported their results of investigations on the effects of wettability and heterogeneities on the recovery of waterflood residual oil with low pressure inert gas injection assisted by gravity drainage. Experiments on forced gravity drainage by gas injection under varying pressures were performed and analyzed. They concluded that tertiary gravity drainage in water-wet systems is most efficient when the oil can spread on water in the presence of gas. Blunt *et al.*²⁸ presented a theoretical and experimental treatment of three phase flow in water-wet porous media from the molecular level upwards. They found that oil spontaneously spreads as a layer between water and gas in most three-phase systems. Their experimental data on gravity drainage in a capillary matched prediction by their theoretical model. Recently Oyno *et al.*²⁹ conducted laboratory experiments on composite cores at reservoir conditions using recombined reservoir fluids to investigate the potential of secondary and tertiary recovery using gas injection, where gravity drainage is regarded as an important recovery mechanism. Although they recognized that the time required to reach capillary/gravity equilibrium depends on oil/gas density difference, gas/oil IFT, and molecular diffusion in both gas and oil phases, they could not identify conditions under which each factor dominates.

In summary, the literature reveals that three different gravity drainage processes in porous media have been investigated: (i) forced gravity drainage by gas injection and controlled flow rate, which occurs when gas is injected into steeply dipping reservoirs, (ii) simulated gravity drainage by centrifuging, which exists only in the laboratory, and (iii) free-fall gravity drainage, which takes place in naturally fractured reservoirs after depletion of oil in the fractures or gas injection into the fractures. The free-fall gravity drainage, which is representative of gas injection into a depleted fractured reservoir, has been investigated by Leverett⁴, Stahl *et al.*⁶, Cardwell and Parsons⁸, Nenniger and Storrow¹¹, Templeton and Nielsen¹³, Dumore and Schols¹⁴, Dykstra¹⁵, Hagoort¹⁶, Jacquin *et al.*¹⁹, Pavone *et al.*²⁰, Stensen *et al.*,²¹ Suffridge and Renner,²² Schechter *et al.*,²⁴ Luan,²⁵ and Oyno *et al.*²⁹

Unlike forced gravity drainage, free-fall gravity drainage cannot be modeled using a Buckley-Leverett approach because flow rate is not pre-specified. A survey of the literature reveals four mathematical models that have been developed for describing the process of free-fall gravity drainage of equilibrium fluids. They are the Cardwell-Parsons-Dykstra (C-P-D) model, Nenniger-Storrow (N-S) model, Pavone-Bruzzi-Verre (P-B-V) model, and Luan Model. The accuracy of these models are found to be poor based on our comparisons with

experimental data. Therefore, we have developed a new mathematical model to simulate equilibrium and non-equilibrium gravity drainage. Comparison of recovery data computed using the new model to experimental data found from both the literature and experiments conducted in our laboratory indicate that the new model can better describe the process of free-fall gravity drainage of both equilibrium and non-equilibrium fluids.

Mathematical Models

There is no mathematical model available from literature to describe non-equilibrium gravity drainage process after gas injection into fractured reservoirs (free-fall gravity drainage). In this study, we simulate the process using mathematical models developed for equilibrium gravity drainage with modifications considering molecular diffusion during gravity drainage. We first tried to select one model among the four existing models: Nenniger-Storrow (N-S) model, Pavone-Bruzzi-Verre (P-B-V) model, and Luan Model. Unfortunately, we found none of them accurate enough to be adopted, even for equilibrium gravity drainage. Comparisons of these models are presented elsewhere.³⁰ Then we decided to develop a new model to simulate equilibrium and non-equilibrium gravity drainage processes. Derivation of the new model is detailed in SPE 35170.³¹ Only the resultant equations are summarized here.

Based on the fact that the volumetric drainage rate is equal to the derivative of draining-phase volume in the porous media with respect to time, the following governing equation for wetting/non-wetting phase demarcator has been formulated:

$$\phi \left[S_{wi} - S_{wr} - \sqrt{\frac{F_s \phi z_D}{5t_D}} \right] \frac{dz_D}{dt_D} + \frac{\phi z_D}{3t_D} \sqrt{\frac{F_s \phi z_D}{5t_D}} - \left[1 - \frac{H_D}{1 - z_D} \right] = 0 \quad (1)$$

where the dimensionless groups are defined as

$$z_D = \frac{z_d}{L} \quad (2)$$

$$H_D = \frac{H}{L} \quad (3)$$

and

$$t_D = \frac{k_e \Delta \rho g t}{\mu L} \quad (4)$$

Equation (1) is non-linear and is difficult, if not impossible, to solve analytically. Therefore, we solved the equation numerically by rearranging it into the following form:

$$\Delta z_D = \frac{-\frac{\phi z_D}{3t_D} \sqrt{\frac{F_s \phi z_D}{5t_D}} + \left[1 - \frac{H_D}{1-z_D} \right]}{\phi \left[S_{wi} - S_{wr} - \sqrt{\frac{F_s \phi z_D}{5t_D}} \right]} \Delta t_D \quad (5)$$

Using initial condition of 0.001 for z_D at a very small time t_D (0.0001 for example) and a small time step Δt_D , the increment of the demarcator Δz_D can be calculated from this equation. Then z_D and t_D can be updated by

$$z_{D_{new}} = z_{D_{old}} + \Delta z_D \quad (6)$$

and

$$t_{D_{new}} = t_{D_{old}} + \Delta t_D \quad (7)$$

Repeated use of Eqs. (5), (6) and (7) gives a numerical solution to Eq. (1). Based on the position of the demarcator and the volume distribution of the liquid above the demarcator, the draining-phase recovery as a function of time is calculated utilizing Eq. (8).

$$R_D = \left(1 - \frac{S_{wr}}{S_{wi}} \right) z_D - \frac{2z_D}{3S_{wi}} \sqrt{\frac{F_s \phi z_D}{5t_D}} \quad (8)$$

Two typical solution curves are presented in Figs. 4.10 and 4.11 for $\phi = 0.1$, $S_{wr} = 0.1$, $H_D = 0.1$, and $F_s = 1$ and 0.5 , respectively. It is clearly seen from Figs. 4.10 and 4.11 that the equilibrium gravity drainage process can be divided into two periods. During the first period, the demarcator drops and the total drainage rate is a combination of rate of full-pore flow and that of film flow. During the second period, the demarcator is stabilized and the total drainage rate is the rate of film flow only. It is interesting to note the effect of the correction factor to the Kozeny equation F_s (discussed in detail in reference 32) on the shape of demarcator and recovery curves indicated by the two figures. When F_s is greater, as shown in Fig. 4.10, the demarcator stabilizes gradually during bulk flow leaving more recoverable fluid behind for pure film flow to occur. When F_s is small, as shown in Fig. 4.11, the demarcator stabilizes sharply at the end of bulk flow leaving less recoverable fluid behind for pure film flow.

Non-equilibrium gravity drainage occurs when a porous medium saturated with one phase is surrounded by another phase not in equilibrium, for instance, injected gas and resident oil. In this case, the surrounding phase migrates into the porous medium due to molecular diffusion causing the IFT of the fluid in the porous medium to change with time. For example, when

an oil-saturated, vertically oriented core is surrounded by CO₂ during gravity drainage, the CO₂ diffuses into the core resulting in continuous reduction of IFT between the CO₂-rich phase and the oil phase as CO₂ moves into the interior of the core. Thus the IFT at any point in the core is time dependent.

Although the new mathematical model is derived assuming that the wetting phase and non-wetting phase are in thermodynamic equilibrium, it is possible to apply the model to simulation of a non-equilibrium gravity drainage process if some modifications are made to account for the non-equilibrium effect due to diffusion. If we divide the core length into many elements along the direction of diffusion, then it is possible to apply the mathematical model to each individual element where uniform fluid properties are assigned to that element. We have developed the following step-wise procedure to simulate non-equilibrium CO₂ gravity drainage in our three cores:

1. Divide the core in the radial (horizontal) direction into 50 cylindrical elements, and estimate the concentration of the gas phase in each element at a given diffusion/drainage time;
2. Estimate the average fluid viscosity, density, IFT and capillary pressure in each element at the time based on the composition of the fluid mixture;
3. Apply the mathematical model to each element to estimate liquid recovery from the element at a given time;
4. Sum up the recoveries calculated from each element to get the total liquid recovery at a given time;
5. Update the time by adding a time step and repeat 1, 2, 3, and 4 until a desired ultimate drainage time is reached.

In order to estimate gas concentration in each element, it is necessary to solve the diffusion equation (Fick's second law). Different analytical solutions to the diffusion equation are available from literature such as Crank³¹ and Carslaw and Jaeger³². It is not clear yet as which of the solutions is more suitable for analyzing gas diffusion into reservoir matrix. To avoid difficulties involved in programming these solutions, a simple numerical solution to the diffusion equation is used in this study. It has been found that the numerical result matches the analytical solution given by Crank³² when the time step is less than 0.5 day for a diffusion coefficient less than 10⁻⁷ cm²/s. This comparison is shown in Fig. 4.12. The numerical procedure to the solution is detailed in reference 31.

Comparisons

Equilibrium Gravity Drainage. The new mathematical model is derived assuming constant capillary pressure at the demarcator, i.e., the wetting phase and non-wetting phase are in thermodynamic equilibrium. This model is compared with existing models and 20 sets of experimental drainage data obtained under thermodynamic equilibrium. In these experiments, the IFT varies between 76 and 0.1 mN/m, the density difference changes from 1.25 to 0.11 g/cc, the effective permeability to the wetting phase covers a wide range, from 6,602 Darcies to 6.1 mD, porosity from 42.72% to 18.4 %, and connate water saturation from 0 to 15.8%. Fig. 4.13 shows comparisons of model calculated and observed C_1/C_7 recoveries from a Fontainebleau sandstone core.²⁰ Other comparisons similar to Fig. 4.13 have been presented in a separate document³⁰. These comparisons indicate that the new model yields better accuracy than other models. The Cardwell-Parsons-Dykstra model and Nenniger-Storrow (N-S) model consider a moving demarcator, while the Pavone-Bruzzi-Verre (P-B-V) model and Luan model assume fixed a demarcator at the bottom of the porous media, which is not a true physical representation of drainage behavior. The C-P-D model neglects a capillary term that appears in the governing equation. The N-S model is an approximate series solution, and the accuracy depends on number of terms (the paper provides expressions for only three terms). The P-B-V model was obtained by assuming a straight-line relative permeability and a logarithmic capillary pressure curve, which also may not be representative of the true behavior. It is believed that these unrealistic assumptions used in model development cause inaccuracies of these models in describing free-fall gravity drainage processes.

Non-equilibrium Gravity Drainage. The concentration of CO_2 in the simulated fracture (annular space around core sample) was estimated based on an Equation of State (EOS):

$$c_f = \frac{p}{zRT} \quad (9)$$

CO_2 concentration in each matrix element was obtained by multiplying c_f by dimensionless concentration calculated from the numerical solution to the diffusion equation presented in Appendix B. Then EOS was used again to determine volume of CO_2 in each element. Oil production due to horizontal diffusion was assumed to be equal to the volume of CO_2 that had diffused into the rock.

The viscosity data provided by Lansangan and Smith² for CO_2 /West Texas oil was utilized in our model. Density and IFT data used in the model were from our measurements as presented in the previous sections. The capillary pressure threshold was calculated using Eq. 10.

$$H = \frac{0.2\sigma}{\Delta\rho g} \sqrt{\frac{\phi}{k_e}} \quad (10)$$

Based on Renner's measurements³⁴, the molecular diffusion coefficient of CO₂ in a decane-saturated Berea core at 100 °F and 850 psig varies from 5.05x10⁻⁵ to 1.08x10⁻⁴ cm²/s. The molecular diffusion coefficient of CO₂ in the pure decane may be back calculated from the following equation:

$$D = \frac{D_0}{F\phi} \quad (11)$$

Using $0.81/\phi^2$ as an approximation to the formation factor F and 0.20 porosity for the Berea core, the molecular diffusion coefficient of CO₂ in the pure decane is estimated to be $D_0=2 \times 10^{-4}$ to 4×10^{-4} cm²/s. This value may be optimistic if applied to CO₂/STO system at 138 °F and 2,000 psig. In the petroleum industry, a practical value of $D_0=2 \times 10^{-5}$ cm²/s for a molecular diffusion coefficient for reservoir liquids is commonly used in simulation of CO₂ miscible flooding.³⁵ However, we have found that the $D_0=2 \times 10^{-5}$ cm²/s results in an over-estimation of oil recovery by our mathematical model. The oil recoveries from our CO₂ gravity drainage experiments were matched by our mathematical model when the molecular diffusion coefficient was tuned to $D_0=6 \times 10^{-7}$ cm²/s.

Figure 4.14 demonstrates the comparison of our experimental data with the recovery curve calculated by the mathematical model for a high permeability Berea core. Figure 4.15 shows the comparison of our experimental data with the recovery curve calculated by the mathematical model for the low permeability Berea core. Figure 4.16 illustrates the comparison of our experimental data with the recovery curve calculated by the mathematical model for the low permeability Spraberry core.

Conclusions

1. A literature survey reveals that four mathematical models have been developed by previous investigators for describing free-fall gravity drainage of equilibrium phases in porous media. They are C-P-D Model, N-S Model, P-B-V Model and Luan Model. Comparison of wetting phase recoveries calculated by these models with experimental data indicates these models to be inaccurate. Discrepancies are believed to be due to unrealistic assumptions made in formulation of these models.
2. Based on Darcy's law and film flow theory, a new mathematical model has been developed to describe free-fall gravity drainage with equilibrium fluids. Comparisons of wetting phase recoveries given by the new model with 20 sets of experimental data obtained under thermodynamic equilibrium show better accuracy of the model over existing models.
3. The diffusion equation has been solved numerically to estimate gas concentration in the porous media. A procedure has been developed to couple equilibrium gravity drainage with diffusion in order to describe non-equilibrium gravity drainage. Using this procedure and

empirical correlations for fluid properties, experimental data obtained under thermodynamic non-equilibrium conditions has been matched.

Nomenclature

c_f	=	fractional concentration, mol/cm ³ .
D	=	effective diffusion coefficient, cm ² /s.
D_0	=	molecular diffusion coefficient, cm ² /s.
F	=	formation factor, dimensionless.
F_s	=	correction factor to Kozeny equation.
G	=	gravitational acceleration, cm/s ² .
H	=	capillary pressure threshold, cm.
H_D	=	dimensionless capillary pressure threshold.
k_e	=	effective permeability, md.
L	=	core length, cm.
p	=	pressure, atm.
R	=	universal gas constant, 8.314 J·mol ⁻¹ ·K ⁻¹
R_D	=	dimensionless fluid recovery, OOIP
S_{wi}	=	initial wetting phase saturation, fraction.
S_{wr}	=	residual wetting phase saturation, fraction.
T	=	time, s.
t_D	=	dimensionless time.
Δt	=	time step size, s.
z_d	=	demarcator depth, cm.
z_D	=	dimensionless demarcator depth.
$\Delta\rho$	=	density difference, g/cm ³ .
μ	=	viscosity, cp.
σ	=	interfacial tension, dyne/cm.
ϕ	=	porosity, fraction.

References

1. Beliveau, D., Payne, D.A., and Mundry, M.: "Waterflood and CO₂ Flood of the Fractured Midale Field," *Journal of Petroleum Engineering*, September 1993, 881.
2. Lansangan, R.M. and Smith, J.L.: "Viscosity, Density and Composition Measurements of CO₂/West Texas Oil Systems," *SPE Reservoir Engineering*, August 1993.
3. King, F.H.: "Principles and Conditions of the Movements of Ground Water," Annual Report, USGS (1899), **19**.
4. Leverett, M.C.: "Capillary Behavior in Porous Solids," *Trans. AIME* (1941), **142**, 152.
5. Katz, D.L.: "Possibilities of Secondary Recovery for the Oklahoma City Wilcox Sand," *Trans. AIME* (1942), **146**, 28.
6. Stahl, R.F., Martin, W.A., and Huntington, R.L.: "Gravitational Drainage of Liquids from

- Unconsolidated Wilcox Sand," *Petroleum Technology*, January 1943.
7. Elkins, L.F., French, R.W., and Glenn, W.E.: "Lance Creek Sundance Reservoir Performance --- a Unitized Pressure-Maintenance Project," *Petroleum Tech.*, July 1948.
 8. Cardwell, W.T. and Parsons, R.L.: "Gravity Drainage Theory" *Trans.AIME* (1949), **179**, 199.
 9. Terwilliger, P.L., Wilsey, L.E., Hall, H.N., Bridges, P.M., and Morse, R.A.: "An Experimental and Theoretical Investigation of Gravity Drainage Performance," *Petroleum Transactions, AIME* (1951), **192**.
 10. Buckley, S.E. and Leverett, M.C.: "Mechanism of Fluid Displacement in Sands," *Trans. AIME* (1942), **146**, 107.
 11. Nenniger, E. and Storrow, J.A.: "Drainage of Packed Beads in Gravitational and Centrifugal-Force Fields," *AIChE* (1958), **4**, No. 3, 305.
 12. Essley, P.L., Hancock, G.L., and Jones, K.E.: "Gravity Drainage Concepts in a Steeply Dipping Reservoir," paper SPE 1029-G, 1958.
 13. Templeton, E.E. and Nielsen, R.E.: "A Study of Gravity Counterflow Segregation," *SPE Journal*, June 1962.
 14. Dumore, J.M. and Schols, R.S.: "Drainage Capillary - Pressure Functions and the Influence of Connate Water," *SPE Journal*, October 1974.
 15. Dykstra, H.: "The Prediction of Oil Recovery by Gravity Drainage," *Journal of Petroleum Technology*, May 1978.
 16. Hagoort, J.: "Oil Recovery by Gravity Drainage," *SPE Journal*, June 1980.
 17. Haldorsen, H.H., Rego, C.A., Chang, D.M., Mayson, H.J., and Creveling, D.M. Jr.: "An Evaluation of the Prudhoe Bay Gravity Drainage Mechanism by Complementary Techniques," paper SPE 13651, presented at the
 18. SPE California Regional Meeting, held in Bakersfield, California, March 27-29, 1985.
 19. Nectoux, A.: "Equilibrium Gas Oil Drainage: Velocity, Gravitational and Compositional Effects," paper presented at the 4th European Symposium on Enhanced Oil Recovery, held October 27-29, 1987 in Hamburg, 779.
 20. Jacquin, Ch., Legait, B., Martin, J.M., Nectoux, A., Anterion, F., and Rioche, M.: "Gravity Drainage in a Fissured Reservoir with Fluids not in Equilibrium," *Journal of Petroleum Science and Engineering* (1989) **2**, 217.
 21. Pavone, D., Bruzzi, P. and Verre, R.: "Gravity Drainage at Low Interfacial Tension," paper presented at the 5th European Symposium on Enhanced Oil Recovery, held October 27-29, 1989 in Budapest, 165.
 22. Stensen, J.A., Skange, A. Monstad, P., and Graue, A.: "The Effect of Interfacial Tension on Gas Gravity Drainage," paper presented at the 2nd North Sea Chalk Symposium, held June 11-12, 1990 in Copenhagen, Denmark.
 23. Suffridge, E.E. and Renner, T.A.: "Diffusion and Gravity Drainage Tests to Support the Development of a Dual Porosity Simulator," paper presented at the 6th European IOR-Symposium, held May 21-23, 1991 in Stavanger, Norway.
 24. da Vilva, F.V. and Meyer, B.: "Improved Formulation for Gravity Segregation in Naturally Fractured Reservoirs," paper presented at the 6th European IOR-Symposium, held May 21-23, 1991 in Stavanger, Norway.

25. Schechter, D.S., Zhou, D., and Orr, F.M. Jr.: "Low IFT Gravity Drainage and Imbibition," *Journal of Petroleum Science and Engineering* (November 1994), 283.
26. Luan, Z.: "Some Theoretical Aspects of Gravity Drainage in Naturally Fractured Reservoirs," paper SPE 28641, presented at the 69th Annual Technical Conference and Exhibition of SPE, held September 25-28, 1994 in New Orleans, Louisiana.
27. Espie, A.A., Brown, C.E., Narayanan, K.R. and Wilcox, T.C.: "A Laboratory Investigation of Gravity Drainage/Waterflood Interaction in Prudhoe Bay," paper SPE 28614, presented at the 69th Annual Technical Conference and Exhibition of SPE, held September 25-28, 1994 in New Orleans, Louisiana.
28. Catalan, L.J.J., Dullien, F.A.L., and Chatzis, I.: "The Effects of Wettability and Heterogeneities on the Recovery of Waterflood Residual Oil with Low Pressure Inert Gas Injection Assisted by Gravity Drainage," *SPE Advanced Tech. Series*, 2, No. 2, 1994.
29. Blunt, M., Zhou, D., and Fenwick, D.: "Three Phase Flow and Gravity Drainage in Porous Media," paper submitted to *Transport in Porous Media* for publication, May 1994.
30. Oyno, L., Uleberg, K., and Whitson, C. H.: "Dry Gas Injection Fractured Chalk Reservoirs -- An Experimental Approach," paper SCA 9527 presented at the 1995 SCA Conference, San Francisco, California, August 20-22, 1995.
31. Guo, B.: "Modeling of Gravity Drainage Under Constant and Varying Capillary Pressure," proceedings of Naturally Fractured Reservoir Forum, New Mexico Institute of Mining and Technology, March 2, 1995.
32. Schechter, D.S. and Guo, B.: "Mathematical Modeling of Gravity Drainage after Gas Injection into Fractured Reservoirs," paper SPE 35170 presented at the SPE Improved Oil Recovery Symposium held in Tulsa, Oklahoma April 22-24, 1996.
33. Crank, J.: *The Mathematics of Diffusion*, second edition, Oxford University Press, New York City (1975).
34. Carslaw, H.S. and Jaeger, J.C.: *Conduction of Heat in Solids*, second edition, Oxford University Press, New York City (1959).
35. Lopez de Ramos, A.L.: *Capillary-Enhanced Diffusion of CO₂ in Porous Media*, Ph.D. thesis, University of Tulsa, Tulsa, Oklahoma, 1993.
36. Stalkup, F.I., Jr.: *Miscible Displacement*, SPE Textbook Series, Dallas, 1984.
37. Widom, B.: "Phase Equilibrium and Interfacial Structure," *Chemical Society Review* (1985), 121-139.

Table 4.1 - Composition of separator oil and produced oil

Hydrocarbon Number	Mole Fraction		
	Separator Oil	Recovered Yellow Oil	Recovered Brown Oil
5	0.09114	0.00122	0.00143
6	0.06631	0.00058	0.00103
7	0.14649	0.00190	0.00612
8	0.10466	0.00585	0.01799
9	0.06115	0.01425	0.03063
10	0.05053	0.03841	0.05731
11	0.03736	0.06110	0.07372
12	0.03561	0.08715	0.09773
13	0.03313	0.10453	0.11466
14	0.02572	0.08705	0.09355
15	0.02151	0.07932	0.08366
16	0.02020	0.07220	0.07295
17	0.02088	0.07893	0.07774
18	0.01485	0.05368	0.05020
19	0.01609	0.05446	0.04840
20	0.01142	0.03545	0.03029
21	0.01068	0.03057	0.02560
22	0.01016	0.02579	0.02109
23	0.00957	0.02142	0.01730
24	0.00898	0.01721	0.01382
25	0.00599	0.01051	0.00853
26	0.00846	0.01187	0.00952
27	0.00574	0.00682	0.00551
28	0.00852	0.00867	0.00711
29	0.00583	0.00488	0.00406
30	0.00566	0.00414	0.00354
31	0.00569	0.00363	0.00320
32	0.00555	0.00320	0.00293
33	0.00536	0.00291	0.00280
34	0.00540	0.00283	0.00283
35	0.00550	0.00285	0.00296
36	0.00822	0.00439	0.00472
37+	0.12763	0.06224	0.00709
Total	1.00000	1.00000	1.00000
Molecular Weight	219.39	251.80	222.34

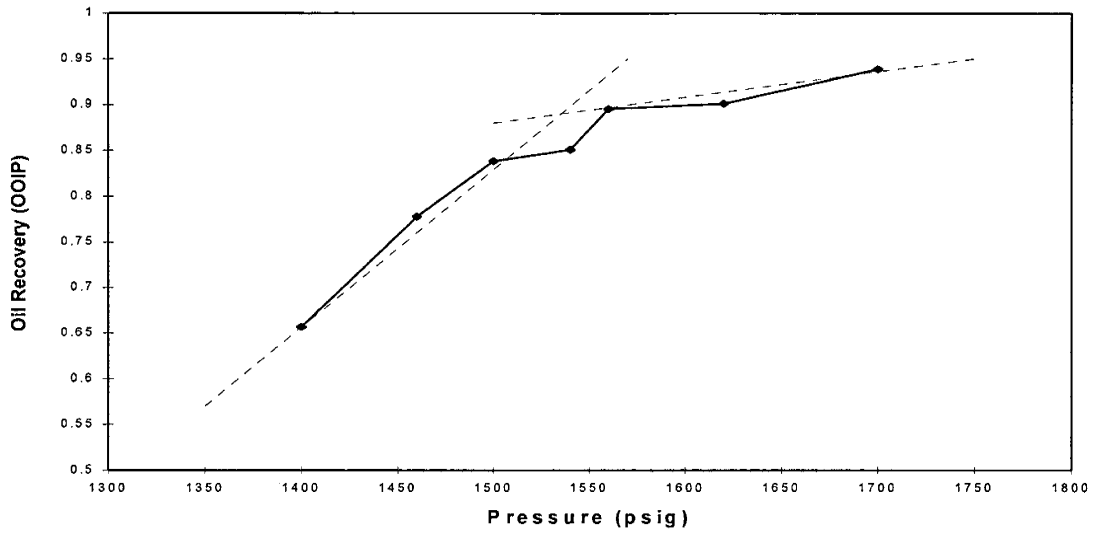


Fig. 4.1 - Results from slim-tube indicate the minimum miscibility pressure for Spraberry separator oil is approximately 1540 psig

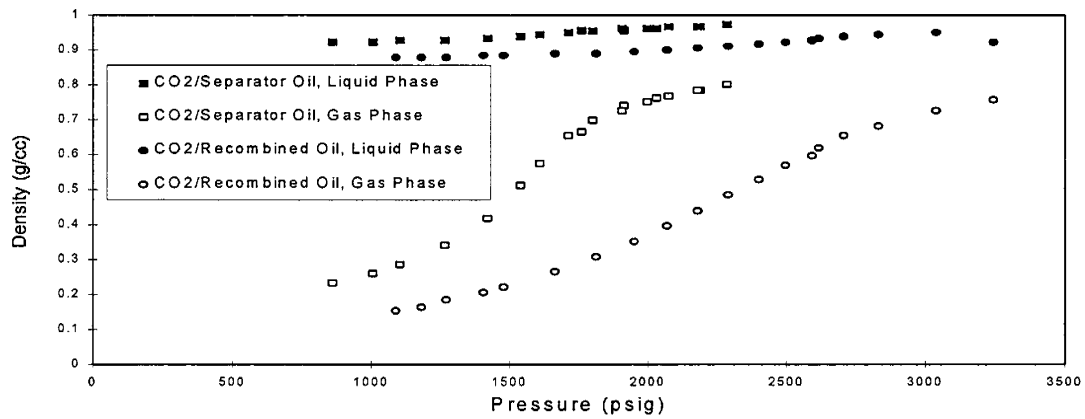


Fig. 4.2 - Measured densities of CO₂/Spraberry oil systems at 138 °F

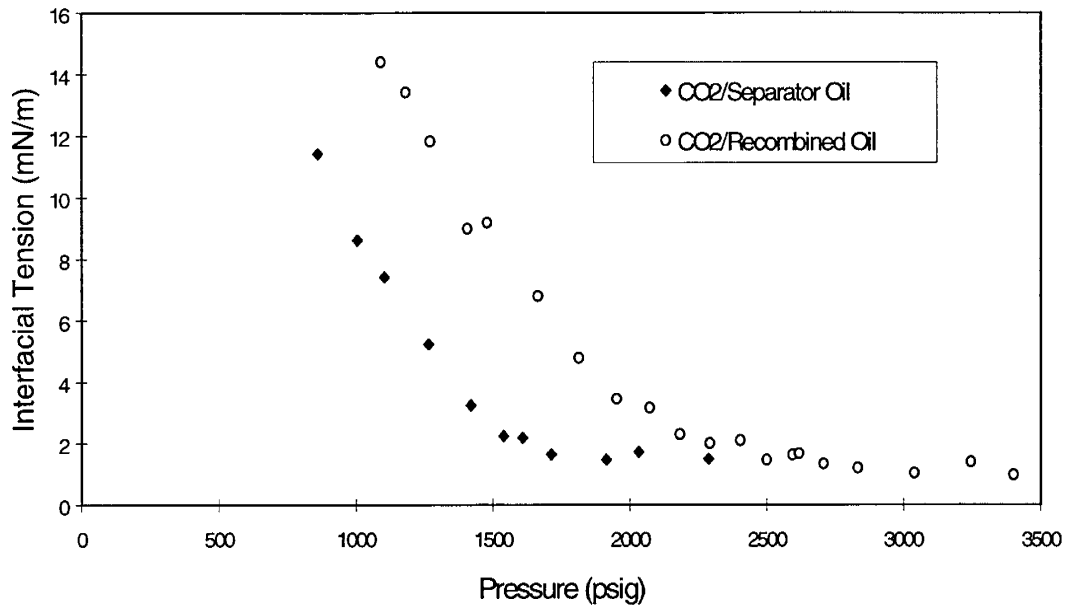


Fig. 4.3 - Effect of pressure on IFT of two CO₂/Spraberry crude oil systems at 138 °F

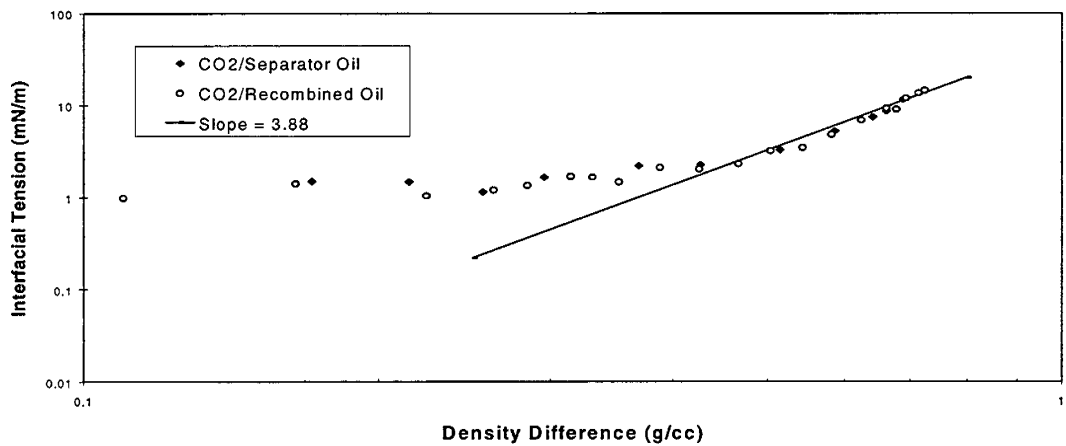


Fig. 4.4 - Relationship between density difference and IFT for two CO₂/Spraberry crude oil systems at 138 F

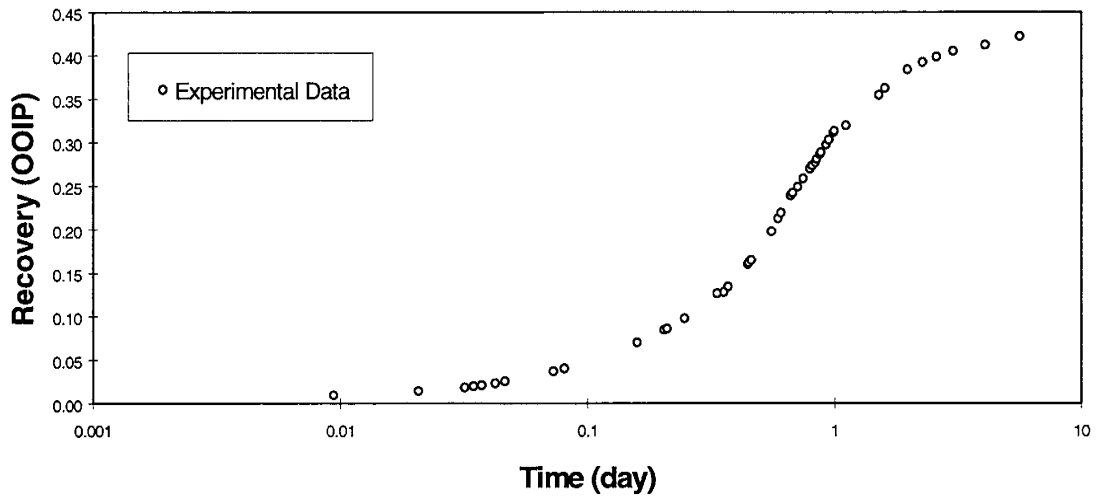


Fig. 4.5 - Oil recovery during CO₂ gravity drainage from a 500 md Berea core

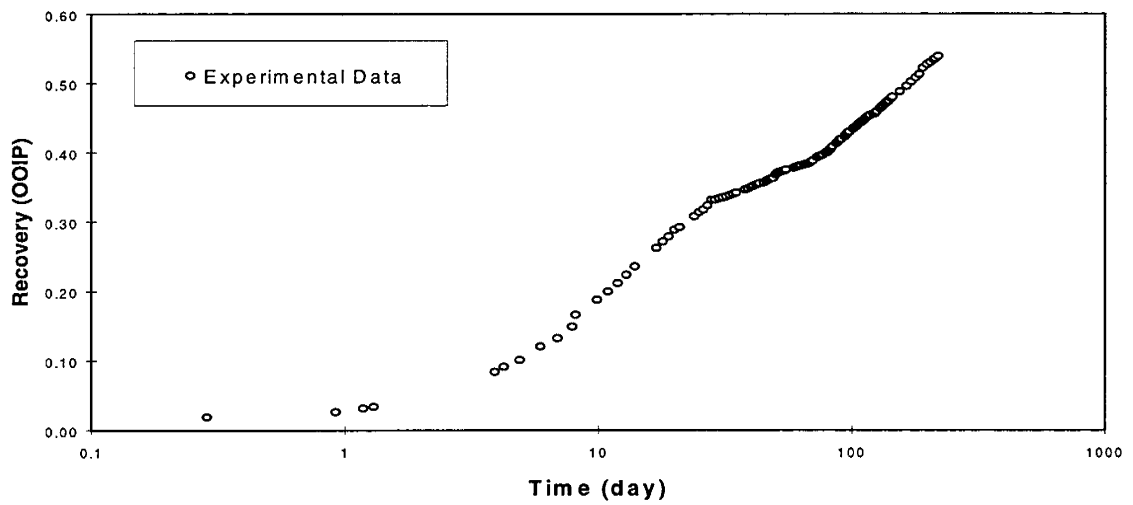


Fig. 4.6 - Oil recovery during CO₂ gravity drainage from a 50 md Berea core

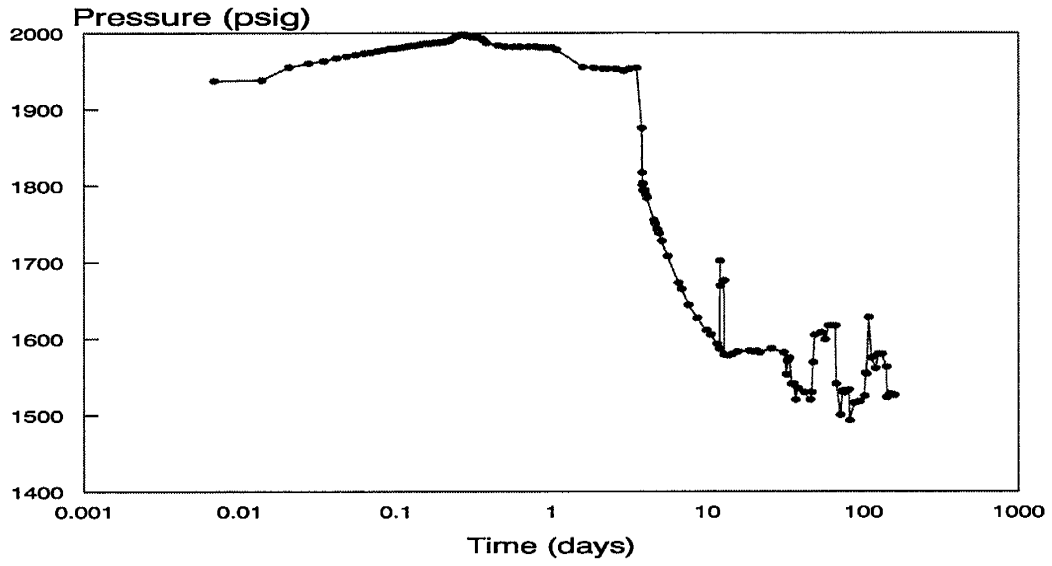


Fig. 4.7 - Pressure history of the Spraberry whole core experiment

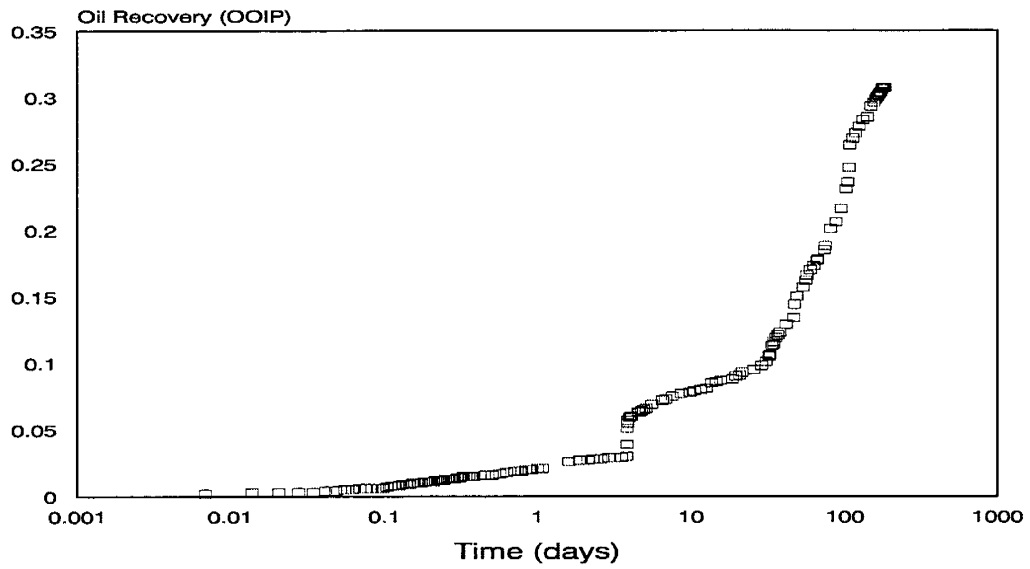


Fig. 4.8 - Oil recovery from the Spraberry core collected at near reservoir temperature

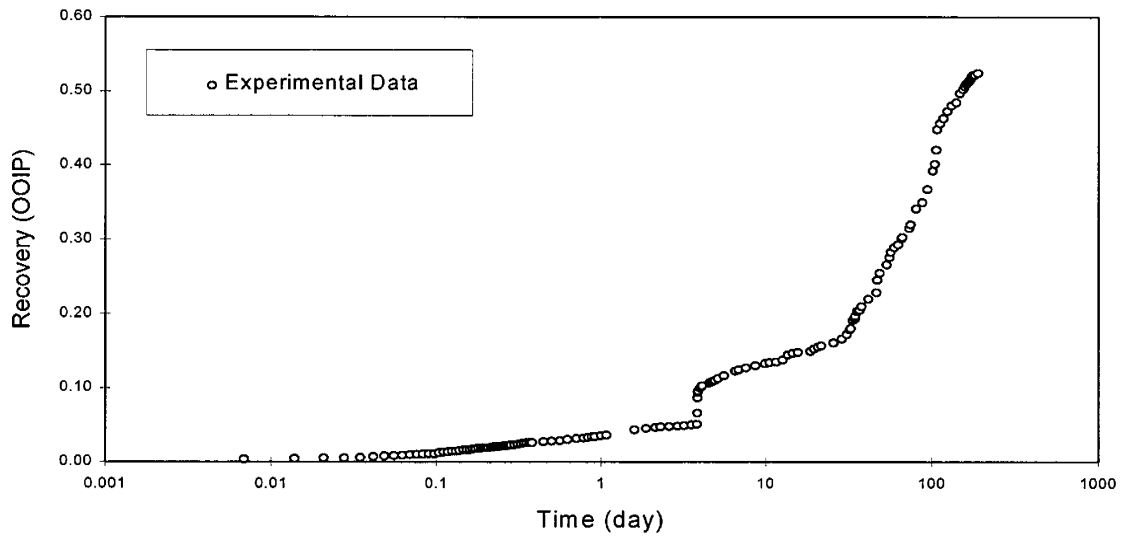


Fig. 4.9 - Oil recovery during CO₂ gravity drainage from a Spraberry core corrected for loss of light ends in CO₂ stream

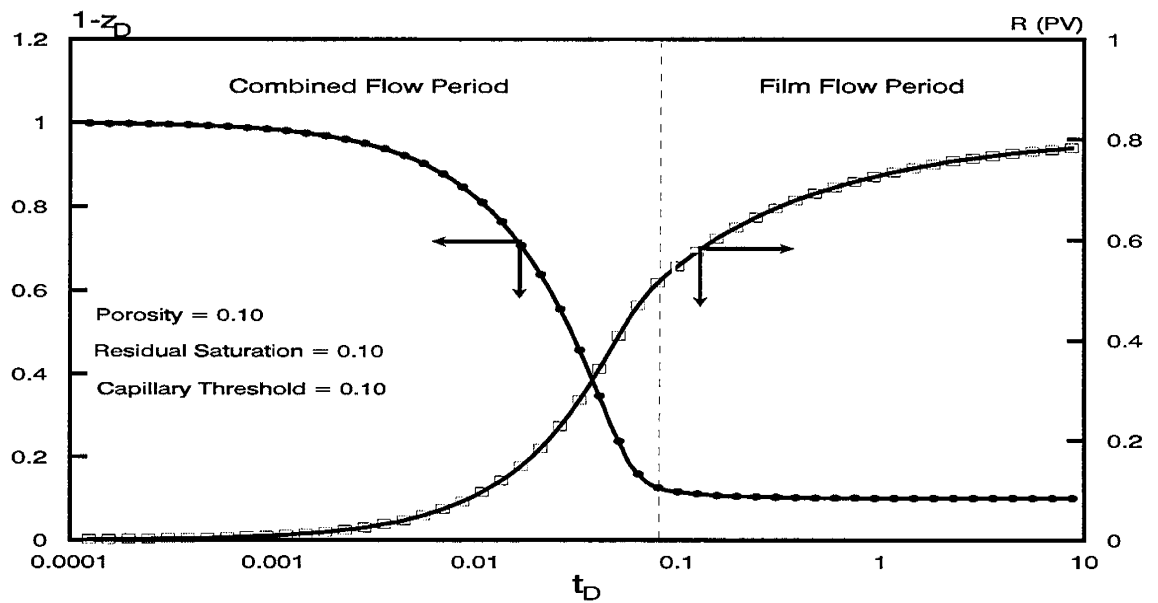


Fig. 4.10 - Solution to demarcator and (z_D) and recovery (R) for $F_s = 1$

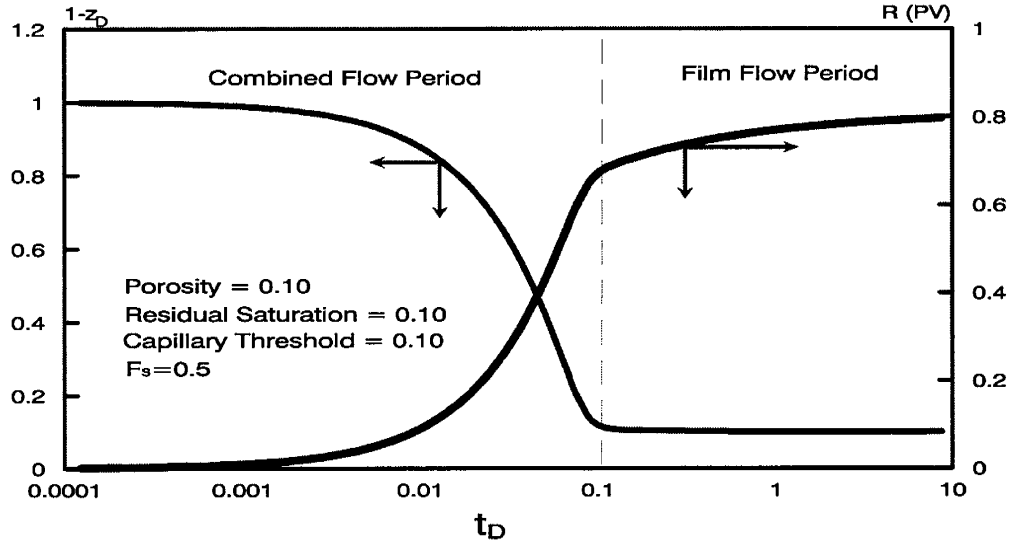


Fig. 4.11 - A typical solution for demarcator (z_D) movement and recovery (R)

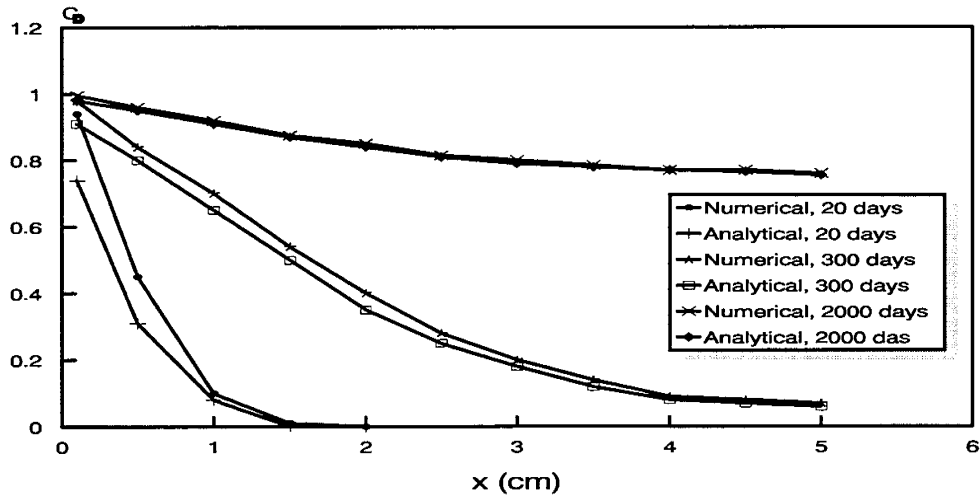


Fig. 4.12 - Model calculated dimensionless gas concentration diffusing into rock matrix from fracture faces

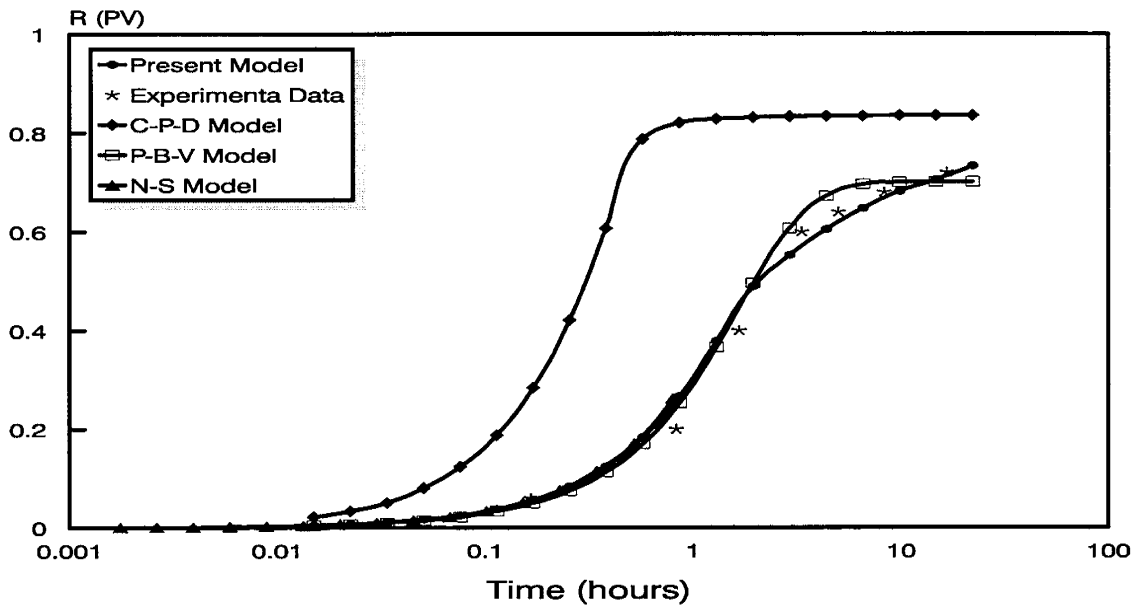


Fig. 4.13 - Comparison of calculated recoveries with experimental data

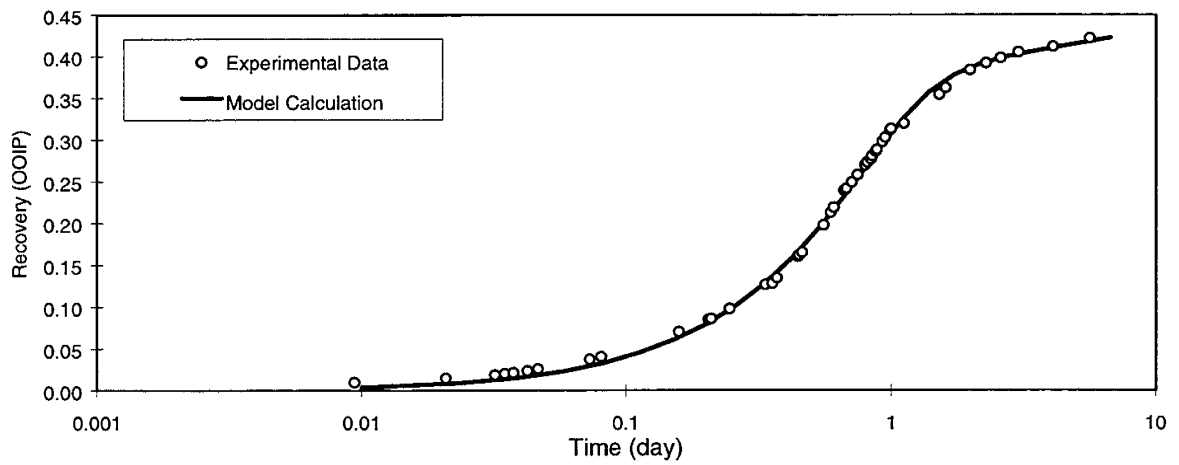


Fig. 4.14 - Comparison of calculated recovery with experimental data, CO₂/oil gravity drainage in a 500 md Berea core

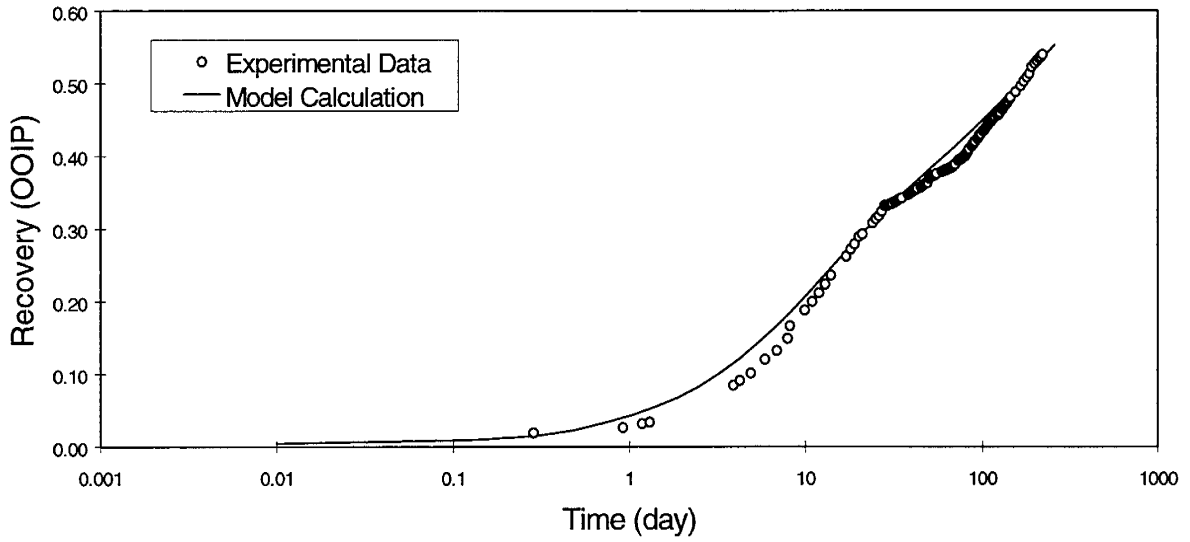


Fig. 4.15 - Comparison of calculated recovery with experimental data, CO₂/oil gravity drainage in a 50 md Berea core

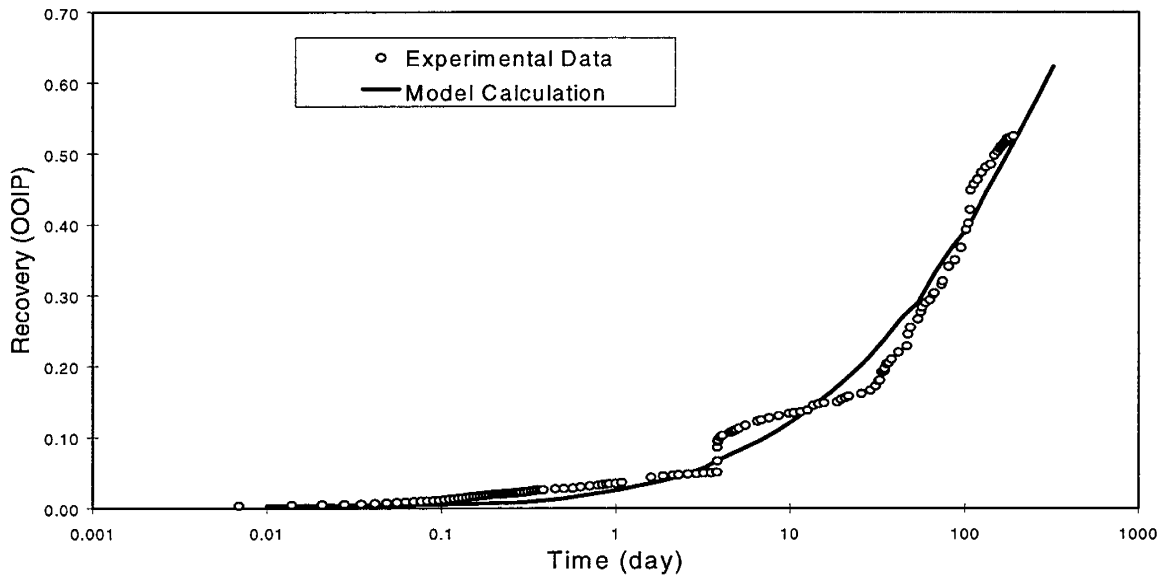


Fig. 4.16 - Comparison of calculated recovery with experimental data, CO₂/oil gravity drainage in a 0.01 md Spraberry core

5. CORING CENTRAL PRODUCTION WELL IN THE CO₂ PILOT AREA

This chapter provides an update for an ongoing field operations in the CO₂ pilot area. We presented reasoning and evidence¹ that stimulated interest in attempting CO₂ injection into this depleted, ill-characterized reservoir. A self-evident conclusion was that the natural fracture system, although universally accepted as dominating all aspects of production behavior in Spraberry, is not well characterized and needs to be rigorously understood before any attempt at process modeling could be attempted. The tremendous area that the productive sands cover also raises questions concerning the relation of these widely occurring fractures to basin-wide tectonics. In this manuscript, we present coring results from the central production well in the 15-well pilot. In addition, we discuss laboratory results and future plans to integrate this data for development of successful process options.

Coring the E.T.O'Daniel # 37

The E.T.O'Daniel #37 is the central production well in the projected 15 well pilot project as shown in Fig. 5.1. This well was sponge cored in the main 5U pay interval. The objective of the sponge core was to determine current oil saturations with a secondary objective of encountering natural fractures.

The following procedure was followed for the central production well:

- 1) Sponge core the main 5U pay zone
- 2) Open-hole logging
- 3) Formation Micro Imaging log
- 4) Complete, stimulate and produce until steady
- 5) Shut-in for pressure build-up test
- 6) Pulse test with existing wells

Core was retrieved from the majority of the Upper Spraberry, although difficulties were encountered and only rotary sidewall cores from the 1U pay zone were retrieved. Acquisition of this core reaffirmed our earlier analysis of previous core wells,² that the net pay in the Upper Spraberry primarily consists of two thin (8–15 ft each) pay zones, the 1U and 5U. Sharp contrasts are observed by fluorescence between shales containing no oil and the 1U and 5U pay zones, a very fine silt with a very low clay content. The 1U and 5U pay zones are easily identified by integration of whole core analysis and open-hole logs into standard shaly-sand algorithms.²

The E.T.O'Daniel #37 was perforated and stimulated in the 1U and 5U with 55,986 gallons of 30 lb. X-link delayed borate and 152,260 lbs. of 20/40 mesh sand. The well was produced (average of 11 bopd) until steady and is currently shut-in for a build-up test. After the

pressure test the central production well will be pulsed while listening in current wells surrounding the pilot area, shown in Fig. 5.1. This test will confirm whether or not the near well-bore orientation data that suggests a predominant east-west fracture orientation extends into the interwell region.

Fracture Description

Several natural and drilling-induced fractures were encountered in the 5U pay zone, occurring from 7220 - 7236 ft. Whole diameter samples were taken for paleomagnetic orientation. Results of core observations along with the interpreted FMI log are shown in Fig. 5.2. Fractures were oriented approximately N85°E. Agreement was excellent between the orientation resolved by the FMI log and the paleomagnetically oriented whole core.

The result of fracture orientation data does not completely resolve the orientation issue. The classic value quoted in the past for Spraberry fracture orientation was near N50°E. Most of the field response data reflects this value, whereas recent near well-bore surveys suggest more of an east-west orientation. Fig. 5.3 is an attempt to summarize all past and current measurements of the fracture system orientation. Fig. 5.3 shows data from pulse tests, pressure surveys, tracer tests and orientation logs. More coring and field testing is planned to resolve the subtleties of fracture orientation in the Spraberry Trend.

Mud losses during coring were generally observed in the shaly zones just above the 1U and 5U. This observation correlates with the observation that natural fractures tend to occur in the pay zones and terminate at gradual or sharp non-pay contacts. This suggests that natural fractures tend to be concentrated in the pay zones. Analysis of a deviated well drilled in 1952¹ demonstrated a qualitative correlation between fracture frequency and lithology with the majority of fractures occurring in sandier horizons exhibiting low gamma-ray response. An injection profile performed in 1968⁴ and shown in Fig. 5.4 tends to validate the premise that pay zones are highly fractured relative to the surrounding shales. Fig. 5.4 shows that the greatest temperature drop occurs within a small interval that correlates to the 1U in the Midkiff Unit.

Discussion

After coring the 1U and 5U of a dual-lateral horizontal well, drilling of the remaining pilot well will commence the purpose of the dual-lateral well is to directly measure the fracture spacing in the primary 1U and 5U pay zone. The information gathered in the reservoir characterizing stage, both lab and field data such as:

- Current reservoir pressure,
- Average fracture spacing,
- Permeability anisotropy in pilot area,

- Rock typing, log interpretation,
- Fracture diagenesis,
- Capillary pressure/wettability determination,
- Measurement and simulation of matrix/fracture transfer rates(water imbibition and CO₂ drainage)

will be used in determining a variety of design parameters for the pilot such as :

- Spacing between pilot wells,
- Orientation of pattern,
- Waterflood injection rate,
- CO₂ injection rate,
- Observation well response,
- Prediction of gas, oil and water production rate.

References

1. Schechter, D.S., McDonald, P., Sheffield, T., and Baker, R.: "Reservoir Characterization and CO₂ Pilot Design in the Naturally Fractured Spraberry Trend," paper SPE 35469 presented at the 1996 Permian Basin Oil & Gas Recovery Conference held in Midland, TX, March 27–29.
2. Banik, A. and Schechter, D.S.: "Characterization of the Naturally Fractured Spraberry Trend Shaly Sands Based on Core and Log Data," paper SPE 35224 presented at the 1996 SPE Permian Basin Oil and Gas Recovery Conference, Midland, TX, March 27–29.
3. Guidroz, G.M.: "E.T. O'Daniel Project—A Successful Spraberry Flood," *JPT* (Sep. 1967) 1137–1140.
4. "Field Test Results of Surfactant Waterflooding and Balanced High Pressure Waterflooding in the Spraberry Midkiff Unit," (1968) Humble Oil Internal Memo, PRRC Spraberry Data Base.
5. Schechter, D.S. and Guo, B.: "Mathematical Modeling of Gravity Drainage After Injection into Fractured Reservoirs," paper SPE 31570 presented at the 1996 SPE/DOE Tenth Symposium on IOR, Tulsa, OK.

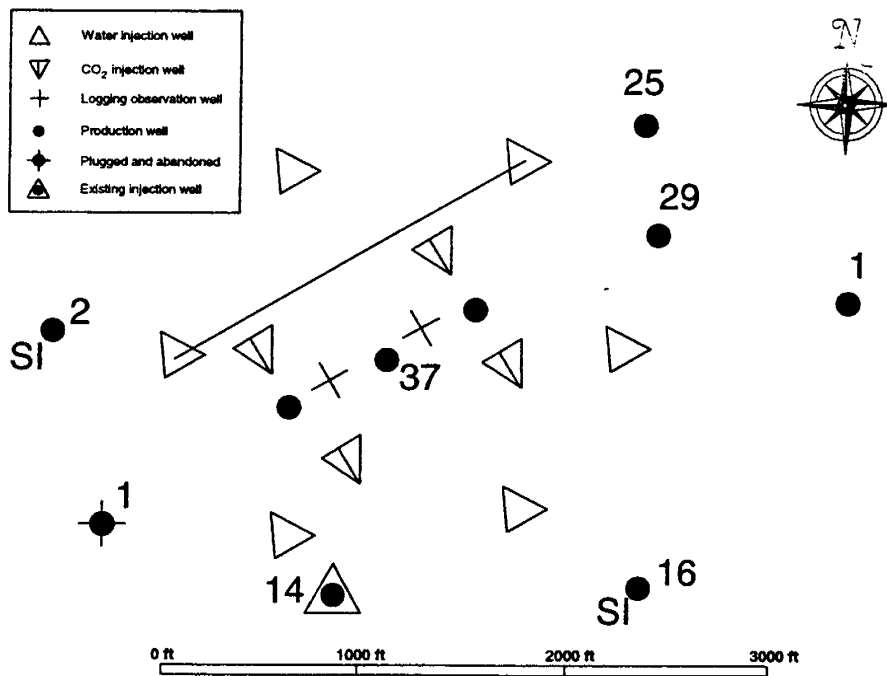


Fig. 5.1. Pilot pattern configuration in E.T. O'Daniel Unit. Existing wells are numbered.

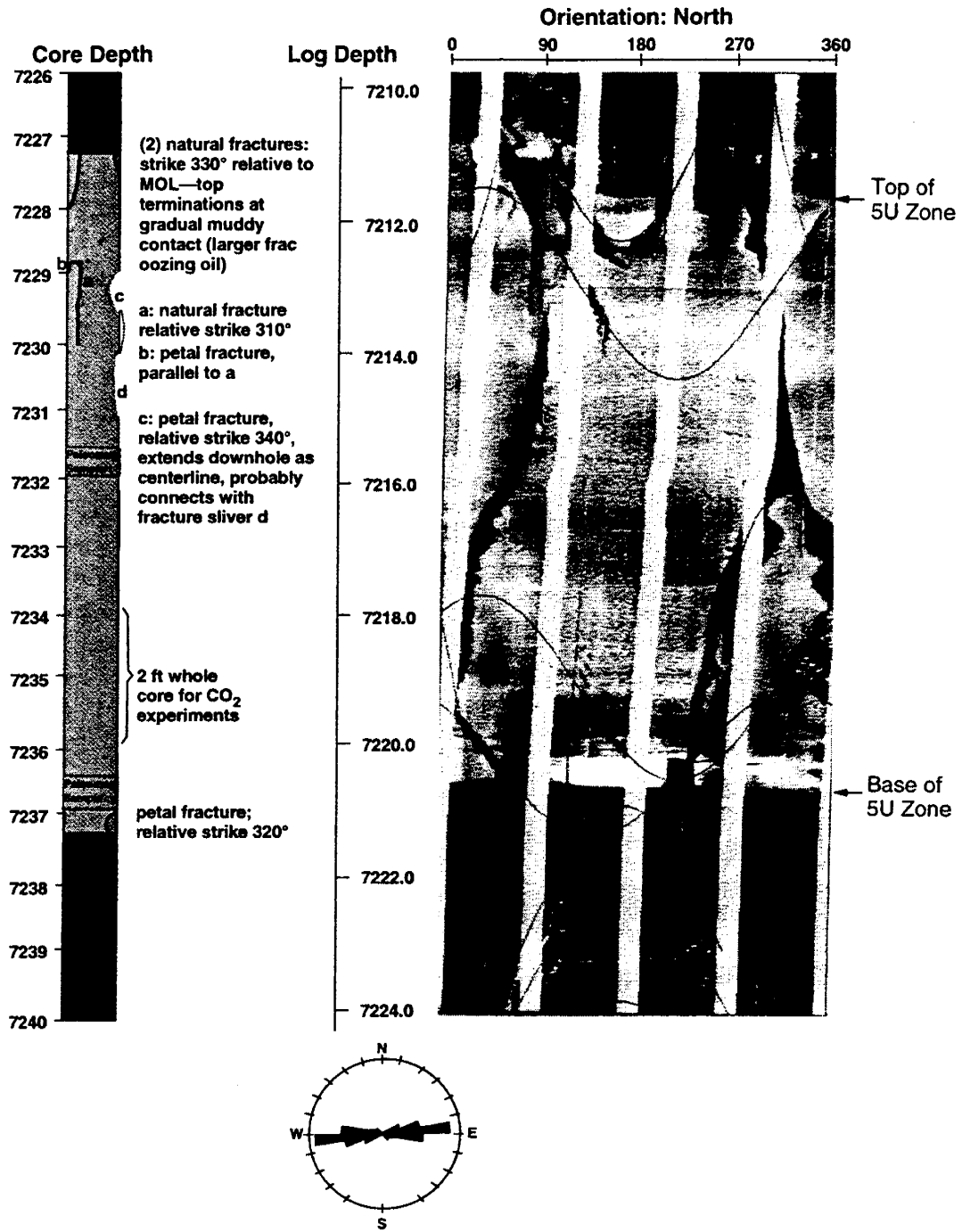


Fig. 5.2. Whole core observation of fractures compared with FMI log for the 5U pay zone. Fractures from core and FMI indicate an E-W orientation. Note sharp interface between pay and non-pay at 7237.5 (core depth) and 7221.0 (log depth).

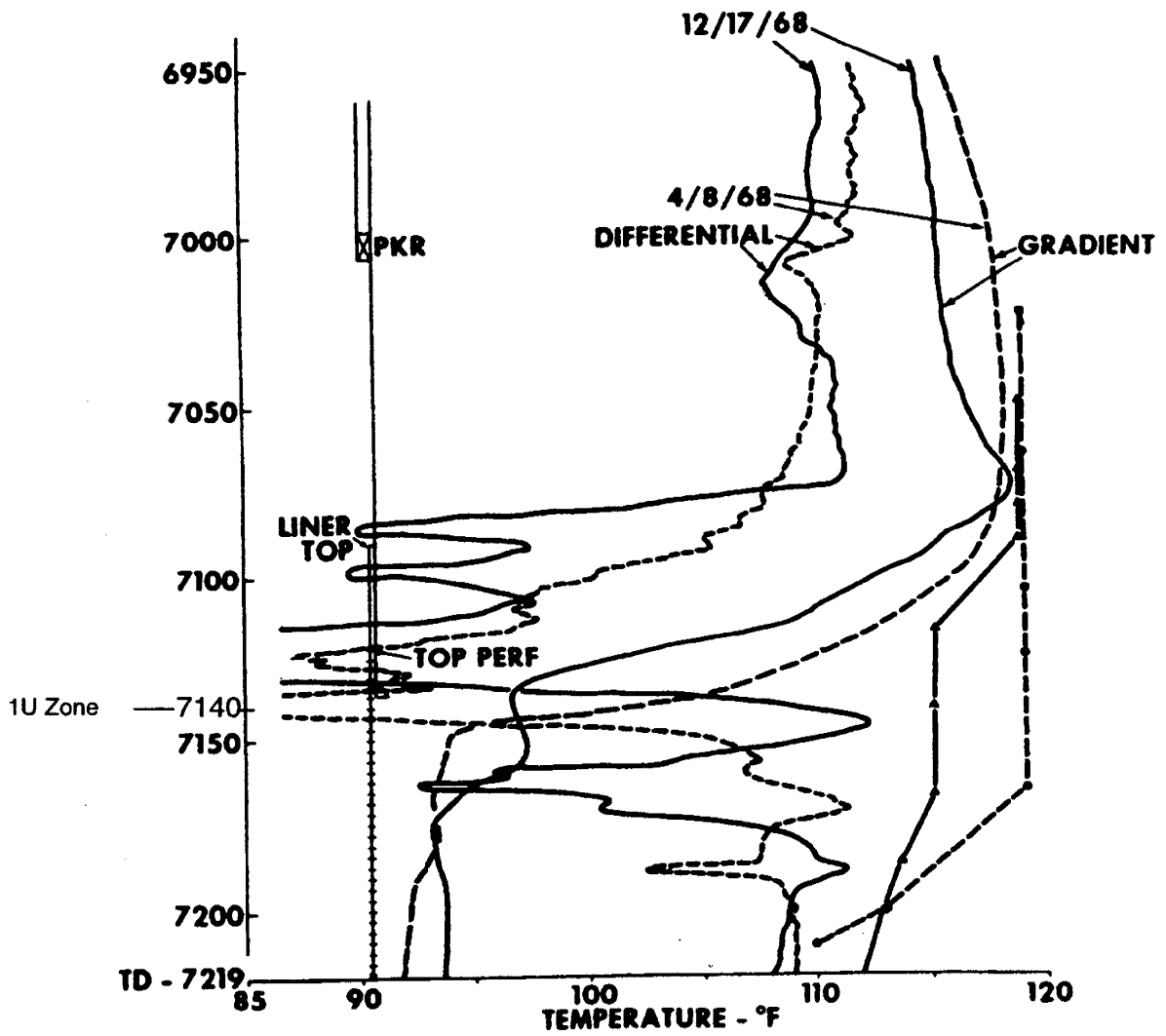


Fig. 5.3. Injection profile performed by Humble Oil Co. in 1968. Most fluid is seen to enter the thin 1U pay zone at 7140 ft.

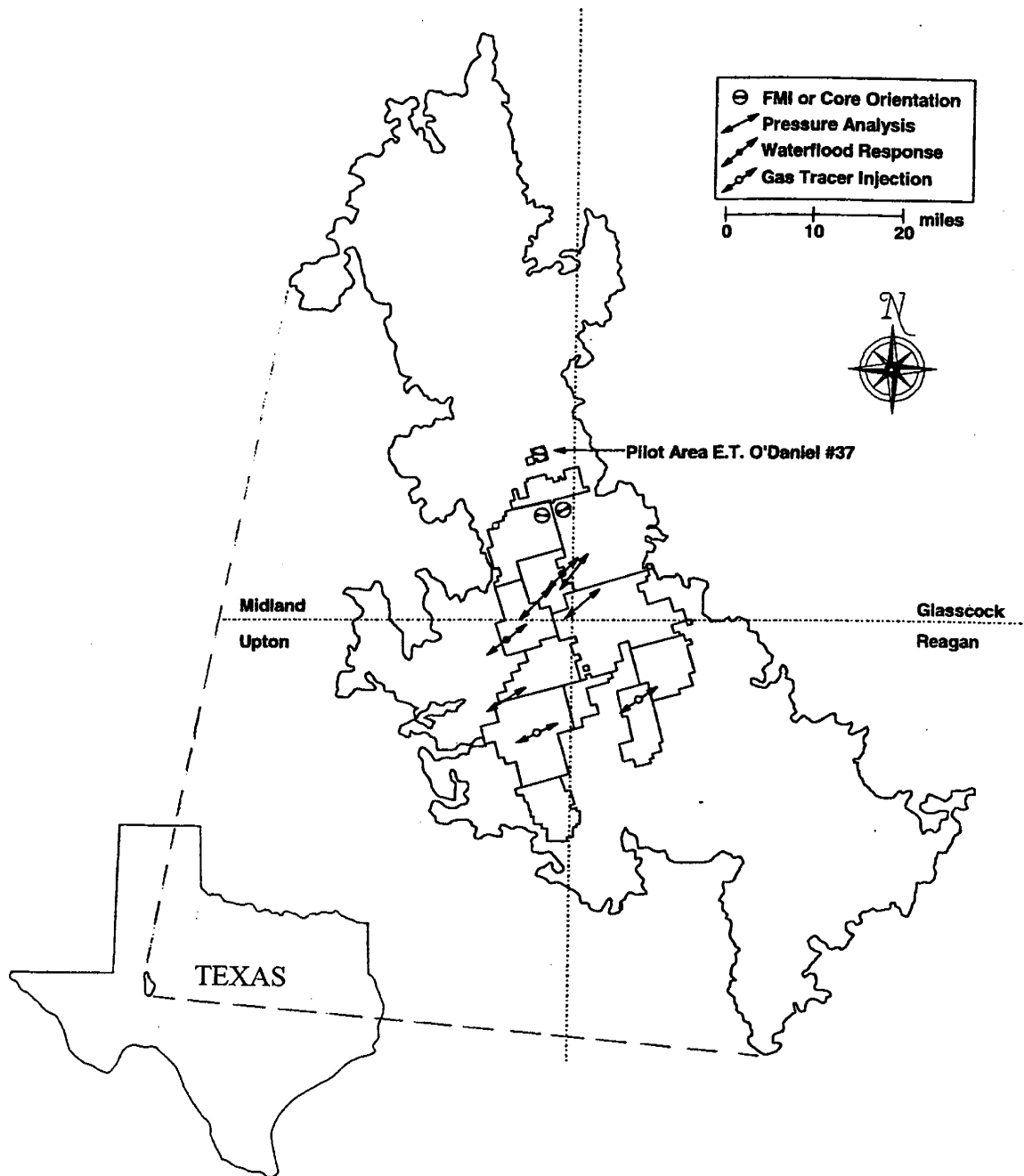


Fig. 5.4. Orientation of fractures in the Spraberry Trend Area. Fluid and pressure response data indicate an orientation near N50°E, whereas more recent borehole orientation data indicate an E-W direction.

III. CONCLUSIONS

During the first year of the project, we focused on understanding the behavior of the Spraberry reservoirs and the feasibility of CO₂ gravity drainage in the reservoirs. We have gained significant knowledge into the behavior of the naturally fractured Spraberry Trend reservoirs through this study. The following conclusions are drawn based on first year of our investigation:

1. A thorough analysis of open-hole logs and core data indicates that Spraberry reservoir sands can be better described by a shaly-sand rock model integrated with geological and petrophysical data. Spraberry pay zones can be identified from open-hole logs by the model, which consists of volume of shale/effective porosity cross plots.
2. Experimental investigations and numerical simulation show that the Spraberry reservoirs are weakly water wet, which may be partially responsible for poor performance of waterflooding Spraberry reservoirs. Other factors attributing to poor performance might include stress-sensitivity of the fractures, high gas saturation in the reservoir, and mineralization of fracture faces.
3. Experimental results of oil recovery from a low permeability Spraberry core during a CO₂ gravity drainage experiment is promising. This result indicates potential for CO₂ flooding Spraberry Trend Area reservoirs and provides the impetus to move this project into Phase II, the actual Field Demonstration.

